Département de formation doctorale en
Automatique et Informatique industrielle

Thèse
présentée à

UNIVERSITE DE LILLE

Ecole Doctorale Sciences Pour l'Ingénieur

Université Lille Nord-de-France

En vue de l'obtention du titre de Docteur dans la spécialité

Automatique, Génie Informatique, Traitement du Signal et des Images

par

MISHRA Maneesh Kumar

Development of Orthopedic Insoles and Shoes 3D Design Process for Atypical Foot Morphologies

« Développement d'un processus de conception 3D de semelles et de chaussures orthopédiques pour des morphologies de pieds atypiques »

Codirigée par Prof. Pascal Bruniaux, Prof. Christine Campagne
coencadrée par Guillaume Tartare

Soutenue le 02 Décembre 2019

JURY		
Ahmed RACHID	Professeur, UFR des Sciences, Amiens, France	Président du jury
Aura MIHAI	Professeur, T.L.I.M Faculty, Iasi, Roumanie	Rapporteur
Dominique ADOLPHE	Professeur, ENSISA, Mulhouse, France	Rapporteur
Pascal BRUNIAUX	Professeur, ENSAIT, Roubaix, France	Directeur de Recherche
Christine CAMPAGNE	Professeur, ENSAIT, Roubaix, France	Directeur de Recherche
Guillaume TARTARE	Docteur, ENSAIT, Roubaix, France	Invité

Development of orthopedic insoles and shoes 3D design process for atypical foot morphologies

Abstract

The needs in the sector of orthopedic insoles are becoming more important. The medical purpose of these plantar prostheses is often to correct the posture or biomechanical imbalance that tends to cause pain in various areas of the body depending on the pathology of the patient. The need for personalization of orthopedic shoes is also increasing. This is due to the progression of people who are increasingly obese or have problems with diabetes or other diseases.

However, the cost of its products can vary from one to two times or more depending on the quality of the product that requires adaptation by a manual process to the morphology of the foot. Whatever the therapeutic product envisaged, the economic model is no longer adapted to the needs of patients and the budgetary imperatives of social security. A new creative process is needed and must incorporate digital tools to reduce these manufacturing costs, while improving the quality of products.

Our study was to take stock of the means of measurement used and analyze the profession of podiatrist by highlighting the medical and economic aspects to detect the technological barrier.

The implementation of the new design process for these therapeutic foot products required the acquisition of morphological, anthropometric and biomechanical knowledge of the foot. In order to characterize the foot dimensionally and morphologically, a process of detection of anthropometric points and creation of morphological curves has been implemented.

At this stage, the process was able to analyze a population of male and female individuals to extract the most representative morphologies of a target population. It was from unsupervised classification methods that has classified the population and detected centroids.

The techniques that were then used to detect the anthropometric points of the foot were incorporated into the process of creating customized insoles. By combining this technique that extracts the outline encompassing the footprint, a method that uses this outline to create the 2D shape of the insole and the 3D shape of the standard shoe-last, the 3D shape of the insole was created and adjusted to foot and the standard shoe-last. This process showed the need to create the custom shoe-last of the person.

After a detailed technical analysis of the shoe-last, set up of a customized shoe-last 3D creation process has been stablished. This process was directly able to take into account the shape of the patient's foot on which detection of the anthropometric points and creation of morphological contours were done. These contours were to support a 3D space of ease on which was hung a network of curves defining the wire model of the surface of the shoe-last. This spatial ease was parametrizable in order to define a specific comfort to the patients or to control their therapeutic needs.

These two customization processes can be connected to each other to improve the wearing comfort of shoes for a patient or for the entire population by applying it to each centroid of the classification.

Développement d'un processus de conception 3D de semelles et de chaussures orthopédiques pour des morphologies de pieds atypiques

Résumé

Les besoins dans le secteur des semelles orthopédiques sont de plus en plus importants. Le but médical de ces prothèses plantaires est souvent de corriger la posture ou le déséquilibre biomécanique qui tend à causer de la douleur dans diverses zones du corps en fonction de la pathologie du patient. Les besoins en matière de personnalisation des chaussures orthopédiques augmentent également. Cela est dû à la progression des personnes de plus en plus obèses ou ayant des problèmes de diabète, voire d'autres maladies.

Mais, le coût de ses produits peut varier de un à deux voire plus en fonction de la qualité du produit qui nécessite de l'adapter par un processus manuel à la morphologie du pied. Quel que soit le produit thérapeutique envisagé, le modèle économique n'est plus adapté aux besoins des patients et aux impératifs budgétaires de la sécurité sociale. Un nouveau processus de création est nécessaire et doit intégrer des outils numériques pour réduire ces coûts de fabrication, tout en améliorant la qualité des produits.

Notre étude a été de faire le point sur les moyens de mesure utilisés et d'analyser la profession de podologue en mettant en évidence les aspects médicaux et économiques permettant de détecter la barrière technologique.

La mise en œuvre du nouveau processus de conception de ces produits thérapeutiques pour les pieds a nécessité d'acquérir les connaissances morphologiques, anthropométriques et biomécanique du pied. Afin de caractériser dimensionnellement et morphologiquement le pied, un processus de détection de points anthropométriques et de création de courbes morphologiques a été mise en place.

A ce stade de l'étude, il nous a été possible d'analyser une population d'individus mâle et femelle afin d'extraire les morphologies les plus représentatives d'une population cible. C'est à partir de méthodes de classification non supervisé que nous avons classé la population et détecté les centroïdes.

Les techniques qui ont ensuite été utilisées pour détecter les points anthropométriques du pied ont été intégrées dans le processus de création de semelles customisées. En combinant cette technique qui extrait le contour englobant l'empreinte du pied, une méthode qui utilise ce contour pour créer la forme 2D de la semelle et la forme 3D de la 'forme' standard, nous avons créé la forme 3D de la semelle ajustée au pied et à la 'forme'. Ce processus a montré le besoin de créer la 'forme' customisée de la personne.

Après une analyse technique détaillée de la 'forme', nous avons mis en place un processus de création 3D de la 'forme' customisée. Ce processus prend directement en compte la forme du pied du patient sur laquelle nous détectons les points anthropométriques et créons les contours morphologiques de celui-ci. Ces contours servent d'appui à un espace d'aisance 3D sur lequel est accroché un réseau de courbes définissant le modèle filaire de la surface de la 'forme'. Cette aisance spatiale est paramétrable afin de définir un confort spécifique au patient ou de contrôler ses besoins thérapeutiques.

Ces deux processus à vocation customisation peuvent être connectés l'un à l'autre pour améliorer le confort au porté des chaussures pour un patient ou pour l'ensemble de la population en l'appliquant sur chaque centroïde de la classification.

ACKNOWLEDGEMENT

Maneesh MISHRA

September 30th, 2019

Contents

LIST OF FIGURES

1

3

LIST OF TABLES

GENERAL INTRODUCTION

Context :

  The needs in the sector of orthopedic insoles are becoming stronger. The medical purpose of these plantar prostheses is to correct the posture or biomechanical imbalance that tends to cause pain in various areas of the body depending on the pathology of the patient. The therapeutic indications that are most often recommended are found in the case of osteoarthritis pain of the knee or hip, legs, unequal length, cavus or planus feet or hyper pressure zones... These pathologies are usually detected by rheumatologists or podiatrists. The latter finalize the prescriptions by the manufacture of custom-made orthopedic insoles that will be worn for about a year (normal life of the orthopedic insoles). These pathologies can be found in particular in children, athletes, disabled and elderly people. Depending on the practitioner, the cost can vary from single to double or more (75 € to 300 €) depending on the quality of the insole and the prescription since the manufacturing techniques are very traditional. In addition, the ceiling for social security reimbursements is not very high and does not take into account the inherent purchase of specific shoes in pharmacy to integrate this additional volume.

  Other needs in the area of customization of orthopedic shoes are also increasing. This is due to the progression of people who are increasingly obese or have diabetes problems. Mostly, these two pathologies are connected. A problem of cost and reimbursement similar to the orthopedic insoles also exists. Costs are strongly related to the design process that tends to remain manual.

  Whatever the therapeutic product envisaged, the economic model is no longer adapted to the needs of patients and the budgetary imperatives of social security. It must be based on the reflection of a coherent value chain to adjust a relevant response to needs by integrating the operating model of podiatrists or medical doctors and their level of acceptance to change, to define the right value chain. Of course, setting up a digital design process for these different products can only help to improve them while reducing production costs.

  The study will need to take stock of the means of measurement used and analyze the profession of podiatrist by highlighting the medical and economic constraints in order to detect the technological barrier. For example, the manufacture of the mold of the plantar arch is a tedious and time-consuming step, generally done in an artisanal way by the orthopedist

for an unattractive remuneration since it must follow the bases of reimbursement (TIPS). A state of the art of all existing diseases in relation to the need to create either orthopedic insoles or orthopedic shoes is therefore necessary to understand the pathology to know the specific needs of these medical and craft trades (medical doctors and practitioners).

The implementation of a new process for the design of therapeutic products for the feet will require the feet's knowledge on different aspects. The morphology of the foot is very useful in the creation of the shoe because it depends on the shoe-last. This object in wood or plastic is or should be a faithful representation of the foot's shape, which is not always the case. Anthropometry is the means of measuring the foot to characterize it dimensionally. But, from one patient to another, with the same size, some dimensions can be very different, which can be problematic. On the biomechanical aspect, the foot's pressure on the insole must be correct because it can cause various disorders or pain mentioned above.

This morphological and anthropometric knowledge of the foot will require the implementation of a reliable 3D digital measurement process. For this, the detection of anthropometric points becomes must, allowing precise measurements by a specific process. Thus, they will not depend on the anthropometric rules or the position of markers placed manually on the foot such as those used by a 3D scanner (industrial measurements).

The classification of the feet of a target population will be an important issue because it may be the start of a new process of creating shoe-last, or shoe, adapted to the morphology and measurements. Depending on the method chosen, it will be possible to know the number of feet typology (morphotype), as well as the number of people respecting a given typology. By this technique, the wearing comfort of the shoe will be increased. Certain classification methods will make it possible to optimize the sizing system or systems depending on whether or not the morphological criterion has been chosen. These morphotype can then be parameterized according to the sizing systems in order to represent the 3D foot's morphology of a patient.

The customized orthopedic insole must be studied to understand how it is located between the foot and the bottom of the shoe. The upper part of the orthopedic insole is supposed to represent the lower surface of the foot in order to correctly distribute the pressure points, the lower part is supposed to represent the inner lower part of the shoe. Podiatrists take into account the first condition by molding the feet, but not the second condition.

The customized orthopedic shoe is therefore desired to obtain good consistency in the creation process. One cannot do one without the other since the foot; the insole and the shoe represent an indissociably whole. Also, the establishment of a creation process of customized

shoe-last is essential for comfort, the medical aspect, not to mention the aesthetic aspect. This concept of comfort worn and unrolled foot on the ground will guide the work on the analysis of the 3D ease allowance between the foot and the shoe-last.

The overall layout of the thesis is organized as follows:

CHAPTER 1 - *State of the art* :

In first, this chapter is devoted to a state of the art of different pathologies of the foot in order to understand them and to know the means of treatment used. After, the anthropometric knowledge of the foot and its various measuring tools, which is essential for the diagnosis of the podiatrist, are presented. The bibliography shows it is from the campaigns of international measurements that this morphological knowledge, but also dimensional of the patient or the population is obtained. The analysis of the plantar pressure is very present in this state of the art because it is an effective means of diagnosis for certain pathologies. Given this desire to design a new process of creating footwear and insole adapted to the morphology of the feet, it was essential to go through the scientific works dealing with foot modeling, shoe-last modeling, without forgetting those that make it possible to understand the interface between the foot and the shoe by the 3D ease allowance.

CHAPTER 2 – *Anthropometric analysis and foot measurement* :

This chapter implements a new measurement method based on the raw data of the 3D scanner. This 3D graphical method aims to accurately measure the foot by reliable detection of anthropometric points. These measurements are compared to those obtained by the 3D scanner measurement software. An anthropometric analysis is detailed because it represents the heart of the measurement process.

CHAPTER 3 – *Clustering of population* :

This chapter deals with the classification of feet. Different methods have been tested according to the purpose and the quality of the results to be obtained. A first dimensional method is proposed in order to define an adjusted sizing system according to a target population. A second, more innovative method uses a 2D shape descriptor to morphologically classify the population independently of the measure. It has the advantage of extracting different foot morphotypes from a population leading to a thorough knowledge of the population.

CHAPTER 4 – *Insole customization* :

This chapter describes a new insole customization process. It is from 3D graphical technique used to detect anthropometric points that has defined the optimal outline encompassing the footprint. A 2D graphic process was associated with him to find the plantar surface of the foot. The shape of a shoe-last standard was then compared with the foot to obtain the 3D shape of the customized insole.

CHAPTER 5 – *Shoe-last customization* :

This chapter emphasizes that the shoe-last is the essential element to design a shoe because the style of the pattern is directly designed in 3D on the shoe-last. For this, a functional analysis of a shoe-last is proposed to better understand the specificity of each zone. Then, an analysis of the 2D/3D ease allowance between the foot and the shoe is performed. This allows integrating the useful data of the comfort and the dynamics of the unfolding of the step on our 3D graphical model of the shoe-last customized.

Respect for the shape of the foot and comparison with orthopedic work is mean to validate the overall concept of creation.

CHAPTER I: STATE OF THE ART

I.1. INTRODUCTION

The human body is very complex. Its anatomy can be disintegrated as follows: the head, the neck, the torso, the two arms extended by the hands, both legs extended by the feet. Generally, these different organs have several very specific functions. In the case of feet, their main role is to carry the weight of the body in a standing position and to allow walking and running. These tasks being of great complexity, nature being well done, the feet anatomy has been therefore created very complex. One foot is composed of 42 muscles, 26 bones, 33 joints, and at least 50 ligaments and tendons made of strong fibrous tissue to keep all the moving parts together, as well as 250,000 sweat glands. This evolution wonder is able to support hundreds of tons representing our weight in motion each day. The innumerable parts of the foot work in harmony to bring us from one place to another. But the stress and the constraints of movement expose them to a greater risk of injury than other parts of our body, risks depending on our overall anatomy. It is therefore important to know the different pathologies of feet to avoid them being precautious than to cure them after. Of course, an anthropometric knowledge of the foot and its various tools of measurement are necessary for the diagnosis of a podiatrist, in the design of the shoe which protects it or which contributes to the treatment of certain pathologies. Many of these diseases lead most of the time to design specific shoes or insoles. Depending on whether or not need of personalization of the products, the morphological and dimensional knowledge of the patient or the population must be known through measurement campaigns. Let's not forget that the knowledge of the shoe design process is essential to understand the interaction between the foot, the insole, and the shoe through a wood object called the shoe-last. This chapter is therefore devoted in summarizing the works tackling this vast problem.

I.2. MEDICAL ANALYSIS

The functional limitations from which older people suffer maybe the result of foot problems. Munro et al. [2] and Menz et al. [3] identified a high prevalence of foot problems (71 and 87% respectively) among older adults, and in both cases, this was more common in women. Older women were more prone to halux valgus and plantar callus, which frequently lead to chronic painful conditions [2][3]. Many of the estimated 110 million individuals in the world with diagnosed diabetes will experience anatomic and pathologic changes of their

lower extremities and a wide range of foot problems. The full extent of the diabetic foot problem is unknown since this heterogeneous pathology is not uniformly defined, classified or reported.

A census of different foot problems is necessary in order to understand the cause of these pathologies and how to avoid or solve them. It can also be seen that the more pathologies, it is not necessarily in the presence of a disease that caused these pathologies

I.2.1. PRESSURE PROBLEM

Many foot problems, including hammertoes, blisters, bunions, corns and calluses, heel spurs, claw and mallet toes, ingrown toenails, toenail fungus, and athlete's foot, can develop due to negligense, ill-fitting shoes, and simple wear and tear. One's feet can also indicate if one's body is under threat from a serious disease. Gout, for instance, will attack the foot joints first. Depending on the perceived problems, the surgical procedure is not always necessary and will be prescribed by the doctor in the last resort.

I.2.1.a. ATHLETE'S FOOT

Caused by a fungus that likes warm, dark, and moist environments like the areas between the toes or on the bottoms of the feet, athlete's foot can inflame the skin and cause a white, scaly rash with a red base. The athlete's foot fungus also causes itching, burning, peeling, and sometimes a slight odor; the infection can also migrate to other body parts.
One can avoid athlete's foot (also called tinea pedis) by keeping feet and toes clean and dry and by changing shoes and socks regularly [4]. Over-the-counter antifungal creams or sprays can be used to treat athlete's foot. If these remedies do not work, however, one may need to see a podiatrist and ask about prescription-strength medication.

Figure 1 : Athlete's foot inflammation [4].

I.2.1.b.   HAMMERTOES

If one's second, third, or fourth toe is crossed, bent in the middle of the toe joint, or just pointing at an odd angle, one may have what is called a hammertoe (**Figure 2**).

Figure 2 : Hammertoes deformities [5][6].

Hammertoes are often caused by ill-fitting shoes. Women are more prone to get ache associated with hammertoes than men because of different kind of fancy footwear and shoe gear. Since muscles of each toe work in pairs, when the toe muscles get out of balance, a hammertoe can be formed [5][6]. Due to this muscle imbalance toe's tendons and joints get so much of pressure and this pressure forces the toe into a hammerhead shape. Hazard for hammertoes include: flat feet, high arch, genetic, arthritis, injury to the toe and aging. For people with diabetes or poor blood circulation hammertoes can be a serious problem as they have a higher risk for infections and foot ulcers [7].

Therefore, customization of orthopedic shoes or last is the only remedy to prevent it from flourishing.

I.2.1.c.   BLISTERS

A blister is a soft pocket of raised skin filled with clear fluid (bubble) develop on a given foot area. This bubble can vary in sizes. Depending on its location, person may have difficulty walking, exercising, or standing for long periods of time. If one has blisters on feet, most probably because of the friction. Walking or standing for several hours a day puts pressure on the heels, soles, and toes; the longer one is on one's feet during the day, the greater the risk of growing feet blisters become [8][9]. Not everyone who walks or stands for long periods develops blisters, in many instances, these fluid-filled bubbles result from poorly fitted or ill-created footwear (**Figure 3**).
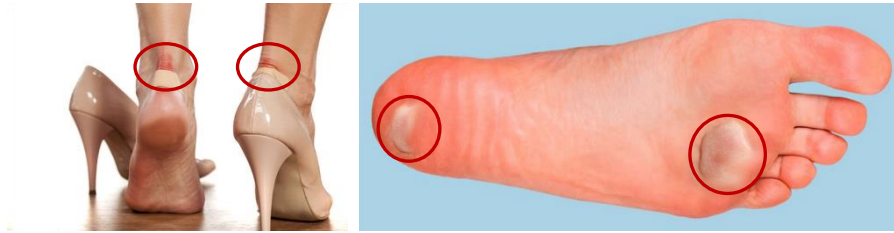
Figure 3 : Foot friction blisters [8][9].

Shoes that fit too tightly or too loosely can rub against the skin. This causes friction, and as a result, fluid builds up underneath the upper layer of skin. Blisters on the feet can be also caused by: frostbite, allergic reaction, chemical exposure, fungal infections, chickenpox, bacterial infection, herpes, dyshidrotic eczema.

Wearing properly fitted shoes is the first remedy to avoid a blister due to friction. Wearing an insole may also provide extra padding and reduce friction along a specific area of your shoe e.g. shop for shoe insoles or moisture-wicking socks.

I.2.1.d.   BUNIONS OR HALLUS VALGUS

A bunion is a crooked big-toe joint that sticks out at the base of the toe, forcing the big toe to turn in (**Figure 4**). A bunion can be painful when confined in a shoe, and for many people, shoes that are too narrow in the toe may be to blame for the formation of bunions [10][11]. Hallux valgus (HV) is one of the most common foot deformities in adults aged 18 to 65 and is characterized with pronation of proximal phalanx, medial deviation of the first metatarsal and medial prominence of the first metatarsophalangeal joint. The prevalence for HV is reported to be 23% in adults is increased with ages and more in female than male which with high dissemination is an important health problem which may cause pain, cosmetic appearance concerns, and reduce in health-related quality of life. Studies reported that individuals with HV had lower thickness and cross-sectional area of abductor halluces and flexor halluces brevis compared to individuals without HV [12].

Figure 4: Bunion or hallus valgus problems [11].

Generally, HV have various grounds, including inborn deformities, arthritis, trauma, and heredity [13]. It has been proposed that atrophied or weak toe flexor muscles are associated with the formation of toe deformities however; there is not enough evidence to support this theory. However, high heels (it forces your toes into the front of your shoes), ill-fitting shoes (too tight, too narrow or too pointed are more susceptible to bunions) may increase the likelihood of suffering with this deformity [14]. The intrinsic foot muscles of older adults with HV and lesser toe deformities are significantly smaller than those of older adults without toe deformities. Therefore, strengthening the intrinsic toe muscles may help to reduce the incidence and severity of toe deformities in older adults [15]. Simultaneously, it is prudent to choose shoes, with wide toe box, no pointy toes and shall be spacious between the tip of your longest toe and the end of the shoe. So, the shoes shall imitate to the wearer's feet shape without squeezing or pressing any part of the foot [16]. Accumulating all the instructions is unlikely to put in practice hence, in such deformity exploitation of modern technology of footwear, orthoses and insole customization is required.

I.2.1.e.   CALLOSITY

Callosity can be divided into two parts: corns and calluses [17]. However, by referring to several medical research papers, it has been quite ambiguous to clearly distinguish between the various types of foot keratotic lesions. Moreover, the terminologies used by different surgeons (British or America) rheumatologists, dermatologists and podiatrists are dissimilar and unclear. For example, podiatrists term corns as heloma (derived from greek helus, stone wedge) [18].

A corn, dry horny mass frequently establish on the dorsolateral aspect of the fifth toe or the dorsum of the interphalangeal joints of the lesser toes, represents a bounded, sharply demarcated area of traumatic hyperkeratosis (**Figure 5**). Corns tend to develop on parts of one'e feet that do not bear weight, such as the tops and sides of your toes and even between toes. It has a visible translucent central core which presses deeply into the dermis, causing pain and sometimes inflammation.

Figure 5 : Corns and calluses [17].

A callus is diffused and a broad based, drawn-out area of hyperkeratosis of relatively thickness, most commonly found under the metatarsal heads, the heels or balls and on the sides of toes (**Figure 5**). Calluses can also be found in weight-bearing areas. A callus is less bounded than a corn, is usually larger, and does not have a central core, and is mostly less or not painful. But, these compressed patches of dead skin cells can also be hard and painful.

Callosities are mainly the problem of shoes and do not occur in people walk barefooted. Low-heeled shoes with a soft upper and a roomy toe-box are compulsory for patients. Moreover, toe separators or some lamb's wool between your toes, has been popular lately. However, this is not enough all the time.

I.2.1.f. PLANTAR FASCIITIS AND HEEL SPURS

Plantar fasciitis is acknowledged as synonym of inflammation of the plantar fascia and the suffix "-itis" integrally suggests an inflammatory disease. It is common for doctors to confuse heel spurs and plantar fasciitis when a patient comes to them with heel pain. Heel spurs are found in 70 percent of patients with plantar fasciitis, but these are two different conditions [19][20]. The heel spurs themselves are not painful; it is the inflammation and irritation caused by plantar fasciitis that can hurt. Heel spurs are often seen on X-rays of patients who do not have heel pain or plantar fasciitis (**Figure 6**) [21].

Figure 6 : Plantars fasciitis and hell spurs [19][20].

Plantar fasciitis is a painful disorder in which the tissue that connects the ball of the foot to the heel and fascia becomes inflamed. Heel spurs are pieces of bone that grow at the heel bone base and often develop after one has had plantar fasciitis.

A process that usually occurs over a period of many months when calcium deposits build-up on the underside of the heel bone as spurs. Strains on foot muscles and ligaments, stretching of the plantar fascia and repeated tearing of the membrane that covers the heel bone, heel spurs are often caused by. Almost 10 percent of injuries occur especially among athletes whose activities include large amounts of running and jumping [22].

Treatments for heel spurs and associated conditions include exercise, custom-made orthotics, anti-inflammatory medications, and cortisone injections as failing by conservative treatments surgery becomes the only option.

I.2.1.g.   MALLET TOES, HAMMER TOES AND CLAW TOES

These terms have been confusing and have been used interchangeably. According to Michel J. Coughlin, a mallet toe involves a contracture of distal interphalangeal joint in which the distal phalanx is flexed on the middle phalanx. A hammer toes involves a similar contracture of the proximal interphalangeal joint in which the middle and distal phalanges are plantar flexed in relation to proximal phalanx. A claw toe has a dorsiflexion deformity at the metatarsophalangeal joint associated with a hammer toe deformity. Mallet and hammer toe deformity is associated with single toe; however, claw toe involves multiple toes (**Figure 7**) [23].
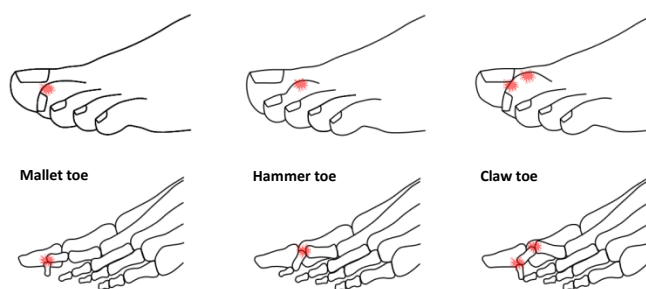
Figure 7 : Mallet toe, hammer toe & claw toe.

Claw toe causes all toes except the big toe to curl downward at the middle of the joints and curl up at the joints where the toes and the foot meet. Calluses and corns may often form when someone has claw toes. While tight shoes can be blamed for claw toes, so can nerve damage to the feet (from diabetes or other conditions), which weakens foot muscles.
With mallet toes, the last joint of the toe bulges and a painful corn will grow near the toenail. Generally the second toe is affected because it is the longest. Injuries and arthritis are among the causes of mallet toe.

Tight shoes can cause the toe muscles to get out of balance. If a shoe forces a toe to stay in a bent position for too long, the muscles tighten and the tendons shorten, or contract which makes it harder to straighten the toe. Over time, the toe muscles cannot straighten the toe, even when one is not wearing shoes. These toe problems form over years and are common in adults where women are affected more often than men because they are more likely to wear shoes with narrow toes or high heels. Less often, these toe problems are linked

with other conditions, such as diabetes, rheumatoid arthritis, stroke, or an injury to the foot or ankle.

Treating the toe joint problem home is possible by changing one's footwear to roomy toe boxes, low heal, good arch support, sandals or athletic shoes that do not rub and custom-made shoes. One may avoid surgery only start at the prima-facie of the problem.

Using products that cushion the toe or hold the foot in a more comfortable position, such as moleskin, toe tubes, arch supports, or other shoe inserts (orthotics) are better for treating a flexible toe; nevertheless, they may also provide some relief for a fixed toe.

I.2.1.h.   ONYCHOCRYPTOSIS (INGROWN NAILS):

From apparent to profound analysis, the nail can be divided into dorsal, intermediate, and ventral nail plates. The nail grows at an assessed rate of 0.1 mm per day. Whenever presented to family physician, approximately 20 percent of patients with a foot problem have an ingrown toenail, also known as onychocryptosis (**Figure 8**). The term ''onychocryptosis'' has been used interchangeably with conditions that are less drastic for example, onychophosis and incurved nail borders. Such usage couples an erroneous diagnostic picture with unsubstantiated therapeutic procedures therefore, it shall be avoided to use interchangeably [24].

When the periungual skin[1] is punctured by its corresponding nail plate, ingrown toenails happens which results in a cataract of external body, inflammatory, infectious, and reparative processes [25][26]. Eventually, the consequences may be painful, draining, and foul-smelling lesion of the involved toe , with soft tissue hypertrophy[2] around the nail plate [27].

Figure 8 : Onychocryptosis around periungual skin [25][26].

Some researchers suggest that the anatomic and behavioral mechanisms are prone to Onychocryptosis. It is not strictly evident, however, it has been stated that a genetic predisposition and family history, hyperhidrosis, and poor foot hygiene increase the

---

[1] Skin that cluster around the fingernail or toenail
[2] The increase in the volume of an organ or tissue due to the enlargement of its component cells

probability of ingrown toenails. Lower limb extremities that may incline to i.e., diabetes, obesity, and thyroid, cardiac, and renal disorder edema can also increase the likelihood of ingrown nails.

Antibiotics are often used for both medical treatments without surgery as well as perioperative adjunct therapy in onychocryptosis. Several kinds of methods have been used for the treatment of onychocryptosis. Every method carries risks of relapse and contagion and there have been few well-designed clinical trials that compare the efficacy of different procedures. As much as the choice of procedure, training and surgical skills are important factors in the success of nail surgery along with some antibacterial insoles which have been tried to use for cure [28].

I.2.2. SHAPE PROBLEM

There are basically two kinds of arches: longitudinal arches (consists of medial and lateral parts-distributes body weight and pressure in different directions with transverse arches together) and transverse arches (**Figure 9**) [29].

Foot bones are arranges in longitudinal plane and transverse arches are supported and controlled by tendons where tendons absorb and transmit forces from body to ground when standing or moving [30]. Transverse arches are across from medial to lateral side where the shapes of different arches can be distinct at various locations. Longitudinal and transverse arches together enables the foot its utility and locomotion. There are two longitudinal arches: medial and lateral. Medial arch is composed of calcaneus, the talus the navicular, the three cuneiforms and the metatarsal 1 to 3 and is higher than the lateral longitudinal arch (called foot arch normally). Soft tissues (the plantar calcaneo-navicular ligament) with elastic properties act as springs.
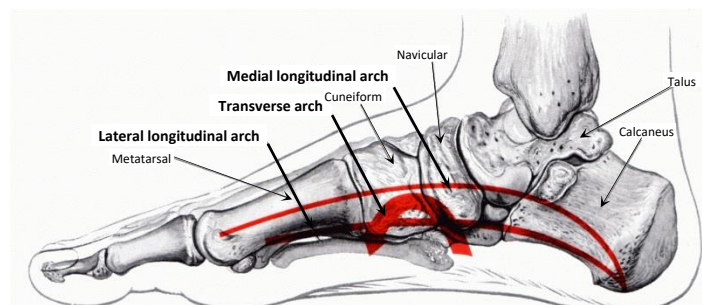
Figure 9 : Arches of foot [30].

I.2.2.a.   HIGH ARCH OR CAVUS FOOT

According to the research performed by Subotnick, 60% of the population have normal arches, 20% have a cavus foot (high arch), and 20% have a planus foot (low arch) [31]. When the longitudinal arches are higher than normal, it termed as high arch (**Figure 10**) [32][33]. It has an imprint with or without a narrow band connecting the forefoot and heel region. The bony structure on the lateral side (over supinated) of the foot is at higher risk of injury due to having smaller area to weight-wearing thereby transmits higher stresses to the foot and leg. High arch (cavus foot) foot is often caused by a neurologic syndrome and other medical condition for instance: cerebral palsy, Charcot-Marie-Tooth disease, spina bifida, polio, muscular dystrophy, or stroke.

Figure 10 : High arch (cavus foot) [32][33].

In other case of cavus foot, the high arch may represent an inherited structural deformity. For this type of foot high level of cushioning and shock absorption would be appropriate [34].

I.2.2.b.   LOW ARCH OR PLANUS FOOT

When longitudinal arches are low, it is called planus foot (**Figure 11**) [35][36]. Plannus foot, like cavus foot, does not transmit forces efficiently and therefore it may lead to foot pain. Moreover, this also affect pressure distribution properly in other parts of body in long term which may cause back pains.

Figure 11 : Low arch (planus foot) [35][36].

Low-arched runners have more eversion excursion and less tibial internal rotation excursion than high-arched runners. This metamorphosis has been the result of the greater inversion of the rear-foot that occurred at heel strike in the low-arched group [34].

I.2.2.c. METATARSALGIA

Metatarsalgia is a common overuse injury. The term describes pain and inflammation in the ball of the foot (**Figure 12**). It is often thought of as a symptom of other conditions, rather than as a specific disease. It can be caused by increased pressure on the metatarsal heads [37]. The cause of increased pressure in this part of the foot can be either due to deformities of the foot, or from pressure from sources outside the foot, such as footwear. Structural issues usually have to do with the metatarsal bone, and the most common variation in people with foot pain is a long second metatarsal. Other variations include abnormal joint alignment (increased extension) of the joint of the metatarsal with the toe (called the metacarpophalangeal joint).
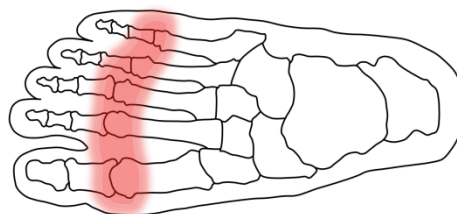
Figure 12: Metatarsalgia (ball of the foot pain).

There are several conditions that can cause enlargement of the metatarsal head, for instance; distinct kinds of arthritis, osteonecrosis, neuromas, tumors, or infections. Lastly, traumatic injuries, including fractures and ligament tears, can cause this type of foot pain. Different remedies exist to treat metatarsalgia. It is possible to use pads or appropriate insoles to eradicate the problem, but also fitting shoes.

I.2.2.d. FOOT JOINTS

There are 33 joints in each foot to enable foot dynamics and to absorb the locomotive shock. Accumulatively, joints can be divided in three parts: ankle joints, intertarsal joints and other joints of foot. Joint pain can occur on one or more joints depending on the pathology. It is characterized by an increase in heat on the affected joints. It is a pathology that can also be diagnosed visually because it usually comes in the form of swelling, redness or bruising. The causes of joint pain can come from infection, inflammation, trauma or arthritis, bursitis, gout.

Generally, the doctor advocates to patient rest to avoid weight on the sore foot. The use of nonsteroidal anti-inflammatory drugs can reduce inflammation. But, personalized orthotic devices can also be prescribed. The goal of these devices is to reduce pain with supporting the foot.

Ankle joints

Ankle joints comprises of talus of foot, tibia and fibula of leg, which creates a synovial hinge joint. A hinge joint is a common class of synovial joint that includes the ankle, elbow, and knee joints. Hinge joints are formed between two or more bones where the bones can only move along one axis to flex or extend which enables dorsiflexion and plantar flexion of foot (**Figure 13**) [38]. Dorsiflexion involves the medial, calcaneo-fibular and posterior talo-fibular ligament whereas plantar flexion involves anterior talo-fibular ligament and the anterior part of medial ligament.

Medial (deltoid) ligaments and lateral ligament stabilize the ankle joints. Ankle ligaments are used frequently during sports activities e.g., walking, running etc. Therefore, most common injuries occur in ankle e.g., sprain (torn ligament) and fracture-dislocation [29]. .
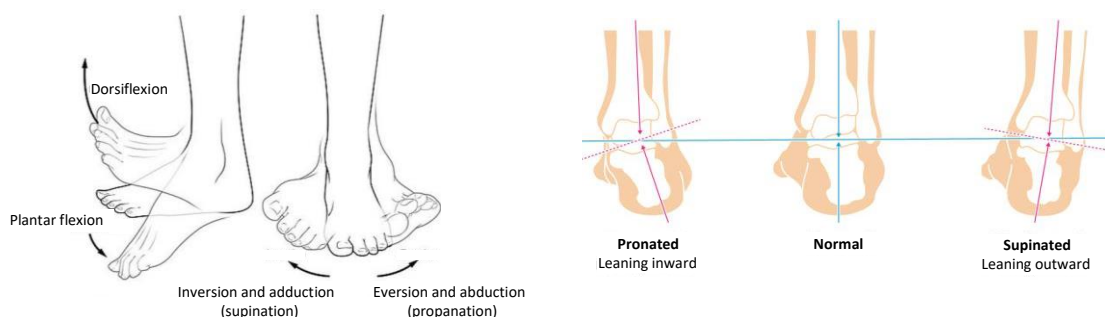
Figure 13 : Foot motions [38].

Intertarsal joints

Joints between tarsals are the intertrsal joints. These joints are mainly transverse tarsal joint (including the talocalcaneonavicular and the calcaneocuboid joints) and subtalar joint (talocalcaneal). These joints are involved in inversion, eversion, pronation and supination.

Cuneonavicular & tarsometatarsal Joints

The cuneonavicular joints and the tarsometatarsal joints have limited movements. Apart from ankle joint, the metatarsophalageal joints are important while in motion (walking and running).

I.3. MORPHOLOGICAL KNOWLEDGE OF FOOT

Morphological analysis is a domain related to the proportion and dimensions of anthropometric measures. Morphological knowledge is prominent in several domains because she can explain for example which may cause ups and downs to phycological health of a person (reference). The prominence of anthropometry has been playing a vital role in forensic researches in order to identify the victim in terms of sex, population group and demographics, not less [39]. In the footwear industry anthropometry has been an important prerequisite to optimize the shoe-last according to the different age groups, races, body composition and be sex-specific. Many works deal with this optimization problem and are connected to measurement campaigns. To measure a foot, there have been several basic methods available in the market such as caliper ruler, blueprints, tape measures, etc. However, today's method like 3D foot-scanners, appear more suitable. Convenient to use and competitive cost procedures, the plaster cast also may be mostly used by orthopaedists to obtain the 3D shape of the foot. But 3D scanner would get more adapted because of its affordable cost and its use for the creation of clients database or for measurement campaigns. Plantar pressure distribution mats can be an useful tool to help orthopaedists in the diagnostic of a plantar problem or morphologic.

Our objective is therefore to inventory the main works dealing with this knowledge essential to the continuity of our work.

I.3.1. ANTHROPOMETRIES OF THE FOOT

By definition, anthropometry is the measurement technique of the human body and its various parts. The measurement of a human body is strongly related to different
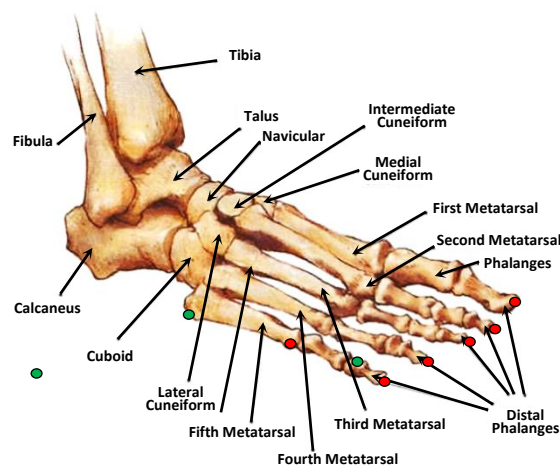
Figure 14 : Different bones of foot. Anthropometric points [40].

anthropometric points defined on the bones [40]. **Figure 14** describes the different bones of the foot by showing in red and green the anthropometric points visible in this point of view to give an example. Complete foot anthropometry will be detailed in the chapter II.

In the case of a complete human body, different planes (sagittal, frontal, transverse) partition it in order to prepare the measurement process [41], which is not the case for the feet. In the works of Witana et al. [42], the anthropometric points are the only measurement references which have been used to classify 18 dimensions by categories according to the length between two points or a point and a plane, the width between two points, the girth of contours positioned with respect to one, two or three points (**Figure 15**): 1) Foot length, 2) Arch length, 3) Heel to medial malleolus, 4) Heel to lateral malleolus, 5) Heel to fifth toe, 6) Foot width, 7) Heel width, 8) Bimalleolar width, 9) Mid-foot width, 10) Medial malleolus height, 11) Lateral malleolus height, 12) Height at 50% foot length, 13) Ball girth, 14) Instep girth, 15) Long heel girth, 16) Short heel girth, 17) Ankle girth, 18) Waist girth.
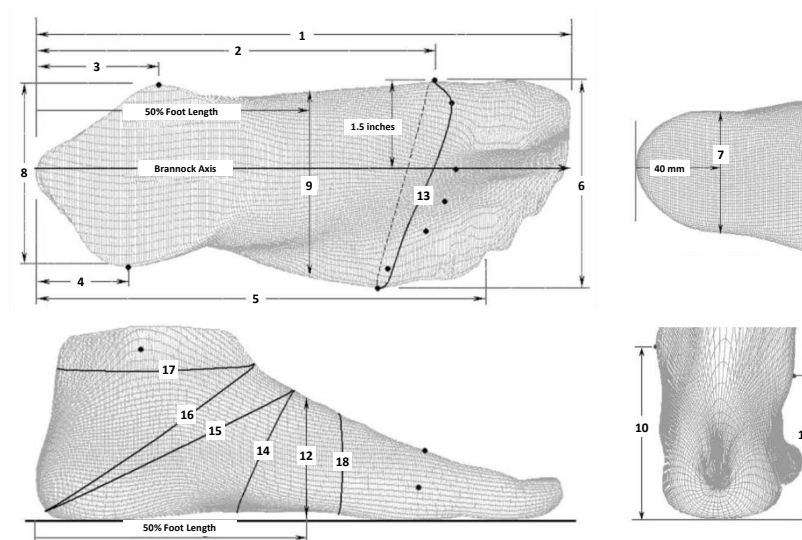
Figure 15 : Foot measurements [42].

To compare foot dimensions between the two genders and also with the corresponding data from other populations, Hajaghazadeh et al. have added others dimensions [43]. Lengths of the second, third and fourth toes measured in the direction of the Brannock Axis have been added to obtain 21 dimensions.

I.3.2. MEASURING TECHNIQUES OF THE FOOT

Manufacturing comfortable footwear relies on anthropometric research, which determines the morphological character of the foot, the behavior of the foot-footwear system and the results of the morpho-functional optimization of the shape of the product. The natural

anatomic-morphological constructions of the foot, its correct static and dynamic functioning are ensured by a rational inner shape of the shoe, the shape which is determined in turn by the construction of the last. The construction of the last, the establishment of the dimensions required to meet the comfort requirements of a larger proportion of consumers with minimal production costs, must be based on the knowledge and the most accurate characterization of the anatomic morphological differences of the types of foot encountered within that population of consumers and the frequency of these types within the population. For this purpose, it is periodically necessary to perform anthropometric studies on the population differentiated according to certain criteria (sex, age, geographical region, etc.) in order to obtain information about the dimensional particularities of the average representative foot for that population, the laws of distribution of anthropometric parameters that characterize the representative average foot of the population of the respective country [44].

The most common approaches include using digital calipers for direct measurements and 3D scanning and footprint analysis for indirect measurements. It is very important to provide adequate training for the technicians to correctly position landmarks on the proper anatomical points.

The main objective of taking measurements of the human foot is to have an approximation to the most precise dimensions of the foot of a person, and consequently to be able to design the shoe last which is the physical support essential to the design of the shoe. This part is devoted to the presentation of different anthropometric measurement techniques, specifying their advantages and disadvantages.

I.3.2.a.   2D TRADITIONAL MEASUREMENT

The ink footprint and digital caliper are the traditional manual approaches used to collect foot dimensions. However, the accuracy of digital caliper measurement tends to be affected by human error. Different technicians may obtain inconsistent measurement results. It is very important to provide adequate training for the technicians to correctly position landmarks on the proper anatomical points [45]. Also, to obtain measurements with reliable results, it is necessary to respect the rules in force and the norms [46]. Other means of traditional measurements then appeared to measure the length of the correctly oriented foot, the strategic angles, anthropometric contour girths correctly identified with respect to the anthropometric points, the footprint with other techniques.

Ink footprint method

In the cas of ink footprint, excellent quality prints have been obtained with a large inkpad and a sheet of plain white paper (**Figure 16**). Due to size concerns, homemade ink pad was used, since it should be larger than any foot which is to be printed. The inkpad used in the study was made with a shallow, plastic, lidded food storage container, lined with a thin layer of foam rubber which was then soaked in stamp pad ink [46]. The extra-large inkpad thus made and a packet of letter-sized paper is easily portable and quick to use, and the lid on the container prevents the ink from drying out. A serious drawback to this method is that it is useful only for static or single footprints, not for making footprint trails. Furthermore, the feet of the subjects should be cleaned after making prints, a messy and sometimes time-consuming chore. However, to avoid the need for clean-up, Kennedy et al. used an "inkless pad" and special chemically-treated paper with excellent results [47].

Using the ink footprint to collect foot dimensions can reduce the experiment time. The ink footprint data can also be used repeatedly for different applications such as calculating the arch index at a convenient time. However, the limitation of collecting foot dimensions using ink footprint method is that it cannot measure vertical dimensions such as navicular height. In addition, the quality of the ink footprint may influence the precision and accuracy of foot dimension measurements.
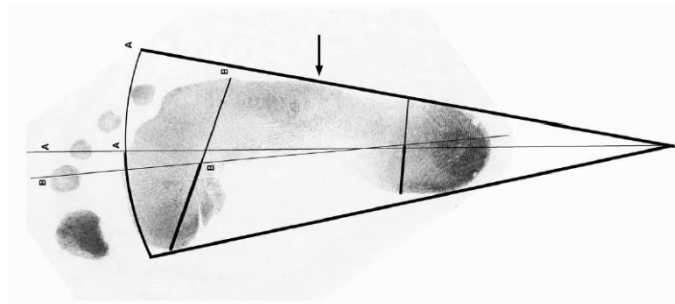
Figure 16 : Ink-print method using homemade ink pad [46].

Footprint was used by Akambase et al. to compare the arches shape of a population and to define the relationship to gender and racial differences [48]. The authors used the plantogram to determine the height of the foot arches by shtriter index method. The ratio of the width of transverse arches to the width of the foot (Flattening index = AC/DE) was the way to distinguish normal, cavus and planus feet (**Figure 17**).

Figure 17 : Plantogram: (a) normal arched foot,
(b) high-arched foot, (c) low-arched foot.

In the same spirit, Özdinc et al. used a similar tracing technique, called pedigraphy, to analyze the effects of ballet training on foot structure [49]. The auhors notice that the ballet training leads to the formation of themedial longitudinal arc in childhood. Their study enable to create a relationship between the body mass index with structural change secondary to ballet training from the footscreen parameters (**Figure 18**).
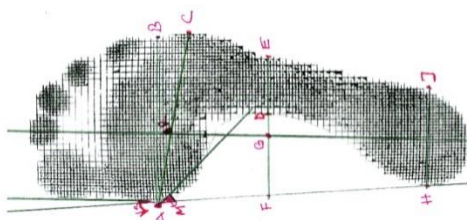
Figure 18 : Footscreen parameters.

Thermography footprint method

The footprint has been used in other research to detect diabetic foot risk based on the anthropometric profile of patients. It is from the thermography footprint (**Figure 19**) that Neves et al. have set up a measurement protocol defining three significant regions (circle on figure) which make it possible to create a link between IMC and diabetic foot risk [7].
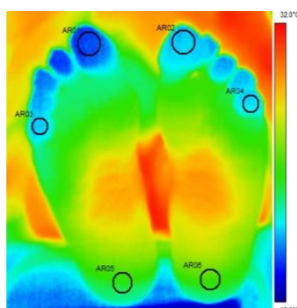
Figure 19 : Plantar foot thermal
image analysis protocol [7].

Digital caliper:

The Digital Caliper (sometimes incorrectly called the Digital Vernier Caliper) is a precision instrument that can be used to measure internal and external distances extremely

accurately. The example shown in **Figure 20** is a digital caliper as the distances/measurements, are read from a LCD display. The most important parts have been labelled.

Earlier versions of this type of measuring instrument had to be read by looking carefully at the imperial or metric scale and there was a need for very good eyesight in order to read the small sliding scale. Manually operated Vernier calipers can still be bought and remain popular because they are much cheaper than the digital version. Also, the digital version requires a small battery whereas the manual version does not need any power source but cannot be used everywhere. Digital calipers are easier to use as the measurement is clearly displayed and also, by pressing the inch/mm button the distance can be read as metric or imperial.
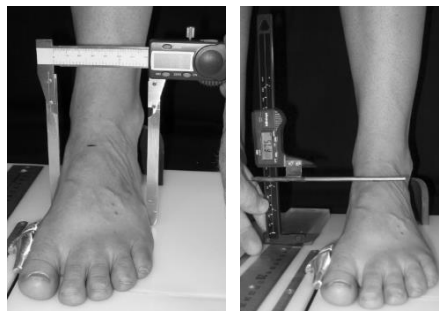
Figure 20 : Dorsal arch height and midfoot
width by digital Caliper [50]**.**

McPoil et al. used the digital calipter to measure and combine several anthropometric measurements to predict the plantar surface [50]. The six measures that were confronted in the study are: total foot length, ball length, dorsal arch height, forefoot width, midfoot width, heel width. The study provides an effective way for the clinician to explain the plantar surface through a combination of measurements and to derive a clinical diagnosis.

Brannock Device:

The Brannock Device (**Figure 21**), designed in 1927 is a foot-measuring device which has become a must in all retail footwear stores.Having been manual, due to the measuring
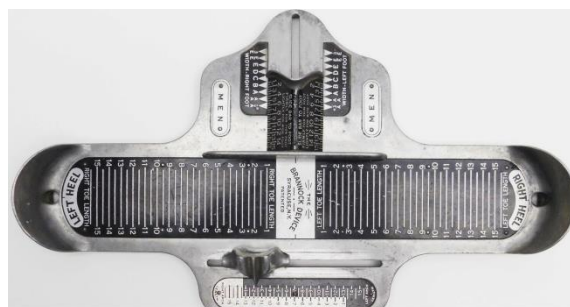
Figure 21 : Brannock foot measuring device [109].

accuracy, quality construction, and simple, yet completely functional, design is what has made genuine Brannock measuring devices the standard in the footwear industry [42].

Although this measurement instrument is considered among the most reliable in measuring the lengths of the foot given its perfect alignment with the Brannock axis, some authors still use the traditional measuring tape in their measurement campaign [51][52].

I.3.2.b.   3D DIGITAL MEASUREMENT

3D digital measurement is usually done with a 3D scanner that can be different depending on the desired measurement height. The company BFTS Human Technology offers two versions of INFOOT 3D scanner [53]. The first version (**Figure 22a**) is able to measure a height of 150mm, while the second version (**Figure 22b**) is 250mm. The interest of the second product could be in the area of the boot which requires a deeper knowledge of the upper part of the foot, or in the sector of orthosis. The 3D foot scanner use the optical laser scanning technology. INFOOT scans a foot form from the anatomical landmark points (**Figure 22c**), and measures automatically almost 20 measuring items (Red marker needed) as maximum.
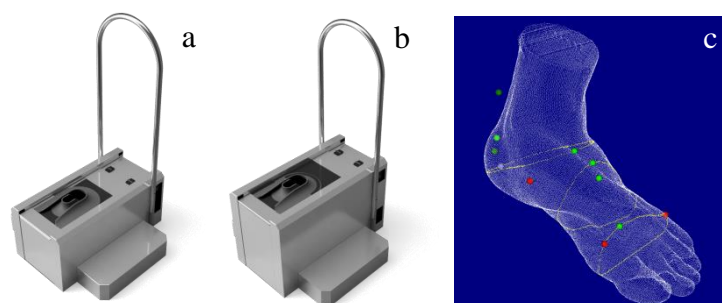
Figure 22 : 3D foot scanners, landmark points on the foot.

Witana et al. shows a great interest in using the 3D foot scanner. The authors have compared in their study the measurement results of a 3D scanner with manual foot measurements. Their work highlights important differences in measurement accuracy come from the measurement tools, the measuring protocol, the time to measure, skill level of the measurer [42]. Lee et al. have achieved similar results by also comparing with conventional foot measurement methods but in particular the digital caliper, ink footprint, and digital footprint [45]. The 3D scanner has been an indispensable tool for the evaluation of anthropometric parameters results obtained by 3D measurements and their statistical and mathematical processing in the works of Pantazi et al. [44]. The 3D foot scanner has also been used by Nácher et al. for its accuracy and rapidity in order to classify the feet of a population

of 316 female participants. This study presents the interest to improve the comfort of shoes by a model for predicting footwear fit on the basis of user data [54].

In the podiatry sector, other techniques are used to directly obtain the 3D form of the underside shape of the foot in order to create orthopedic insoles adapted to the patient. The box with double imprint for example, can be quoted [55] (**Figure 23a**) that allows, from footprint (**Figure 23b**), to realize the 3D shape of the two feet in plaster or resin (**Figure 23c**) and finally obtain the orthopedic insoles (**Figure 23d**). This manual technique is not direct and expensive because it requires consumable, expertise for molding and the creation of the insole. This process could be done numerically and more quickly in CAD, would be less expensive in the long term as it can be seen in chapter IV.
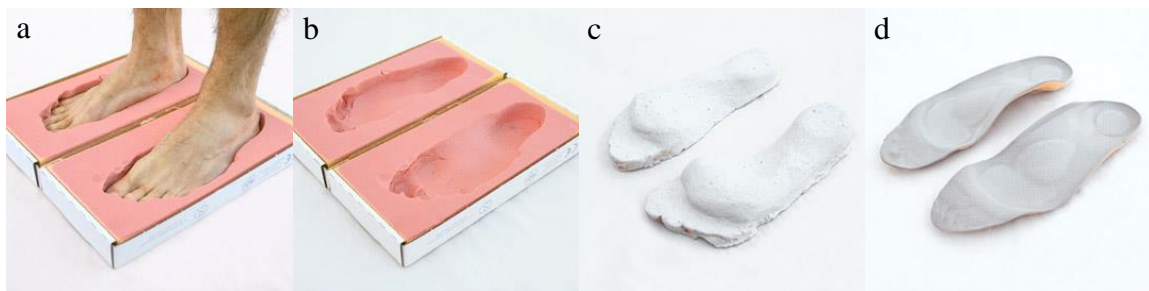
Figure 23 : Creating process of orthopedic insoles [55].

I.3.3. ANTHROPOMETRIC STUDIES AND ANALYSIS

This part is devoted to the analyse of anthropometric data for targeted population. Two directions are taken. The first one allows the comparison of the measures between them to give proportion rules. The second leads us to the classification of the feet to create a new sizing system for feet or analyzes the shape of the feet to extract morphotypes.

I.3.3.a. STATISTICAL ANALYSIS:

From childhood, the evolution of foot starts. The statistical analysis of Vrdoljak et al. on in children aged 2-7 years shows length and shape of the foot have changed with evolution, adapting to the upright posture of man and the change in the manner of weight-bearing [51]. The tarsus has increased by over 50% in length of the foot, and with the development of the transverse and longitudinal arches, a foot for walking and running developed, as opposed to climbing and grasping. The greatest changes in length and shape of the foot occur in the earliest years, where the foot must develop sufficiently in width to allow for balance while a child learns to walk [44].

In the works of Hasanzadeh et al., a complementary study on a population of school children aged 10 to 12 was conducted [52]. The authors note that the length of the foot of a child during growth reaches its ultimate dimensions more proportionally than any other element of the body. The foot of a girl 1 year old and that of a boy 18 months old approaches 50% of their final length at the end of growth because a wide base of the foot compensates for the weakness and lack of muscle coordination in a child. Foot length in growing children is standardized in individual countries and varies according to geographic position and ethnic differences. Foot length is taken as a fundamental measuring unit which allows for following the growth of the foot and can be used to compare other anthropometric measures which would be important for standardization of foot sizes in children

Commendably of anthropometry on kinetic abilities of speed, agility, balance and power have been studied in several domestic and international studies. For example, Koley et al. investigated the relationship between anthropometric characteristics and kinetic performance in elite volleyball players and concluded that there is a positive and significant relationship between height, weight and length of the lower limb and the fat percentage and vertical jump [56][52].

The feet statistical analysis results of Akambase et al. claims it will serve as a reference point for other studies regarding stature estimation in other ethnic groups in Cross River State and Nigeria at large [48]. These authors have studied the anthropometric parameters of the foot in relation to gender and racial differences. In the estimation of the stature, Rademene et al. show that foot breadth in the males and foot length in the females present the strongest association with stature and are the most reliable for estimation of stature in Efik males and females, respectively [57]. Nevertheless, its regression equations obtained from the study must be validated by forensic experts.

Others researchers have worked on stature estimation and dimensions of the foot of Nigerians. The dependability of predicting stature from the foot dimensions was established by Ogugua et al. [58] using three hundred (300 individuals: 170 males and 130 females) adult Nigerians of Igbo descent, aged between 18 and 30 years.

Iheanyi et al. have estimated stature from measurement of foot length using 262 healthy medical students of Imo State University, Owerri, aged between 18 and 28 years was also carried out [59]. In similar study of Mansur et al., the regression equations was derived which can be used in estimating stature from foot length for Nepalese individuals which consisted of 440 students of age group 17–25 years [60].

Three measurements have been particularly targeted in Turkey. Works of Ozaslan et al. have been to predict the stature in Turkish adults (224 males and 132 females) whose age ranged from 20 to 51 years according to the measured dimensions of hand and feet. [61].

Due to the limited number of studies on Iranians and the smaller number of dimensions, a study of Hajaghazadeh et al. aimed to measure the important dimensions (21 measurements) of the foot for both genders in northwestern Iran and also to compare the means of the corresponding measurements using available data from other published studies [43]. Significant differences were reported for foot morphology between Caucasian in North America and Japanese Korean males, Taiwanese and Japanese females, and French and Japanese males. The incidence of digital patterning also varied across nationalities. Therefore, due to various foot morphologies among populations, country specific data of the foot needs be made available to designers, study says.

In Romania, a lot of work has been realized to analyze the feet with different goals. Initial work was conducted on the methodology for obtaining the anthropometric data of human foot (21 measurements) using 3D scanning systems [62]. Sarghie et all used mathematical statistics tools to validate the results. So, from a population of 23 male subjects, authors have demonstrated that between left and right foot does not appear difference.

I.3.3.b.   CLUSTER ANALYSIS

In Romania, others works have been oriented on an elderly people populations. The goal of the works of Sarghie et al. was to develop and manufacture footwear according to the needs of this population [63]. To solve the comfort problem during the wearer of shoe, customized made footwear for the elderly female population was obvious. For that, 92 female subjects were measured and analyzed. The classification result give different groups in which the specific needs will lead to specific shoes. Works of Costea et al. used the plantar footprints to analyze the feet of an elderly people population [64]. 67 women, aged between 52-84 years old has been classified into 5 groups (subjects with Normal Foot, High Arched Foot, Flat Foot, Hallux-Valgus Foot and Hallux Varus Foot) according to the foot typology. The shape descriptor of the footprint used Chippaux-Simark Index and Hallux-Valgus Angles. In Taiwan, study has been realized by Lee et al. to obtain a new sizing system for feet from 12 foot dimensions (foot length, ball of foot length, outside ball of foot length, foot breadth, heel breadth, ball circumference, instep circumference, toe height, navicular height, instep height, toe 1 angle and toe 5 angle) [65][66]. Right foot scanning of 1835 male population

(aged from 18 to 60 years old) were used in the classification process. To classify subjects' foot shapes, authors used the principal component analysis (PCA) and K-means cluster analysis. The results are interresting because it allows to reduce the size numbers giving 6 foot clusters.

Classification have also be done for female [67]. To cluster foot shapes, 936 females' 3D foot has been scanned.

Similar works has been done in Spain by Bataller et al. [68]. The classification process is identical. 39 foot dimensions (foot and footprint) has been measured on 1100 people population. But, a group of 177 men of size 41 were selected for the study. The results give 3 clusters giving 3 specific shapes of foot.

I.4. PRESSURE ANALYSIS OF FEET

Static and dynamic analysis of feet pressure is widely used in the medical and sports sector. A biomechanical examination can be used to evaluate the functioning of the human body during walking or during a sport such as running. By measuring the feet pressure, the practitioner studies osteo-articular and muscular functioning under static and dynamic conditions. Numerous information can then be detected and useful to the diagnosis, i.e.: points of maximum and average pressure, trajectory of the center of mass, length and frequency of the steps, the asymmetry between the two feet, the time spent on each foot during a step, ... During a postural examination, the practitioner can detect a plantar misalignment, explain the back pain, understand the abnormal wear of shoes or even optimize the performance of athletes.

The focus therefore would be on the different measurement techniques that have been developed in recent years and identify the latest scientific work explaining the interest of pressure cards in the diagnosis of a given pathology.

I.4.1. MEASURING TECHNIQUES OF THE FOOT PRESSURE

A lot of works has been realized in how to measure foot pressure by more or less precise means. Previous work by Grieve et al. used ductile aluminum foil to record the footprints [69]. The goal was that the foot pressure compresses the foil in a sandwich betwen 5mm sheet of high-density foam and a rubber undermat whose upper surface embossed with a pyramidal lattice (3-54 mm repeat distance). This process was interesting at the time but then came other works involving sensor physics to take in account dynamic and static

measurements resulting in different design techniques depending on the application (medical or sport). The most commonly used sensors in the deformable structure devices are: strain gauge, conductive /resistive, capacitive, piezoelectrics. The article by Rosenbaum et al. presents an complete inventory of the different devices existants to measure the plantar pressure distribution [70]. The technical background and clinical applications are very detailed in order to help us to choose the measurement device the more adapted at the need of the application. The authors highlight the major directions of development that have been taken, i.e.: pressure distribution platform systems, in-shoe systems, matrix devices, sole systems with discrete sensors.

Among the first interesting works, the method of Duckworth et al. is interesting [71]. The device developed in this study captures the image of the pressure of both feet resting on ice/transparent window (**Figure 24**). A deformable thin sheet of opaque reflective plastic is located between the feet and the ice to improve the zoned measurement of foot pressure and to obtain a more significant distribution of the contact zone by reflection. An image processing is then used to calculate the distribution of the foot pressure according to the gray level of the image and to visualize its color map thanks to a color interface. This technique is interesting because the distribution obtained gives zones of distribution of the pressure easy to exploit by the practitioner in clinical application.
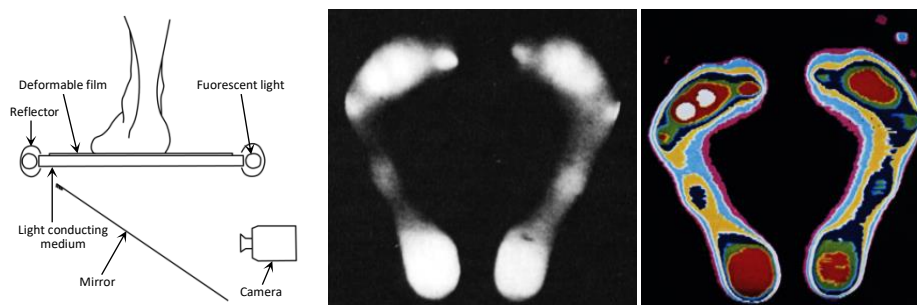
Figure 24 : Basic foot pressure measurement device with pressure results.

In India, works of Syed et al. have established normative data on pressure distribution under the feet and create an association between arch type to that of the plantar pressures (**Figure 25**) [72]. Plantar pressure measurements were quantitatively recorded using a baropodometric platform (i-Step). The new version of i STEP LUNA use 3.744 barometric sensors to measures the pressure exerted by the foot every 0.25cm^2 [73].

In Romania, the Mihai's team has realized a lot of works with the plantar footprint platform developed by Rsscan (**Figure 26a**). Different orientations were taken according to the target population. Some works have led to defining a good fit of the shoe for the elderly people [64]
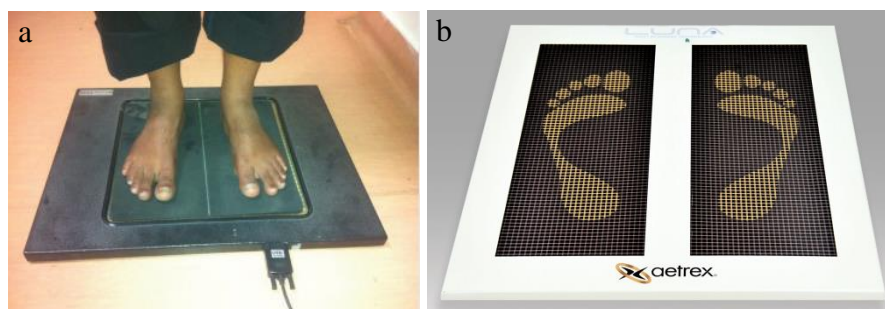
Figure 25 : Digital pressure scanner with barometric sensors [73].

(**Figure 26b.c**). Within the framework of the SIMSANO project, scientist work has been realized in the production of therapeutic footwear for those with locomotors disabilities inflicted by diabetes and arthritis [74]. From gait analysis and plantar pressures measurements, data of the 3D foot scanning and interactive 3D modelling of the new shoe-last, they have developped a complete solution for Virtual Prototyping (VP) of a shoe-last for therapeutic footwear.

Figure 26 : Plantar footprint platform developed by RSscan.

In the context of work on the integration of sensors in insoles, the research work of Almusallam et al. is mentionable [75]. Authors have developed screen-printed piezoelectric composites that can be printed on flexible substrates like insole (**Figure 27a**).
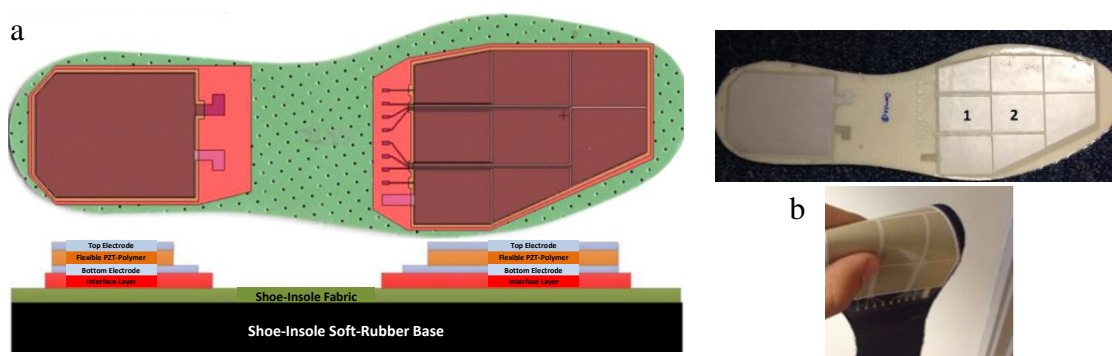
Figure 27 : Screen-printed piezoelectric composites in insole [75].

The proposed materials are mixtures of PZT ceramic powder mixed with polymer materials. The sensor is based on piezoelectric property d33. A screen-printed piezoelectric shoe-insoles has been developed as a self-powered force mapping sensor. Results show that the product is very flexible and interesting because each separate element can deliver a no-load voltage of 2V (**Figure 27b**). Mateu et al. used also piezoelectric film to insert in insole [76]. They study the bending properties of this beam-type shoe insert to optimize the product in term of walking confort and measurement quality.

Works of Zhao et al. are quite impressive because they have used piezoelectric properties for two types of applications. The most recent works is in energy recovery. The goal of their study is to harvest mechanical energy from human motion during walking [42]. Their device is composed of multilayer PVDF film which can measure the dynamic foot pressure distribution (**Figure 28a**). The energy harvester provides an average output power of 1 mW during a walk (frequency 1 Hz). Their devices has advantages of a thin geometrical shape, high performance and an excellent durability (**Figure 28b**). The other works has been directed to plantar pressure measurement [77]. The device developped based on 3-D forces piezoelectric sensor is of an insole with eight measure points, a wireless data transmission and embedded computer. Each measurement point located according to human anatomy characteristic have three sensors assembled in 3D directions.
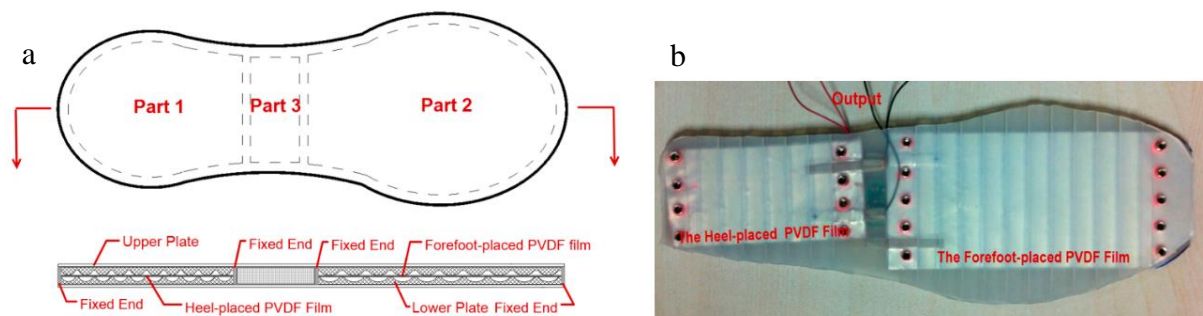
Figure 28 : Schematic and real prototype of flexible energy harvester.

I.4.2. MEDICAL ANALYSIS

The goal of this part is to classify according to the pathology of the foot the different scientific works which use the plantar pressure to diagnic according to its distribution a given disease.

I.4.2.a. OBESITY & DIABETIC

Birtane et al. evaluated the effect of different obesity categories on the plantar pressure values [78]. Their study has been realized on the feet (left and rigth feet) of 50 participants classify in two groups as non-obese and class 1 obese according to their body mass index values. Pressure zones which has been investigated are: peak phalanx pressure, medial forefoot peak pressure, middle forefoot peak pressure, lateral forefoot peak pressure, middle foot peak pressure, rearfoot peak pressure, plantar contact area. Static pedobarographic parameter show that the values of forefoot peak pressure, total plantar force and total contact area in the feet of class 1 obese subjects are higher than non obese. Dynamic pedobarographic parameter show only middle foot peak pressure was found to be higher in class 1 obese subjects. But this study has to be completed.

Veal et al. quantified the weight increase [79]. For that, the authors verified if the increase in weight had an impact on the mean peak foot pressures by controlling foot function, deformity, and structure. Novel's in-shoe dynamic pressure measuring system (Pedar system) has been used to measure peak plantar foot pressures. Two types of shoes and two additional weight has given three conditions of the test. the result shows that a significant increase in mean peak plantar foot pressures under the metatarsal heads, heel, and midfoot during the incremental increase of weight.

In obese or overweight people, the risk of becoming diabetic is very important because diabetes is the consequence of being overweight. Prabhu et al. analyzed the effects of subject weight, walking speed and duration of high pressures in all areas of the insole on diabetic patient subjects belonging to different levels of plantar sensation loss which is an important factor in this disease [80]. Semmes-Weinstein nylon monofilaments has been used to quantify the different levels of sensation loss in diabetic neuropathy. The foot pressure parameters which has been used are the normalized peak pressure, the pressure contact ratio, and their gradients. An optical pedobarograph allowed to obtain the walking foot pressure patterns and measure the ten specified areas. A statistical study led to find correlations between the quantified levels of sensation loss and foot pressure parameters in the areas where there is a high incidence of plantar ulcers [79]. The study confirms that specially designed footwear could prevent plantar ulcer in reducing foot pressure parameters of diabetic neuropathic feet. The works of Rahman et al. analyzed the plantar pressure essentially in diabetic type 2 subjects with and without neuropathy [81].

In this work of Teh et al. [82], the pressure distribution under the feet in obese and non-obese subjects has been also finely studied and complete the Prabhu'works. Authors conclude that the increase in the peak pressure is due to the shift of the center of the body forward because of the excessive adipose tissue causing excessive forefoot loading. An increase in the middle foot contact area is due to collapse of the longitudinal arch caused by overweight.

A very interesting study is that of Gefen et al. which have developed foot numerical model to calculate the stress distribution in the plantar neuropathic tissue [83]. The plantar soft tissue under the medial metatarsals was analyzed for simulations of diabetic versus normal conditions. The finite element method is used to solve for internal stresses under static ankle joint reaction and triceps surae muscle forces through five anatomic planar cross-sections in the directions of the foot ray. Tissues were assumed to be homogenous, isotropic and elastic materials, with nonlinear stress-strain relations. This numerical model is very interesting because it can simulate de numerous test conditions allowing to understand the process of injury in diabetic feet.

I.4.2.b. PEAK PRESSURE

As part of the work of Cavanagh et al., an analyze of plantar pressure distributions is realized with normal people during barefoot standing [84]. Peak pressures have been detected more strong under the heel than the forefoot. The forefoot peak pressure were under the second or third metatarsal heads. This study can help the clinician in evaluating plantar pressure findings to diagnostic specific problem.

From a larger population sample of healthy individuals, Pomari et al. finds similar results with those of Cavanagh et al. Their study is carried out on a population of 238 female and 193 male individuals aged between 2 and 69 years. Significant differences are detected according to the age of the people given three groups: A1 (2-6 years), A2 (7-10 years), and A3 (11-69 years). Peak pressures have also been detected more strong under the heel than the forefoot but differently in the groups.

A clinical study was conducted by Tenten et al. in the goal to improve foot orthoses in patients with rheumatoid arthritis by using the in-shoe plantar pressure measurements [85]. Specific adaptation protocol for patients with rheumatoid arthritis has been developed. This protocol takes into account of the custom made foot orthoses by the podiatrist, his evaluations of the in-shoe plantar pressure measurements for the forty-five rheumatoid arthritis patients

with foot problems. The evaluation was to define the peak pressures plantar on the foot nine regions of the patient from the feet plantar pressure distribution. Traditional care methods have been compared with this method using plantar pressure measurements, a series of tests have shown a marked improvement with this new method of care.

I.4.2.c. FOREFOOT PAIN CLASSIFICATION

Estimate pain in relationship with the foot plantar pressures was addressed by Keijsers et al..

In first, authors have developed a new method to normalize foot plantar pressures [86] for future classification. Previous works use 6–11 areas are used to analyze average and maximum plantar pressure under the foot in order to compare subjects. These techniques can lead to a loss of important information about the plantar pressure distribution pattern. Keijsers et al. propose a method to normalize the plantar pressure pattern depending on the foot size, foot progression angle, and total plantar pressure. For that, the plantar pressure pattern has been aligned over the foot progression angle and adjusted for foot size.

After, the authors have worked with 297 subjects without apparent foot deformities in order to classify of forefoot pain on plantar pressure measurement [87]. In this population, 50% had forefoot pain. Following a PCA, neural networks made it possible to classify subjects with and without forefoot pain from the plantar pressure measurements and a questionnaire defining the level of pain and clinical evaluation. Results show the performance of forefoot pain classification by neural networks is good quality and that the forefoot pain is more connected with the distribution of the pressure under the foot.

I.5. MODELLING OF THE FOOT

The interest of a 3D foot model is that it is parameterized according to the measurement data of customer or patient to create shoes adapted to the morphology. However, this 3D model has imperatively to be connected to a 3D deformable shoe-last according to this 3D foot model otherwise it would be useless in the creating shoe process. Few studies have really focused on 3D modeling of feet in this type of context.The approach of Luximon et al. is very interesting [88]. Their 3D prediction model is parameterized with the most relevant measurement data of the customer: foot length, foot width, foot height, foot curvature. In their process, a 3D prediction model is used to create the customer's foot according to their measurements. In first, authors measure a population of 65 Hong Kong

Chinese men. 40 Chinese men are chosen to defining a 3D standard foot considered like morphotype of the population. This shape is used to create the foot shape prediction model. The others 25 Chinese men were used for the validation of the 3D prediction model. During the feet scan process, 11 points marked on the foot ahs been chosen (**Figure 29a**). 7 points (Points 1 to 7) on the metatarsal- phalangeal joint was chosen to model Metatarsal-Phalangeal curve using polynomial regression. The flex line of a shoe should match this curve. 2 points on the dorsal surface of the foot (Points 8 and 9) and 2 points on the plantar side of the foot (Points 10 and 11) were chosen so that each scanned foot could be aligned during processing using polynomial regression. Metatarsal-Phalangeal curve is a strategic curve because it adjust the prediction model with measurements of foot length, foot width, foot curvature of customer's feet (**Figure 29b**). In plus, this curve is connected also with the cross-sectional curves perpendicular to the heel center line of the prediction model which are ajusted with foot width and foot height of customer's feet (**Figure 29c**).
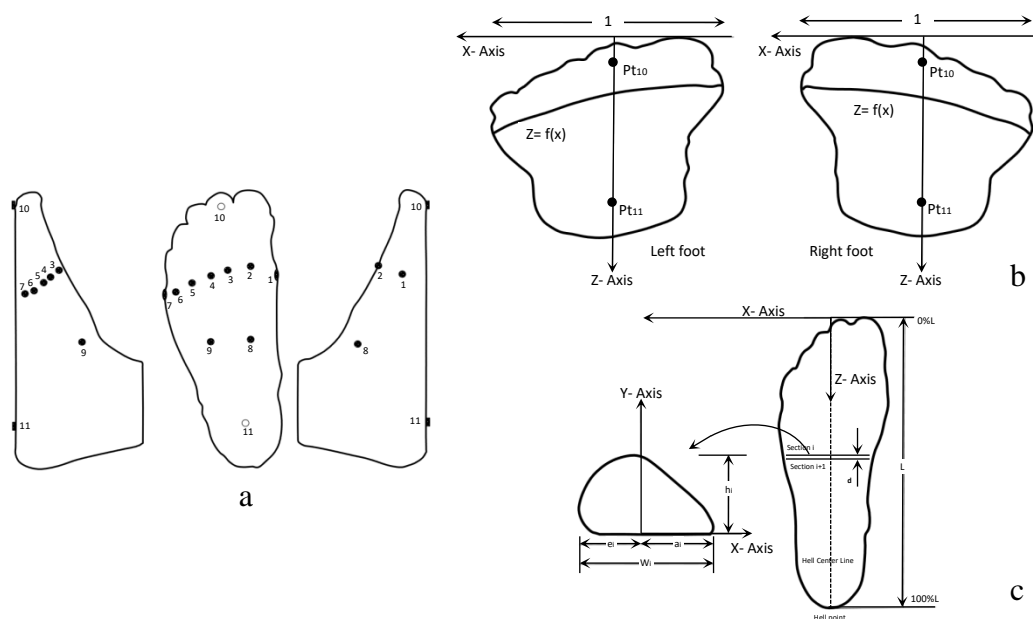
Figure 29 : 3D modelization of feet by Luximon.

I.6. MODELING OF THE SHOE-LAST

The first investigation to understand mechanisms of ulcer formation has been done by Chen et al. [1]. They analyze the relationship between shoe last design, foot measurement and shoe fitting for orthopedic footwear. Shortly after came the work of Bao et al. [89]. Authors describe ideal production line to create custom-made shoes or also commercial shoes. The process start by the digitize the foot with two CCD cameras with 512x512 digital images, the

creation the geometry of a shoe-last from the foot model and finish by the generation the tool cutter paths for a numerical cutting machine. Different options allow deforming the foot to get the shape according to the requirements of the operator and aesthetic and functional needs of the patient. This process is critical because it is very subjective, but it represents the departure of many CAD systems in this area to replace manual work of the expert.

Some works deal with problems related to custom-ordered shoe-lasts. These custom-tailored products have to meet the customer's different tastes or requirements various are size and shapes. But a production process not organized can take longer. Hwang et al. [90] have solved the problem by using a database of many template shoe-lasts to detect the most similar template shoe-last. For that, a classification is realized for the creation of different clusters. An evaluation criterion has allowed determining the similarity of the shapes of the template shoe-lasts depending in shape, ignoring the size of them. After, their process creates a template shoe-last from each group with the smallest size. The custom-ordered shoe-last is machined from the shape of this template. Like previous work, the generation the tool cutter paths for a numerical cutting machine is generated automatically.

Zhang et al. present a very interesting state of the art in the framework of mass-customized shoe design system, of shoe style customization system, of customized shoe-last design system. All these systems are based on commercial CAD software [91]. With their, consumers can directly be involved in footwear design lead to the more efficient production of shoe-lasts adjusted.

Shi et al. proposes a CAD system for designing the customized shoe last based [92]. They take into account the requirements of the customers on the shoe style and their foot features. Eighteen foot features are extracted and used in the deformation the base shoe last of the customer preferred style to the customized shoe last. This process gives a better fit to the customer's foot. The evaluation of the fit is evaluated through a color-coded map representing the gap between the customer's foot and the customized shoe last.

I.7. EASE AND FIT

Works developed by Nácher et al. are oriented in the same analysis spirit of Hwang. These authors have worked predicting footwear fit from user data, anthropometric measures, and fit preferences [54]. To take into account the style of the commercially shoes, classification has been realized to represent a typology of footwear. Eight clusters have been found integrating the design elements which had bearing on fit: shoe-last, toe cup, upper

flexibility, fastener adjustments, and sole. User data were: anthropometric characteristics of the foot and user preferences. Eighteen anthropometric measures are calculated from the 3D mesh of the foot. For user preferences, two questionnaires were used to analyze the fit shoe, the first one by the users according to a three-level scale, the second one by expert according to a three-level scale. **Figure 30a** show the four areas which has been defined to analyze the fit of the shoe. Others questionnaires were used to analyze the perception of pain in fifteen areas (**Figure 30b**) according to a four-level scale, overall comfort was according to a seven-level scale. The statistical fit models developed from user data and data of the classification has given an accuracy rate of approximately 65.7%. Results have shown that final shoe comfort depends not only on foot dimension but also on fit preferences.
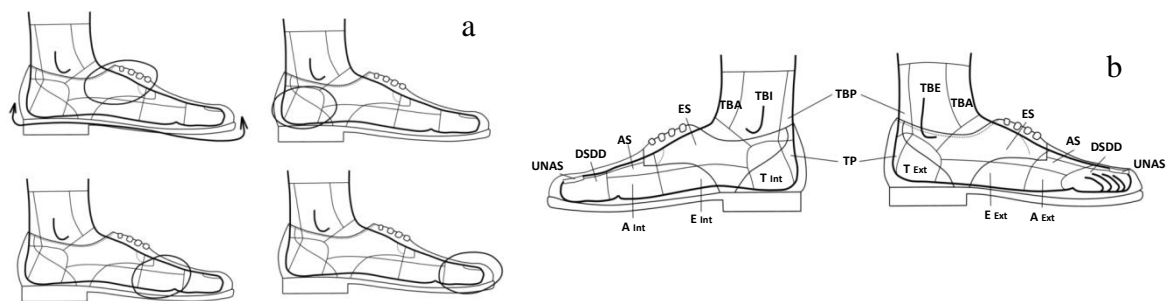
Figure 30 : Shoe areas during fit tests & evaluation of discomfort and pain.

The work of Chen's thesis on the investigation fundamental mechanisms of ulcer formation by measurement of plantar pressures in diabetic neuropathic patients, are fundamental [1]. This authors is alone who investigate into shoe last design in relation to foot measurement and shoe fitting for orthopedic footwear. However, it is important not to discuss about it further in this chapter because it has been a priority reference of chapter V.

I.8. CONCLUSION

This chapter presents the main diseases and pathologies of the foot. At the end of this pathological assessment, the main research interest is to understand the foot by its morphological analysis and an anthropometric study leading to a review of existing measures.

The ultimate objectives of these measures are very diverse. The bibliography shows that some measuring devices help in the diagnosis of the practice (chiropodist), whether it is in the footprint, the pressure of the foot, its morphological or cutaneous appearance. But these 2D or 3D measurements also contribute to the treatment of foot diseases. In many cases, it is necessary to design shoes adapted to the morphology of the feet to alleviate the suffering of

the patient, to curb or eradicate the disease. The sole design adapted to the morphology of the footprint is also increasingly recommended to distribute the plantar pressure in the right place.

The literature review clearly shows the need to define anthropometric reports from measurement campaigns on the population. This knowledge will then help to develop a digital foot model leading to shoe-last models. These are essential to a shoe design adapted to the patient or client in a context of improved ready-to-wear. The next chapter, therefore, represents the departure of the knowledge of the foot necessary for this custom design process.

CHAPTER II: **ANTHROPOMETRIC ANALYSIS AND FOOT MEASUREMENT**

II.1. INTRODUCTION

The previous chapter shows that the foot measurements can be done manually or automatically depending on the measurement tools used. Manual measurement generally leads to measurement errors depending on the operator and their fatigue if it is performed on many people. To avoid this type of problem, the industry has developed different types of 3D foot scanner. But the measurement protocol and the exploitation of the results of these new foot measurement tools can affect the precision of the measurements. This chapter is devoted to the implementation of our own measurement method based on the 3D raw data of the scanner. These measurements will be compared with those obtained directly by the software sold by the manufacturer of the scanner that the one has been chosen. An anthropometric analysis is necessary because it represents the central core of the measurement process.

II.2. ANTHROPOMETRIC ANALYSIS OF FOOT

II.2.1. ANTHROPOMETRIC POINTS

The measurements of a foot depend essentially on the anthropometric points defined in precise places of its skeleton. The manual foot measurement instrument, which is used and validated scientifically, is a device that was invented by Brannock. The positioning of the foot in this instrument makes it possible to define a reference axis for the measurements: Brannock axis. As a general rule, for a foot that does not have a deformation problem (typical deformation: indicate diseases), the reference axis is a virtual line between pternion to tip of second toe (A). Since there may be slight differences between measurements made by hand using a tape measure, Brannock's instrument, and a 3D scanner, it seems important to recall first of all what the anthropometric points are necessary to measure a foot (**Figure 31**) and how should these measures be taken or interpreted in order to find the best compromise between these different methods. 19 anthropometric points are recognized today:

1) Pternion :
2) Metatarsal tibiale : Most medially prominent point on the 1st metatarsal bone
3) Medial malleolus : Most medial point of medial malleolus
4) Lateral malleolus : Most lateral point of lateral malleolus
5_n) Toe n^{th} : n^{th} toe tip

43

6) Instep: Top of instep point

7) Metatarsal fibulare : Most laterally prominent point on the 5th metatarsal bone

8) Highest point of 1st metatarsal : Top of ball girth point

9) Sphyrion :

10) Sphyrion fibulare :

11) Landing point : Back heel point

12) Junction point :

13 & 13') Calcaneum points : Most medially and laterally prominent points on the calcaneum bone

14) Navicular :

15) 5th metatarsal : Tuberosity of 5th metatarsal
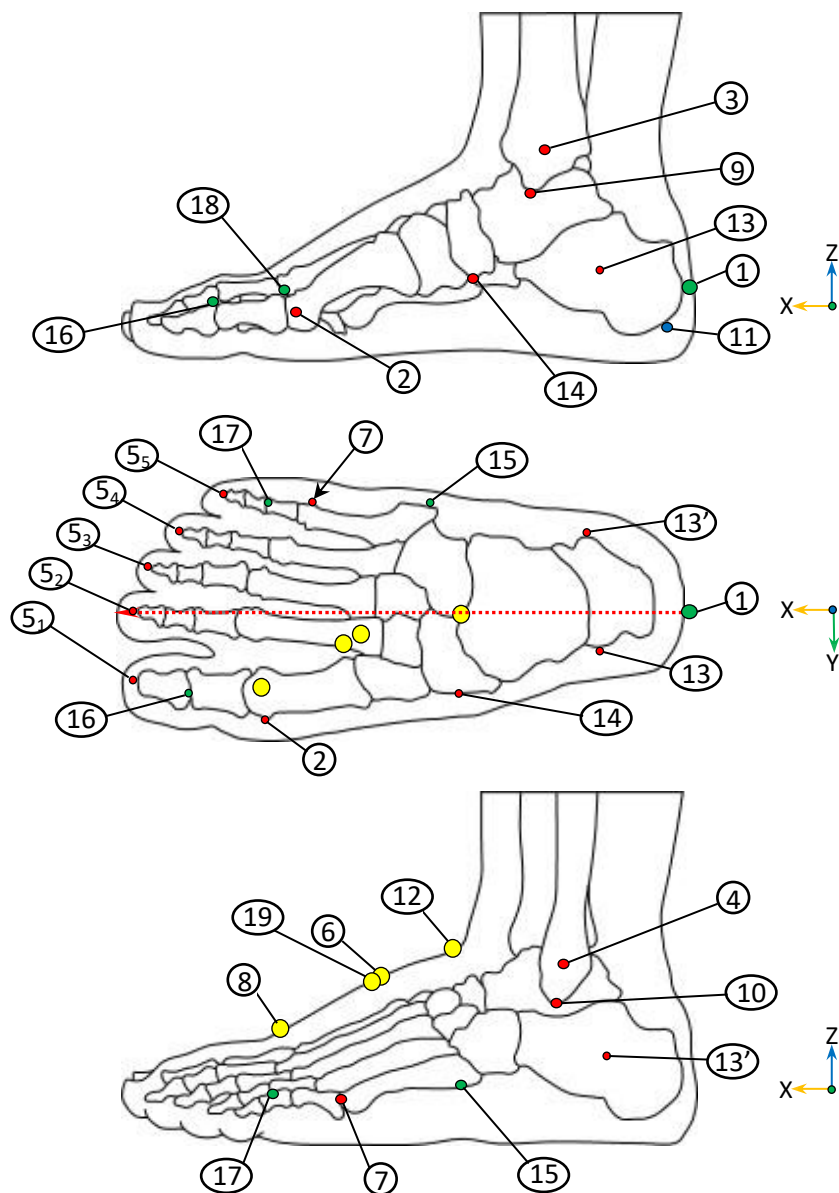
Figure 31 : Anatomical bones, anthropometric points.

16) Toe 1st joint : Highest point of Toe 1st joint

17) Toe 5st joint : Highest point of Toe 5st joint

18) 1st metatarsal : Highest point of 1st metatarsal head

19) Mid-foot highest point : Highest point of the Vertical girth at 50% foot length from the pternion

Figure 31 allows locating the position of these points relative to the skeleton of the foot, these joints. Of course, in practice, these points will be positioned with a slight shift caused by the muscular surplus that surrounds the bone structure.

II.2.2. FOOT MEASUREMENTS

Foot measurements are generally classified into 4 categories (Lengths, Heights, Widths, and Girths). A fifth category (Angles) required for the design of footwear products (sole, shoe) is extracted from the previous measurements:

Lengths: The whole distances are measured along the Brannock axis (X-direction)

L1 - Foot length: distance from point 1 to the tip of the longest toe.

L2 - Arch length: distance from point 1 to point 2.

L3 - Heel to medial malleolus: length from point 1 to point 3

L4 - Heel to lateral malleolus: length from point 1 to point 4

L5 - Heel to fifth toe: distance from point 1 to point 5.

L6 - Heel to Sphyrion: distance from point 1 to point 9.

L7 - Heel to Sphyrion fibulare: distance from point 1 to point 10.

Heights: The whole distances are measured in the vertical direction (Z-direction)

H1 - Medial malleolus height: distance from the floor to point 3.

H2 - Lateral malleolus height: distance from the floor to point 4.

H3 - Height of instep: distance from the floor to point 6.

H4 - Sphyrion height: distance from the floor to point 9.

H5 - Sphyrion fibulare height: distance from the floor to point 10.

H6 - Mid-foot Height: Maximum height measured with a line at 50% of foot length from the point 1

Widths: The whole distances are measured in the direction perpendicular to the Brannock axis (Y-direction). There may errors with this type of measurement because in manual mode with a cephalometer, or with some 3D scanners, these distances may be the shortest distance between the measuring points.

W1 - Foot width: distance from point 2 to point 7

W2 - Bimalleolar width: distance from the point 3 to point 4

W3 - Mid-foot width: Maximum breadth measured with a line at 50% of foot length from the point 1.

W4 – Heel width: distance from point 13 to point 13'

Girths: This type of measurement can represent the contour drawn on the shape (ex: scanner or CAD) or an equivalent contour representative of a stretched tape measure.

G1 - Ball girth: Girth of foot passing through point 2, point 8 and point 7.

G2 - Instep girth: Smallest girth passing through point 6.

G3 - Long heel girth: Girth of foot passing through point 6 and point 11.

G4 - Short heel girth: Minimum girth passing through point 12 and point 11.

G5 - Ankle girth: Horizontal girth passing through point 12.

G6 – 50% foot length girth: Vertical girth at 50% foot length from the point 1.

Angles: Angle as a function of the side lines of the foot (plane B and C later).

A1 - Toe 1st angle: Angle with the plan B.

A2 - Toe 5th angle: Angle with the plan C.

II.3.   MEASUREMENT PROTOCOL FOR THE FOOT SCAN

A first measurement campaign was carried out to start developing a sufficient database to validate our 3D graphical process. The number of people who were scanned is 100. No distinction was made between the feet of women and men. At this stage of the study, the morphology of the feet does not depend on sex. The distinction will be made later in the creation of footwear according to the population targets envisaged by the industry sector (foot industry).

The measuring device used to scan the different feet to create database of this research was 'INFOOT USB Scanning system, IFU-S-01'. A measurement protocol is imposed by the designer. In a first phase, eight patches must be glued on the foot of the person to be scanned

Figure 32 : Landmarks for the scan process.

so that the software can size the overall volume of the foot (**Figure 32**).

A tactile analysis of the bones of the foot is carried out in order to better detect the following anthropometric points: metatarsal fibulare 7, sphyrion fibulare 10, lateral malleolus 4, instep 6, metatarsal tibiale 2, navicular 14, sphyrion 9, and medial malleolus 3 (Figure2).

The five red stickers localize the points of reference for the calculation of the different anthropometric points and the positioning of the morphological contours. Anthropometric reports on which the user can intervene contribute to the automatic calculation process and its calibration if need be. **Figure 33** shows the result obtained on the morphology that to be tested.
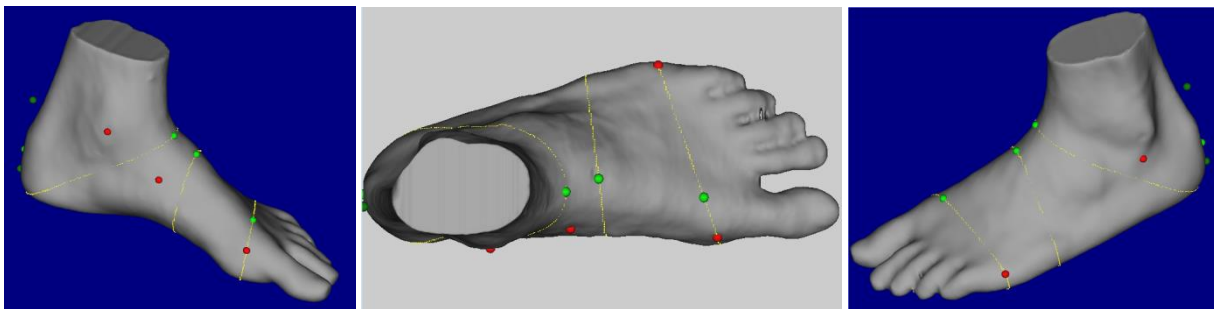
Figure 33 : Anthropometric points detection and morphological curves results on real foot.

Figure 34 shows the results of measurements (lengths, widths, heights, angles and girth) taken under the normal conditions of use of the scanner i.e. the feet must be positioned between the two green lines.

	Right	Left
Foot length	276,9	280,6
Ball girth circumference	270,1	278,7
Foot breadth	113,2	115
Instep circumference	267,2	282,7
Heel breadth	68,4	67,2
Instep length	203,5	203,4
Fibular instep length	181,6	175,7
Height of top of ball girth	44,1	47,6
Height of instep	75,8	75,9
Toe 1st angle (°)	-3,3	-8,4
Toe 5th angle	10,6	4,9
Height of navicular	57,7	38,6
Height of sphyrion fiburale	54,7	78,2
Height of sphyrion	88,2	67,8

Figure 34 : Scan and measurements of feet.

II.4.   3D GRAPHICAL PROCESS

This part is devoted to the implementation of a new method of foot anthropometry. It is a very precise method that is applicable, or even adaptable, to each foot because it is semi-automatic, i.e. commendable with a set of parameter specific to the morphology of the patient or client. Each step of the process must be followed with rigor given the anthropometric links integrated into the process.

II.4.1. OUTLINE ENCOMPASSING THE FOOTPRINT

The first step of the 3D graphical process is to wedge the foot in a trapezoid composed of six planes to define the geometry of the optimal outline encompassing the footprint. For this, two techniques are used whose goal is to find the contact area or areas between a plane perpendicular to the ground and the 3D shape of the foot.

As the method is to follow the manual process during the measurement of the foot, at first the heel on a vertical plane A was wedged to define the zero of the coordinate system along the X axis, which allowed to detect a contact zone which gave an approximation of the position of point 1, called 1' (**Figure 31** et **Figure 35a**). Then it was translated and turned the foot so that it could stick on a vertical "plane B" to the "plane A", which lead to two contact zones. In this method, the procedure was reversed since the foot was fixed and spotted in an absolute coordinate system "R0(O,x,y)" (**Figure 35a**).It was required to look for the "plane-B" before the "plane-A". A movable coordinate system "R1(O1,x,y)" was therefore designed which was related to "R0 (R zero)" and controlled by two translations along the X-axis and Y-axis and a rotation along the Z-axis. Two lines aligned on the X-axis and Y-axis of "coordinate-R1" was supporting the two planes to be able to translate and rotate to enable
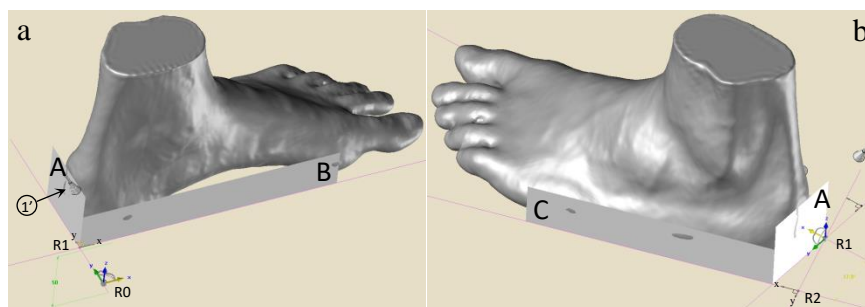
Figure 35 : Wedging the heel by two plans, detection of medial and lateral contact points. them for the visualization of the areas by their associated planes.

In the same way, "plane-C" was positioned by a movable coordinate system "R2(O2,x,y)" (**Figure 35b**). This coordinate system was designed with relation to

"coordinate-R1" and controlled by a translation along the Y-axis and a rotation along the Z-axis. The line aligned on the X-axis of "coordinate-R2" supporting the plane will translate and rotate so that can the two zones could be visualized by its associated plane.

The plane-D made it possible to search for the angle of inclination of the first finger is positioned by a movable coordinate system "R3(O3,x,y)" whose origin "O3" slide by translation on the line representing the Y-axis of "coordinate-R1" (**Figure 36a**). The coordinate system "R3" pivots about its Z-axis to manage the angle of inclination of its X-axis on which was aligned a line supporting the detection plane of the contact zone with the foot.

The plane-E observed for the angle of inclination of the fifth finger (**Figure 36b**). It is positioned by a movable coordinate system "R4(O4,x,y)" whose origin "O4" slide by translation on the line representing the Y-axis of coordinate-R1. The coordinate system R4 pivoted around its Z-axis to manage the angle of inclination of its X-axis on which was
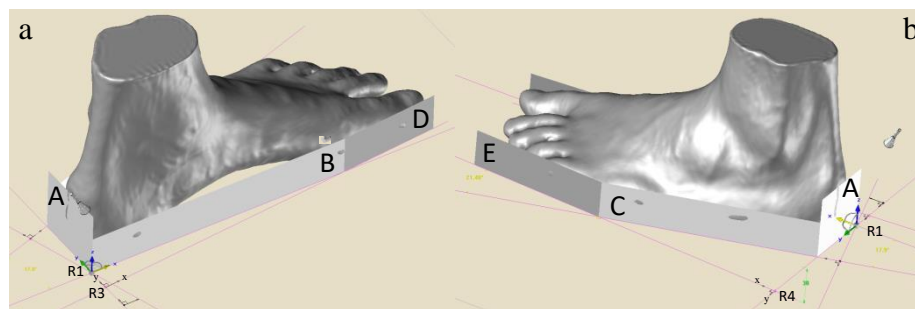
Figure 36 : Detection of medial and lateral contact points of toes.

aligned a straight line supporting the detection plane.

At this point in the process, the location of the Brannock axis was required. In the first phase, a median axis between the two plane-B and plane-C was created to detect the point of intersection B_1 between this axis and the line associated with the plane-A (**Figure 37a**). This point was the starting point B_1 of the Brannock axis because it represented the projection on the ground of the anthropometric point 1 (re-adjustment of point 1').

The other edge was at the end of the second toe (**Figure 37b**). The detection of this edge went through the creation of a movable coordinate system "R5(O5,x,y)" whose origin "O5" slide by translation on the line representing the X-axis of coordinate-R1. The reference R5 rotated around its Z-axis to manage the angle of inclination of its Y-axis on which was
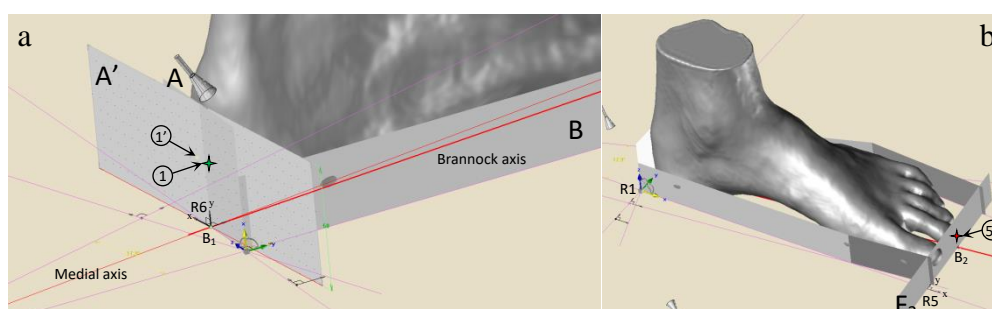
Figure 37 : Detection of contact points 1, 5_2, creation of Brannock axis.

aligned a line supporting the detection plane F_2. This angle was required to be adjusted so that plane-F_2 was perpendicular to the Brannock axis. Once the "endpoint-5_2" was found, the projection was on the right representing the Y-axis to this point to create the second "endpoint-B_2" of the Brannock axis. This axis could then be plotted from "point-B_1". Consequently, a new coordinate system "R6(O,x,y)" was created on point-B_1 which is perpendicular to the Brannock axis (**Figure 37a**). A detection plane-A' was created from the line representative of the X-axis of "R6" in order to readjust the final position of "point-1". The condition was that "point-1" must have been at the same height as was in the area detected by plane-A'.

At this stage, the finalization of the outline encompassing the footprint has been done by creating the last plane-F_1 that detected the "point-5_1" of the first finger (**Figure 38a**). This plane was aligned on the line representing the Y-axis of a coordinate system "R7(O7,x,y)" whose origin "O7" translated on the Brannock axis. Among other things, the Y-axis of this coordinate system was perpendicular to the Brannock axis. **Figure 38b** shows the contour that was detected on which location of remaining anthropometric points relied.
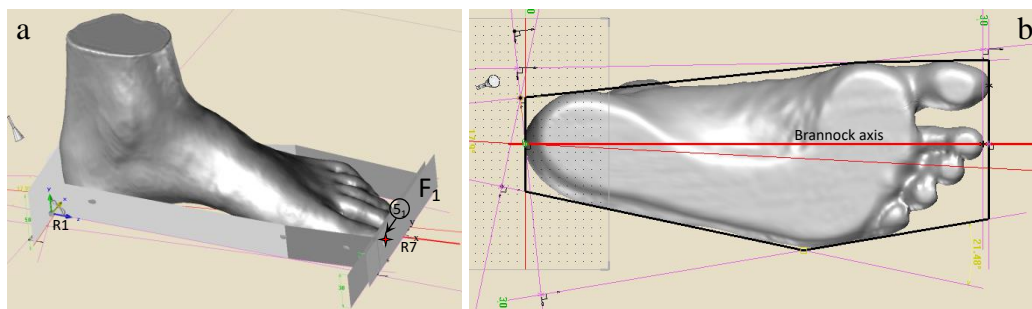
Figure 38 : Detection of contact point-5_1, outline encompassing the footprint.

II.4.2. ANTHROPOMETRIC POINTS DETECTION AND MEASUREMENT

II.4.2.a. TOES TIP (5_1, 5_2, 5_3, 5_4 AND 5_5)

In the same analytical way as the first toe, the different coordinate systems "R8(O8,x,y)", "R9(O9,x,y)" and "R10(O10,x,y)" were placed along the axis of Brannock to create the different lines representing the Y-axis of each coordinate system (**Figure 39a**). Then, detection planes: F_3, F_4 and F_5 were created on each line (**Figure 39b**). The three end points: 5_3, 5_4, 5_5 of the last fingers, detected by these planes, were at that time projected onto the Brannock axis. The length of each toe with respect to point-B_1 (projected from 1) can be measured directly on X-axis of the coordinate systems of: 5_1, 5_2, 5_3, 5_4 and 5_5.
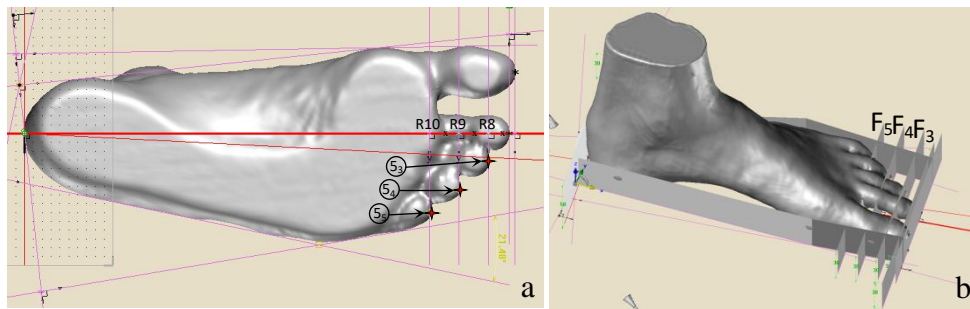
Figure 39 : Detection of contact points $5_3, 5_4, 5_5$.

II.4.2.b. JUNCTION POINT (12) AND LANDING POINT (11)

The junction point was defined from two inclined planes, first plane-G in the oblique direction of the top of the foot (in side view) and second plane-H in the direction of the contact zone of the lower part of the tibia (in side view) (**Figure 40a**). These two planes, perpendicular to the plane-B, were created from two lines, one oriented along the X-axis of coordinate system "R11(O11,x,y)", the other oriented along the Y-axis of coordinate system "R12(O12,x,y)" (**Figure 40c**). These coordinate systems rotated around the Y-axis of coordinate-R1 in the XY-plane of coordinate-R1 in order to respect the perpendicularity. The orientation of these coordinate systems and their relative position in respect to the reference R1 made it possible to manage the zones of tangency of the planes in contact with the foot.

Moreover, a coordinate system "R13(O13,x,y)" was created at the intersection of the two lines defining the contact planes: G and H. This coordinate system had a Y-axis aligned with the X-axis of "R11". A cylinder was then created and centered at "O13", its main axis being aligned on the Z-axis of "R13" (**Figure 40b**). The Z-axis of "R13" was also at the intersection of the two planes: G and H. By modifying the diameter of this cylinder, contact zone of the heel representing the landing point-11 were identified.
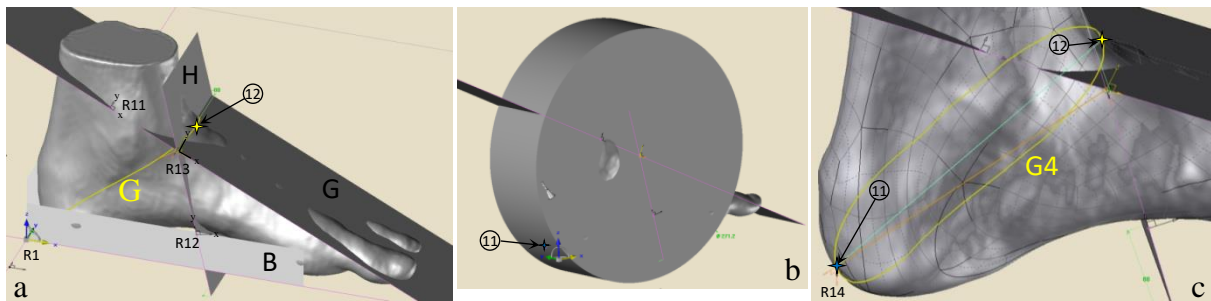
Figure 40 : Detection of contact points 11 and 12.

It was from a straight line connecting the origin point O13 of R13 and the landing point-11 that was positioned and directed on the point-11 a cutting coordinate system

"R14(O14,x,y)" (**Figure 40c**). The yellow curve resulted from the section of the foot by the cutting plane of "R14" represented the short heel girth "G4". The junction point-12 was at the extremum of this curve in a vertical direction upwards.

II.4.2.c.   INSTEP POINT (6)

The instep point-6 was a point detected with the plane G. It was located in the lower part of the contact zone (**Figure 41a**). This point was one of the three points of passage of the curve of the instep girth "G2". The second point A_{rs} was located at the upper part in the arch (**Figure 41a**). The intersection between a plane-B1 parallel to plne-B and the foot made it possible to create a portion of the curve symbolizing the shape of the internal arch. The third point B_{mid} was defined in the middle of two points B_{max} and B_{min} located at the ends of the tangent areas of the plane-C. These points were defined on the creation line of the plane-G (**Figure 41a**). Since the B_{mid} point did not belong to the surface of the foot, it was needed to create a "R15(O15,x,y)" cut mark on "6" to create curve-G2. The curve-G'2 was a curve perpendicular to the Brannock axis representing the instep girth-G'2 proposed by the foot
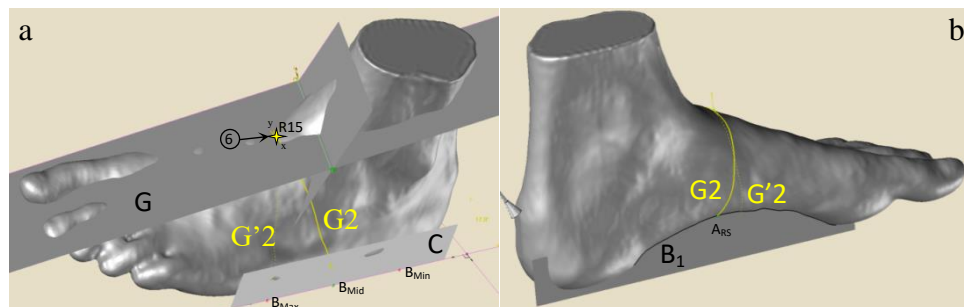
Figure 41 : Detection of contact point 6.

scanner.

II.4.2.d.   METATARSAL TIBIALE (2), METATARSAL FIBULARE (7), HIGHEST POINT OF 1ST METATARSAL (8)

The metatarsal tibial point-2 and metatarsal fibulare point-7 were detected from the outline encompassing of the footprint (**Figure 42b**). To do so, intersections between the creation lines of planes B and D were looked for, as well as planes: C and E at the lower level, i.e. the ground. These two points were sufficient to create the axis of articulation of the foot. At the end of this axis a coordinate system R16(O16,x,y) was created such that its X-axis was on this axis of articulation (**Figure 42a**). Ball girth "G1" was obtained with the XY cutting plane which is orientable along the X-axis of "R16" to detect the highest point of 1st

metatarsal 8 (**Figure 42c**). The tibial metatarsal "2" and the metatarsal fibulare "7" represents the extreme points on the "G1" curve in the direction: X and -X (towards the outside of the foot). In the figure, curve "G'1" is perpendicular to the ground aligned on the axis of articulation representing the ball girth "G'2" proposed by the 3D foot scanner.
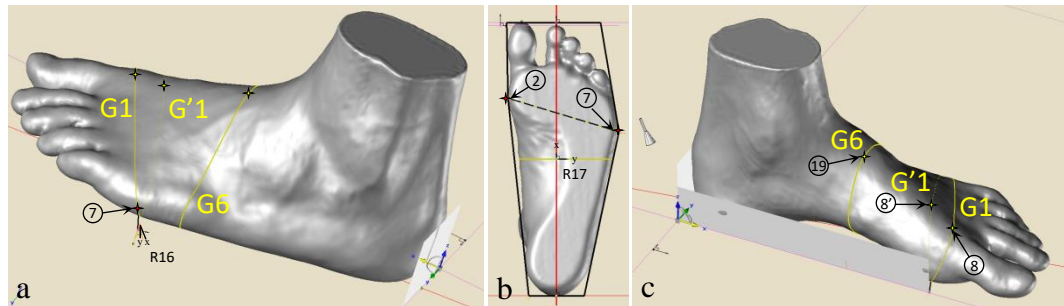
Figure 42 : Detection of contact points 2, 7, 8, 19.

II.4.2.e.   MID-FOOT HIGHEST POINT (19)

The curve representing the girth at 50% foot length from the pternion was obtained from a cutting coordinate system "R17(O17,x,y)" located along the Brannock axis with the same method that was used for R8, R9 and R10 (**Figure 42b**). On that curve G6 was detected the mid-foot highest point "19" which represents the extremum point in the direction of "-Y" (**Figure 42c**).

II.4.2.f.   MEDIAL MALLEOLUS (3), LATERAL MALLEOLUS (4)

The Medial malleolus "3" and the lateral malleolus "4" were obtained respectively from two parallel planes: B' and C' to the planes: B and C. For the second point, a second zone of contact superior to the first was taken into account (**Figure 43a & b**).
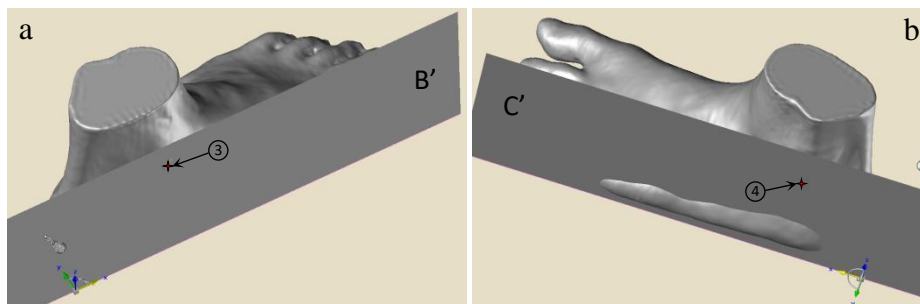
Figure 43 : Detection of contact points 3 and 4.

II.4.2.g.   SPHYRION (9), AND SPHYRION FIBULARE (10)

To detect Sphyrion "9" and fibular sphyrion "10" the technique similar to points "3" and "4" was used. The two detection planes B'' and C'' moved a little deeper in the foot to surround the malleolus. At this point, it was possible to create two curves surrounding each malleolus by looking for the intersection between these two planes and the foot. As illustrated in **Figure 44**, the Sphyrion "9" and the fibulare sphyrion "10" are at the lowest point of these, representing the extremum in "-Z".
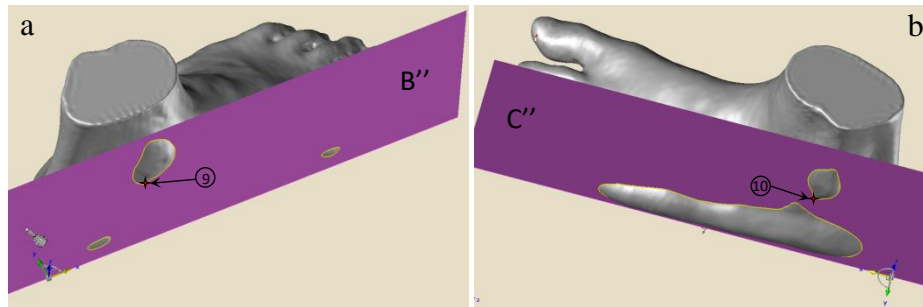
Figure 44 : Detection of contact points 9 and 10.

II.5.   MEASUREMENT PROCESS ANALYSIS

From the anthropometric points and the morphological curves that were detected and created by the 3D graphical process, the set of measurements necessary for the dimensioning of the foot were calculated (**Table 1**: L1 to G6). **Table 1** : Difference measurement between compares the results from our method with those from the scanner. Since the scanner offers other complementary measures (italic measurements) to the standard measures (scanner-specific terminology), it was required to be added to the list (L8 to A1) so that the comparison was complete.

The results show that all the measures useful for sizing the foot have a very small error. Only the "H5" measurement has an error mainly from the scanned measurement. Since this depended on the positioning of the patch that has been glued to the foot of the person to scan to locate the fibulare sphyrion, imprecision is naturally generated by this manual mode. Similar problem was found for H7 (patches positioned manually).

Since the scanner did not measure "G" as specified in the scientific bibliography (now "G'" for the scanner), point "8" became a point "8'" for the scanner, which explained this difference for "H8". This difference was strongly reduced if one would have taken the measurement as it is practiced by the scanner (measure between parentheses for the 3D graphical process).

The measurement of the two angles is highly criticized in the case of the scanner. This measurement was very important to define the basic shape of the insole, depending on outline encompassing of the footprint.

The measurement technique of the proposed process was based on the 3D foot shape whereas the technique used by the scanner was different and was based on the line of the heel thus, leading to often negative angles.

Table 1 : Difference measurement between 3D graphical and scan measurement.

	3D graphical measurement(mm)	Scan Measurem ent (mm)	Erreur (%)
L1 - Foot	277.5	280.6	1.1
L2 - Arch	200.6	203.4	1.3
L3 - Heel to medial malleolus	68.1		
L4 - Heel to lateral malleolus	41.3		
L5 - Heel to fifth toe	229.6		
L6 - Heel to Sphyrion	63.2		
L7 - Heel to Sphyrion fibulare	50.1		
H1 - Medial malleolus	92.0		
H2 - Lateral malleolus	79.2		
H3 - Instep	77.9	75.9	2.6
H4 - Sphyrion	65.5	67.8	3.3
H5 - Sphyrion fibulare	63.4	78.3	21.7
H6 - Mid-foot	75.2		
W1 - Foot	110.6		
W2 - Bimalleolar	70.8		
W3 - Mid-foot	95.2		
W4 - Heel	68.1	67.2	1.3
G1 - Ball	276.9 (277.5)	278.7	0.6
G2 - Instep	273.0 (267.7)	282.7	3.4
G3 - Long heel	372.0		
G4 - Short heel	353.2		
G5 - Ankle	272.3		
G6 - 50% foot length	266.7		
L8 - Fibulare instep	*166.6*	*175.7*	*5.1*
H7 - Arch or Navicular	*29.9*	*38.6*	*22.5*
H8 - Top of 1st metatarsal	*26.4 (53.2)*	*47.6*	*44.5 (11.7)*
W5 - Foot breadth	*115.9*	*115*	*0.7*
A1 - Toe 1st	*5°*	*-8.4°*	*159*
A1 - Toe 5st	*21.4°*	*4.9°*	*336*

II.6. **CONCLUSION**

In this chapter, a 3D graphical process has been developed to detect the anthropometric points of the foot. These anthropometric points are crucial to obtain all the measurements characterizing the foot shape and dimensions. This non-contact measurement method proposes a tracking technique using virtual adjustable planes.

A comparison was realized with the industrial measurement data from specific software to the 3D foot scanner. Overall, the results showed a good match between the data measured with the 3D scanner and process anticipated. Nevertheless, the industrial methods were very reprehensible because they were influenced by the positioning of the markers on the foot and anthropometric ratios which were integrated into the measurements process. This explained the few differences on some measures. Among other things, the use of anthropometric reports was disagreeable and could lead to many more errors if the foot to be measured was out of the ordinary, i.e. with non-negligible deformations. Proposed method has the advantage to adapt to this problem because it could be tested on feet with hallus-valgus or hammertoes deformities during the measurement campaign and the analysis of foot-shape of the following chapter.

CHAPTER III: CLUSTERING OF POPULATION

III.1.   INTRODUCTION

Feet's classification according to their morphology makes it possible to extract the different foot morphotype from a population and then to find the right match between the morphotype and its adjusted size system. This strategy improves the fit and comfort of the shoe. Similar studies on the human body have validated this concept in the context of clothing [93][94]. The morphological foot classification is a process that can be defined in several stages.

The first step is the detection of anthropometric points and contours to ultimately obtain the measurements necessary for the classification process. Therefore, in Chapter II 3D graphic process has been employed that detects the anthropometric points on which the process of proposed method (non-contact numerical method) relied to create the morphological contours to be measured. Some anthropometric points were enough for themselves to take the measurements. The anthropometry that is represented for new measurement technique characterizes the foot dimensionally. Dimensional comparison between each foot then defines a size system. This classification with measurement data, considered to be one-dimensional, is a 1D classification giving overall results for the entire population, ignoring the morphological criterion, hence fit and comfort.

The second step in the morphological foot classification process was to find the proper signature of the foot morphology to express its characteristic shape. Therefore, two directions could be taken, i.e.: the 2D classification or the 3D classification. The 2D classification required defining a 2D shape descriptor that could be the plantar surface (top view of the foot) or the outer contour of the foot (side view). In a 3D classification process, the 3D shape descriptor could be the arch shape of the foot arch. This choice depends mainly on the needs of the proposed study. The 2D shape can provide the necessary information to define foot morphotype (Greek foot, Egyptian foot, Roman foot, Germanic foot, Greek foot, Celtic foot etc.) or classify people for medical reasons (flat foot, hollow foot etc.). The 3D shape can lead to the detection of 3D feet's deformation.

The next step was to apply one of the 2D/3D descriptors to all the feet of the 3D database, to classify the population into different morphological clusters by an unsupervised classification process. In this chapter, different ways have been tested depending on the goal and the quality of the results to obtain.

III.2.   1D CLUSTERING METHOD

III.2.1. ANTHROPOMETRIC DATA ACQUISITION AND PROCESSING

III.2.1.a.   SUBJECTS AND PROTOCOL

Anthropometric data of 100 French people has been used in this study. The subjects were males as well as females. The foot-scan campaign was conducted in April 2017 where both left and right feet were scanned while to save time, only right foot data has been used in this study. The age of the female subjects ranged from 19 to 70 years, however for males it was from 21 to 60 years. **Table 2** presents the basic demographic information of participants.

Table 2 : Fundamental demographic data of participants (measurements in millimeters).

Term	Males (n=50)		Females (n=50)	
	Mean	SD	Mean	SD
Age (years)	32.2	9.3	36.8	15.07
Stature (cm)	180.5	8.3	164.1	7.02
Weight (kg)	78.34	10.9	74.2	72.03
Foot length (mm)	269.9	13.4	241.8	13.6
Ball girth (mm)	256.5	12.9	234.3	13
Foot breadth (mm)	106.2	6.1	96.7	5.9
Instep girth (mm)	258.2	10	233	12.3
Heel breadth (mm)	68.4	4.2	62.1	3.9
Toe #1 angle	6.2	4.6	8.3	9
Toe #5 angle	13	4	12	5.6
Height of navicular (mm)	34.1	8.5	30.8	6.2

III.2.1.b.   EXPERIMENT APPARATUS

Because of its accuracy which is 1.0 mm, INFOOT USB Scanning system, IFU-S-01 (**Figure 45**) was used to collect the foot data [44][95]. It is comprises of 8 CCD cameras and 4 laser projectors to architype the structure of the foot. Each foot scan took about 10 seconds where every subject was asked to stand in natural pose so that body weight distribution would evenly be on medial and lateral part. The measurement protocol which has been used is the same in part II.3.

Figure 45 : INFOOT USB foot scanner standard.

III.2.2.STATISTICAL ANALYSIS

In this study principal components analysis (PCA) was applied to obtain significant factors for foot shape representation to be practiced in the clustering of 3D foot shapes [65]. Principal component analysis is generally defined as a data analysis method that has the particularity of transforming a certain number of variables correlated with each other into a smaller number of variables de-correlated so-called main components. Depending on the area of application, it is also named the transformation of Karhunen-Loève, the transformation of Hotelling or orthogonal decomposition to eigenvalues. The ACP has been invented in 1901 by Karl Pearson in 1901[96]. Very often used as a data mining technique, it has nowadays been oriented towards predictive models of reconstruction. In this application, Nine foot dimensions (**Table 2**) were considered as input to calculate PCA as they are the most relevant in shoe and insole designing [45].

SPSS statistics 23.0 version was used to perform non-hierarchical cluster analysis in order to categorize the foot type. To cluster the homogeneous individuals into groups for approach, K-means cluster analysis was used.

Table 3 : Gender differences in the measures of similar foot length (measurements in mm).

Variables	Foot length 200-220 (mm)			Foot length 220-240			Foot length 240-260			Foot length 260-280			Foot length 280-300			Foot length 300-320		
	Male	female	MD	Male	female	MD	Male	female	MD	Male	female	MD	Male	female	MD	Male	female	MD
Ball girth		223.1			228.8		250	238.9	11.1	256.4	250.4	6	265.9	231.4	34.5	256.8		
Foot breadth		91			94.4		102.9	98.6	4.3	106.4	103.6	2.8	110.5	96.1	14.4	104.9		
Instep girth		228.9			228.9		253.5	236.2	17.3	258	247.8	10.2	264.9	224.9	40	261.9		
Heel breadth		64.4			60.9		66.2	62.9	3.3	68.2	63.6	4.6	70.7	60.8	9.9	74.1		
Height of Instep		65.5			62.6		71.8	64.9	6.9	71.2	64.6	6.6	72.8	59.7	13.1	67.1		
Toe #1 angle		7.3			6.8		4.4	8.8	-4.4	7.3	14.25	-6.95	5.3	12.6	-7.3	3.7		
Toe #5 angle		1			10.7		13.5	14	-0.5	11.7	10.5	1.2	13.4	12	1.4	10.5		
Height of navicular		27.8			31.6		39.5	25	14.5	22.9	41.9	-19	32.7	23	9.7	23.9		

III.2.3.RESULTS AND DISCUSSION

III.2.3.a. GENDER EFFECT ON FOOT SIZES

Foot length ranging from 200-320 mm was selected and the other dimensions pertaining to this size range were compared between males and females. According to **Table 3**, slight differences in dimensions between both the genders were testified. There was no dimension data found below 240 mm sizes for male; however, there was no foot size above 300 mm recorded for female. Yet, foot length 280-300 male showed greater measures in ball girth, foot breadth and instep girth than females. In size 260-280 mm females for height of navicular showed greater measures than men while toe-1 angle has been greater in entire size set than male.

III.2.3.b. PRINCIPLE COMPONENT ANALYSIS

Principal component analysis was used to extract the most important variables with highest factors scores to consider as independent variables for cluster analysis. **Table 4** shows that ball girth, fibulae instep length, foot breadth, instep length and height of navicular and heel breadth exhibit the higher scores.

Table 4 : Results of principle component analysis for foot dimensions.

Variables	Male			Female		
	PC1	PC2	PC3	PC1	PC2	PC3
Foot length	0.736	.595	.056	.827	-.497	.026
Ball girth	0.891	-.348	-.052	.886	.352	-.163
Foot breadth	0.879	-.308	-.094	.873	.270	-.203
Instep girth	0.867	-.281	.088	.773	.156	.035
Heel breadth	0.730	-.015	-.243	.628	-.558	.281
Instep length	0.770	.461	.055	.534	.510	.174
Fibulae instep length	0.353	.826	.241	.026	.173	.935
Height of instep	0.490	-.522	.200	.670	-.597	-.041
Height of navicular	-.038	-.191	.940	.890	.245	.008

III.2.4.K-MEANS CLUSTERING

To cluster the feet, Euclidian distance method was applied. Thus, three distinct clusters were extracted, respectively. The clusters presented in **Table 6**, **Table 7** are the variables of k-well-spaced observations and were used for next stage hierarchical clustering using K-means clustering analysis. During cluster analysis, maximum numbers of iterations

were set 10 to obtain rectified clusters of the data. The **Table 5** gives an example in the evolution of the iteration of the method.

Table 5 : Number of iterations during K-means clustering female.

Iteration	Changes in cluster centroids		
	1	2	3
1	19.534	14.619	18.991
2	1.513	4.114	0.490
3	0.866	6.938	0.860
4	0.735	3.821	0.0
5	0.0	0.0	0.0

The convergence was successful because there are few or no changes in the cluster centers. The maximum value for modifying absolute coordinates for a center is 0.00. The current iteration was 5 then. The minimum distance between the initial centers was 46.3 which show these are the noticeable values to be utilized in foot analysis. Analysis of PCA results in terms of females represents ball girth, height of instep and height of navicular represents with higher values. Therefore, K-means of these anthropometric measures was executed and results are presented in **Table 6**. Correspondingly, the clustering for the men was performed with ball girth, fibulae instep length and height of navicular (

Table 7) due to its higher value in PCA results.

Table 6 : K-means cluster center female.

Terms	Cluster (mm)		
	F1	F2	F3
Ball girth	246.2	241.1	226.0
Height of instep	66.3	65.0	62.2
Height of navicular	33.8	29.4	30.2

Table 7 : K-means cluster center male.

Terms	Cluster (mm)		
	M1	M2	M3
Ball girth	257.5	263.7	241.4
Fibulae instep length	172.1	173.6	176.8
Height of navicular	31.6	37.1	34.3

Table 6 describes the three kind cluster centers for three different kind of foot model (rest dimensions can be chosen from the size table accordingly) F1, F2 and F3 for female

which can be utilized to create ideal foot for a size given. These ideal foot models can be utilized for the purpose of shoe last, shoe manufacturing and insole making.

Similarly,

Table 7 depicts the cluster center of three main dimensions M1, M2 and M3 for male.

III.2.5. RESULT AND DISCUSSION

Having been compared foot measures, there was no dimension data found below 240 mm sizes for male; however, there was no foot size above 300 mm recorded for female. Yet, foot length 280-300 male showed greater measures in ball girth, foot breadth and instep girth than females. In size 260-280 mm females for height of navicular showed greater measures than men while toe-1 angle has been greater in entire size set than male. Obtained results suggest that the gender differences on foot dimensions should be taken into consideration for shoe-last and in manufacturing of shoes.

Ball girth, height of instep, height of navicular and fibulae instep length was considered for the clustering analysis of both the genders. Consequently, three different foot types for both the genders (M1, M2 and M3 for male and, F1, F2 and F3 for female) were acquired. Based on foot classification presented here a new planning for customized foot or a new production planning can be industrialized.

III.3.   2D CLUSTERING METHOD

The unsupervised classification of morphologies from 3D scans is a complex and delicate process. To overcome the limitations of manual methods, data analysis techniques have been studied to interpret information. Indeed, promising results have been achieved. In these approaches, the goal is to group the feet in homogeneous sets sharing the same features. Such a process must be robust, precise and adapted to the final application. **Figure 46** presents the different steps of the methodology needed to be followed:

- **Pretreatment of data**: The foot 3D scan is represented by a triangle mesh that requires corrections. Indeed, the tools that make it possible to detect the points and anthropometric curves apply on 3D objects whose surface comes from a clean and totally closed mesh. Hence, pretreatment of the 3D scans consisted of filtering the noisy data, resealing the holes corresponding to the shadow areas, especially the toe areas and smoothening the mesh. A surface model was designed from this mesh.

- **2D descriptors of the 3D foot shape**: Each 3D foot was standardized and then represented by a 2D shape descriptor representing the signature of it.

- **2D unsupervised classification:** Unsupervised classification was applied to 2D foot descriptors. In this part, study the use of a graph-based approach was articulated, the spectral classification to classify the feet. Unlike parametric methods, graph-based methods are non-parametric, in the sense that they do not require a priori assumptions about the size, shape, or distribution of classes [97]. The classification implies the integration of the feet in a space where they are linearly separable into different homogeneous classes.

Figure 46 : 2D unsupervised classification process for feet.

III.3.1. PRETREATMENT OF DATA

The point cloud of the 3D representation of the foot, obtained after the 3D scan of this foot, was subjected to different preprocessing in the Rapidform software. These steps comprised of correcting the imperfections of the scanner mentioned above. The preprocessing process was as follows:

- Importing the 3D scan into Rapidform (**Figure 47a**)
- Re-meshed the 3D object to extract the reference points (**Figure 47b**)
- First automatic smoothing of the resulting surface with edge extension (to close the easy holes) (**Figure 47c**)
- Hole selection (**Figure 47d**)
- Clearing holes (to remove bad edges) (**Figure 47e**)
- Block the hole (with a suitable surface mode) (**Figure 47f**)
- Second smoothening of the 3D object
- Placing a cutting plane to cut off the top of the object (**Figure 47g**)
- Results of the cuts in yellow (**Figure 47h**)
- Adding a surface on the top to close the 3D object (**Figure 47i**)
- Creation of a surface model whose number of facets depended on the accuracy of the desired 3D model (**Figure 47j**)

- If necessary, modifying the position of the nodes in order to avoid the folding of the facets on itself or on the neighbors (**Figure 47k**)

- Final result that were exported in IGS format in 3D design software (Design Concept 3D) (**Figure 47**)
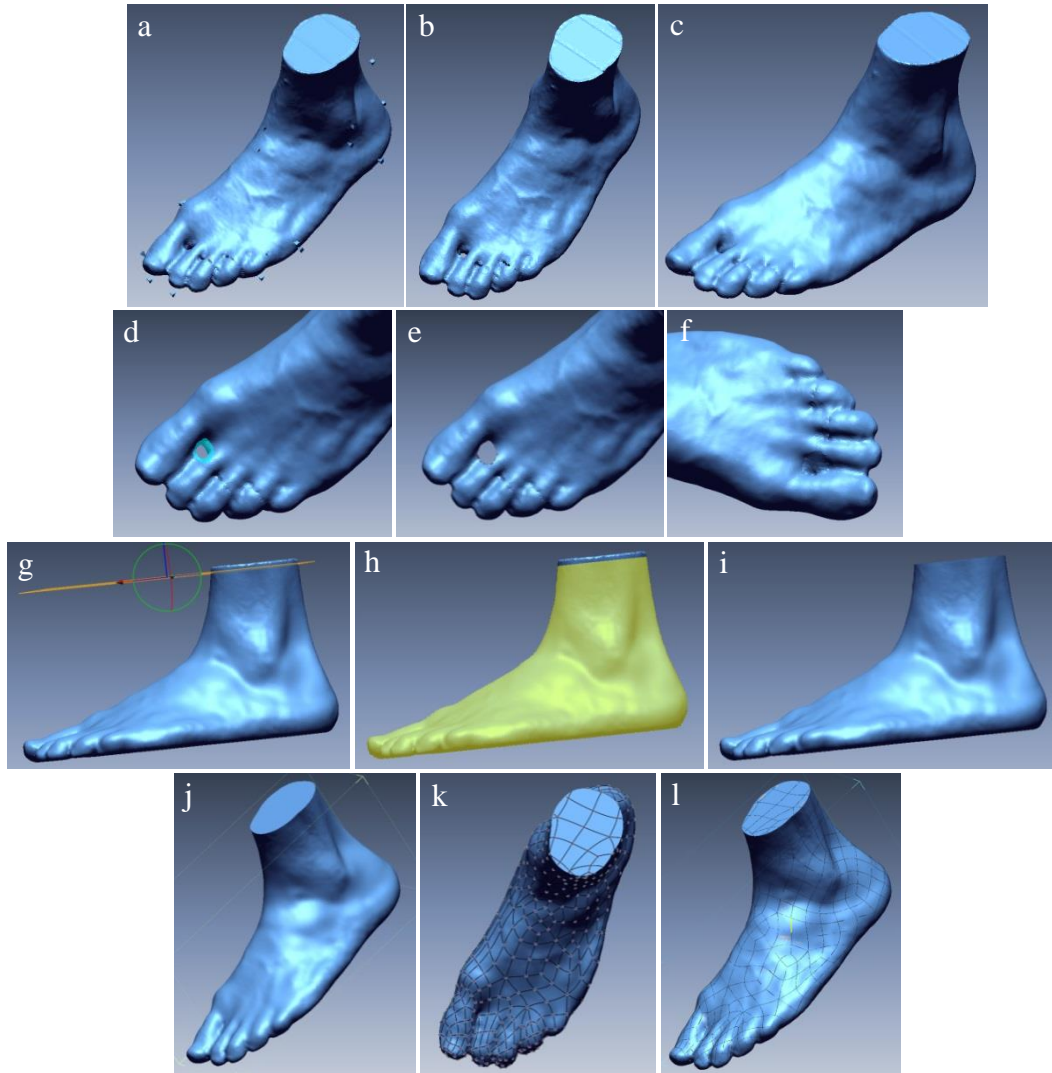
Figure 47 : Pretraitment of scanned data.

III.3.2.2 D DESCRIPTORS OF THE 3D FOOT SHAPE

Each foot was then processed in the 3D design software to extract its non-standard 2D shape descriptor. 3D graphical process (Lectra 3D Design Concept) was utilized to get the trapezoid shape composed of the six plan A, B, C, D, E and F1 (see II.4.1) of the optimal outline encompassing of the footprint.

Data standardization is an important step in pattern recognition. In this case, it was required to go back to a canonical representation to ensure that the shape descriptor was

invariant. So, three operations were necessary: the translation (the centering), the rotation (the alignment) and the scaling.

The first two operations represent the wedging and alignment of the foot contours that was also practiced when measuring a foot with the Brannock device. The two reference points P_{r1} and P_{r2} allowed to identify the heel wedging line (**Figure 48a**), line perpendicular to the Brannock axis. The points of intersection between these two lines were considered as the origin of the coordinate system of the set of outlines. Each contour was then aligned with a common Brannock axis by rotating around the origin of the coordinate system (**Figure 48b**).

The third operation consisted of scaling the 2D contours with the Gärtner's algorithm. It consisted in defining the minimal sphere (d = 3) or the minimal circle (d = 2) which made it possible to encompass a set of points via an iterative approach. This technique was applied in dimension d = 2 to look for the enclosing minimal circle of each 2D contour (**Figure 48c**).
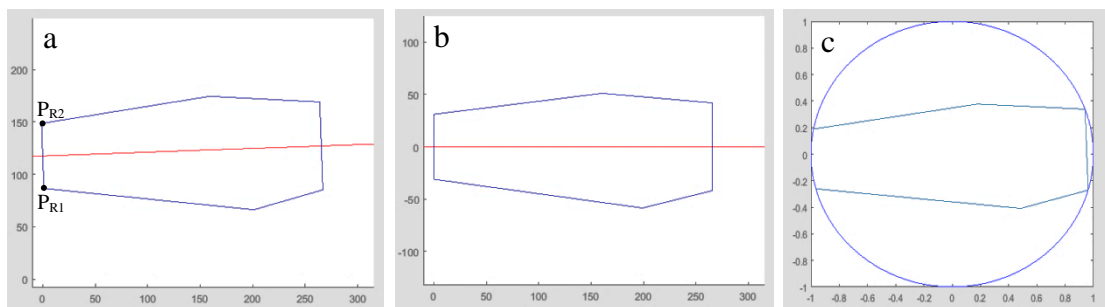
Figure 48 : Standardization of the 2D shape descriptor.

The shape descriptor is then transformed into a vector composed of the polar coordinates of the points P_1, P_2, P_3, P_4, P_5 and P_6 (**Figure 49**).
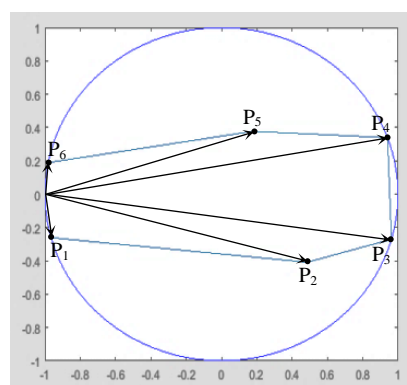
Figure 49: Vectorization of the 2D shape descriptor.

III.3.3.2D UNSUPERVISED CLASSIFICATION OF FEET

In general, the purpose of the unsupervised classification was to search in a set of points, natural groups (called clusters) such that the points of the same group were the most similar between them while the points belonging to different groups were the least similar to each other. There were many unsupervised classification approaches. These are distinguished by the implicit assumptions about class properties:

- *Classes far apart:* A class is a set of points close to each other and distant from any point of the other classes. In fact, this assumption is satisfied only when the classes are far apart from each other.

- *Prototype-based clusters:* A class is a set of points closer to the prototype that defines the cluster than any prototype of another class. The cluster prototype can be the center of the points of the class or the medoid that is to say the most representative point of the class. Example of algorithms: k-means, k-medoids.

- *Density-based clusters:* A class is an area with a high density in points and is surrounded by a low-density area. Example of algorithms: mixing of Gaussian densities, search of modes.

- *Graph-based clusters:* A class is a set of points connected to each other. The data points are represented as graphs, where the nodes are the points and the links represent connections between the points. Example: the spectral classification, the graph partition.

In the following, unsupervised classification was done based on the graph from the spectral classification.

The spectral classification was based on graph theory and matrix theory. The advantages of this method was its performance in classifying data of various shapes, including convex, its solid theoretical bases and its recent successful applications in the fields of signal and image. The spectral classification takes its name from the spectrum, a set of eigenvalues of the Laplacian matrix of the graph extracted from the similarity matrix of the data. The properties of the vectors and eigenvalues of the Laplacian matrix play a fundamental role in the determination of the projection space in which the data are more easily separable.

Let us recall, in the following, some notions of the theory of the graphs necessary for the comprehension of the spectral classification.

III.3.3.a. SOME NOTIONS ON GRAPH THEORY

The unsupervised classification based on graphs consists of associating a graph G $(V,$ $E, W)$ with the set of given points $X = \{x_1, \dots, x_n\}$ so that at each point x_i of X corresponds to node v_i of the set of nodes $V = \{v_1, \dots, v_n\}$ and that to the similarity w_{ij} between any pair of points (x_i, x_j) corresponds the weight of the connection between the pair of nodes $(v_i, v_j) \in E \subset V \text{x} V$ corresponding. Moreover, the similarity matrix W of the graph was defined by its general term w_{ij}, $W = (w_{ij})$. the matrix W is considered symmetrical. To illustrate, further examples of weights corresponding to the similarities between couples of points have been given.

To get the outcome the context of simple graph (without loops) undirected and weighted, and considered the case of partitioning a graph into two groups of nodes A and B and introduce the following concepts:

- degree d_i of a node v_i : $d_i = \sum_{j \in V} w_{ij}$

- the degree matrix of a graph is a diagonal matrix defined by:

$$D = \begin{cases} d_{ii} = d_i \ for \ i \ = \ 1, \dots, N \\ d_{ij} = d_{ji} = \ 0 \ for \ i \ \neq j \end{cases}$$

- volume of set A : $vol(A) = \sum_{i \in A} d_i$ and $vol(B) = \sum_{j \in B} d_j$

- section a graph in A and B disjointed or not: $cut(A, B) = \sum_{i \in A, j \in B} w_{ij}$

- coupe normalisée: $ncut(A, B) = cut(A, B) \left(\frac{1}{vol(A)} + \frac{1}{vol(B)} \right)$

- the Laplacian of a graph is a matrix of the form: $L = D - W$

- D is the degree matrix and W is the similarity matrix. Note that the Laplacian matrix L has a zero eigenvalue whose eigenvector is the vector 1 of components 1.

The goal of the graph section is to search for groups A and B such that the weights of connections between A and B are minimum and their volumes are maximum. It is thus necessary to look for A and B such that $ncut$ (A, B) is minimal:

$$\min_{A,B} ncut(\text{A}, \text{B}) = \min_{A,B} cut(\text{A}, \text{B}) \left(\frac{1}{vol(A)} + \frac{1}{vol(B)} \right)$$

Note that there are different types of graph section criteria in the literature: *min-cut*, *ratio-cut*, *min-max cut*, and so on. The *ncut* criterion is the most suitable for the classification problem.

Relationship between the normalized section and the Laplacian matrix of a graph

There is a relationship between the normalized graph section criterion and the Laplacian matrix of the graph. Indeed, consider the vector $u = (u_1, \ldots, u_n)^T$ indicator of membership of the points (or nodes) to classes A and B with :

$$u_i = \begin{cases} \frac{1}{vol(A)} & si \ x_i \in A \\ -\frac{1}{vol(B)} & si \ x_i \in B \end{cases}$$

The following relationship between the Laplacian and the graph section criterion can be easily demonstrated:

$$\frac{u^T L u}{u^T D u} = \frac{1}{2} cut(A, B)(\frac{1}{vol(B)} + \frac{1}{vol(B)})$$

Indeed,

$$u^T D u = \sum_i d_i u_i^2 = \sum_{i \in A} \frac{d_i}{vol(A)^2} + \sum_{i \in B} \frac{d_i}{vol(B)^2} = \frac{1}{vol(A)} + \frac{1}{vol(B)}$$

Because

$$\sum_{i \in A} d_i = vol(A)$$

According to von Luxburg [98] :

$$u^T L u = u^T (D - W) u = \frac{1}{2} \sum_{i,j} w_{ij} (u_i - u_j)^2$$

Indeed,

$$u^T L u = u^T (D - W) u = u^T D u - u^T W u$$

$$= \frac{1}{2} \left(\sum_i d_i u_i^2 - 2 \sum_{i,j} w_{ij} u_i u_j + \sum_i d_i u_i^2 \right)$$

$$= \frac{1}{2} \sum_{i,j} w_{ij} (u_i - u_j)^2$$

$$= \frac{1}{2} \sum_{i \in A, j \in B} w_{ij} \left(\frac{1}{vol(A)} + \frac{1}{vol(B)} \right)^2$$

$$= \frac{1}{2} cut(A, B) \left(\frac{1}{vol(A)} + \frac{1}{vol(B)} \right)^2$$

The *ncut* criterion becomes:

$$\frac{u^T L u}{u^T D u} = \frac{1}{2} \frac{cut(A, B) \left(\frac{1}{vol(A)} + \frac{1}{vol(B)} \right)^2}{\left(\frac{1}{vol(A)} + \frac{1}{vol(B)} \right)}$$

$$\frac{u^T L u}{u^T D u} = \frac{1}{2} cut(A, B) \left(\frac{1}{vol(A)} + \frac{1}{vol(B)} \right)$$

$$\frac{u^T L u}{u^T D u} = \frac{1}{2} ncut(A, B)$$

The *ncut* minimization becomes:

$$\min_{A,B} ncut(A, B) = \min_{u} \frac{u^T L u}{u^T D u}$$

The search for *A* and *B* which minimize *ncut* is solved by making the vector of membership *u* continuous (solution relaxed). It is an optimization problem in the form:

$$\min_{u} \frac{u^T L u}{u^T D u}$$

The trivial solution is the vector 1 whose components are 1 and corresponds to the zero eigenvalue. The vectors *u* must therefore check:

$$u^T D 1 = 0$$

By normalizing the denominator, this problem has for equivalent:

$$min \ u^T L u \ \text{ under the constraint: } u^T D u = 1$$

With *u* non-zero vector checking $u^T D 1 = 0$

The vector *u* of non-trivial solution is the second smallest eigenvector of the system of generalized eigenvalues:

$$Lu = \lambda D u$$

Since the vector *u* is continuous, it is sufficient to thresholding *u* with respect to 0 to obtain the assignments of the points to classes *A* and *B*:

$$x_i \in A \ si \ u_i \geq 0 \ \ et \ x_i \in B \ si \ u_i < 0 \ .$$

It may be noted that the components u_i of u are none other than the projections of points x_i on the axis u. These projections verify:

$$u^T L u = \frac{1}{2} \sum_{i,j} w_{ij} (u_i - u_j)^2$$

The minimization of $u^T L u$ therefore amounts to find the components of the vector "u" so that the closest pairs of projections on this axis, thus satisfying $(u_i - u_j)^2$ minimum, represent pairs of points (x_i, x_j) the most similar ones in the input space having a maximum weight w_{ij} and vice versa.

In a general way, the partition of a graph in k groups, $\{A_1, \ldots, A_k\}$ amounts to minimizing the standard cut criterion defined by:

$$ncut(A_1, \ldots, A_k) = \sum_{i=1}^{k} \frac{cut(A_i, \bar{A}_i)}{vol(A_i)}$$

With $\bar{A}_i$ is the set of complementary nodes of the set A_i in V. The general solution is also optimization problem of the form:

$$min_U \ trace(\ U^T L U) \ \text{under duress:} \ U^T D U = I$$

This leads to the search for the k eigenvectors associated with the k smallest nonzero eigenvalues. The projections in the spectral space generated by the k eigenvectors constitute an image of the given points. It is enough to classify these projections by a simple algorithm like the k-means and then to classify the given points according to the classes of affectation of their projections.

Spectral classification algorithms

Several spectral classification algorithms exist. Spectral classification algorithms usually consist of the following three basic steps:

- Pretreatment:
    - Construction of the graph *G (V, E)* representing the data
    - Creation of the similarity matrix *W*
- Representation in the spectral space:
    - Elaboration of the Laplacian matrix of the graph *L*
    - Calculation of the eigenvalues (spectrum) and eigenvectors of the Laplacian matrix *L*.

- Projection of each point in the spectral space based on the eigenvectors retained.
- Classification:
  - Application of K-means in the spectral space to classify the image of the data in the spectral space
  - Assignment of each point in the original space to the class.

The different steps of the spectral classification algorithm are summarized in **Figure 50**.

| Data X | Graph G(V,E,W) | Similarity matrix | Laplacien L=D-W | Values Vectors | Post Traitment |
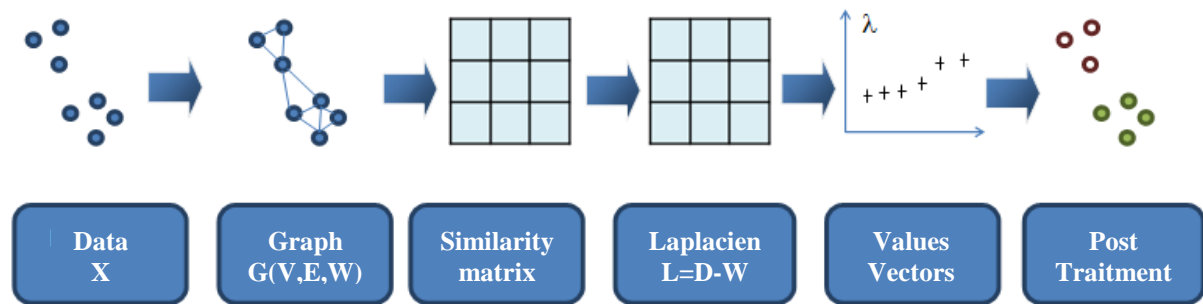
Figure 50 : Schematic steps diagram of the spectral classification algorithm.

Algorithm of Shi and Malik

The method proposed by Shi and Malik [99] is based on a recursive resolution of bi-partitioning. To do so, the authors extract the second smallest eigenvector from the symmetric normalized Laplacian matrix and then separate the points into two subsets *A* and *B*. At the next iteration, they extract the second eigenvector from the symmetric standardized Laplacian matrix constructed thanks to the similarities computed between the points of the same group (*A* or *B*), then partition the points again.

The algorithm, summarized below, converges when the desired number of groups is reached or when the value of the cut is greater than a threshold set by the user.

Algorithm
- Pretreatment
  - 1. construct the data graph $G\ (V,\ E,\ W)$
  - 2. construct the matrix of degrees D
- Spectral representation
  - 3. calculate the symmetric standardized Laplacian matrix
  - 4. extract the second smallest eigenvector z_2 from the symmetric normalized matrix

- Partitioning
  - 5. store the elements of $D^{-\frac{1}{2}}z_2$ in descending order
  - 6. partition the graph G (V, E, W) into two subsets according to the values of the elements of u
- Recursivity
  - 7. Repeat steps 1 to 6 on each remaining group of points until you obtain K groups.

Algorithm of Von Luxburg

Von Luxburg [98] defines K indicator vectors f_k as $f_k = (f_{1k}, \dots, f_{Nk})$ or $f_{ik} = \frac{1}{\sqrt{vol(C_k)}}$. These vectors are listed in the columns of matrix F. The problem is expressed as:

$$\min_z J(A_1, \dots, A_K) = \min_z \sum_{k=1}^{K} z_k^T L z_k$$

$$F = D^{-1/2} Z$$

$$F^T D F = 1$$

This problem is solved by using the first K eigenvectors of the Laplacian matrix which minimize the criterion. They make it possible to estimate the K indicator vectors. The goal was to find discrete values for these indicator vectors. The extraction of the spectrum is followed by a step of classification of the points which represent the lines of $F = D^{-\frac{1}{2}}Z$.

Algorithm
- Pretreatment
  - 1. Construction of the data graph G (V, E, W)
  - 2. Construction of the matrix of degrees D
- Spectral representation
  - 3. Calculation of the symmetric standardized Laplacian matrix
  - 4. Extraction of the K smallest eigenvectors
  - 5. Construction of the Z matrix
- Partitioning
  - 6. Application of a partitioning algorithm on the rows of the matrix F.

The pretreatment phase of the spectral classification is summarized here in the constitution of the graph and its similarity matrix.

73

III.3.3.b. PRETREATMENT

The pretreatment phase of the spectral classification consists of the establishment of the graph corresponding to the data. The time/intensity curves become the nodes of a connected graph and the similarity between two nodes is the weight of the connecting arc which links them.

Construction of the graph representing the data

Prime interest was in non-oriented graphs, simple and weighted with variants:

- Fully connected graphs, where all the nodes are connected to each other.
- ε neighborhood graphs, which connect a node to its neighbors if the points are in the hypersphere radius ε.
- K nearest neighbor graphs (K-ppv), the nodes are connected to the k-ppv nodes.

These graphs are shown in **Figure 51**.

Fully connected graph ε neighborhood graphs K-ppv graphs (K=2)
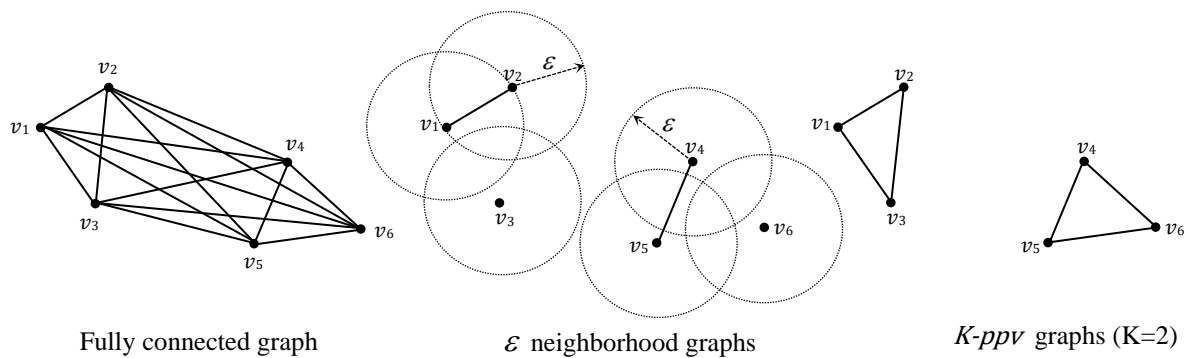
Figure 51 : Examples of graph construction.

From the graph, illustrates the similarity matrix.

Creating the similarity matrix

The similarity matrix W makes it possible to define the degree of resemblance between the nodes of the set V. The similarity functions are based on the distances (for example: Chebyshev, Manhattan, Euclidian, Minkowski), but unlike the measure of distance which takes values between zero and infinity, the similarity measure provides values between 0 and 1, which are easier to interpret.

- The *inverse similarity* of Euclidean distance is defined by:

$$w_{ij} = \frac{1}{1 + d^2(x_i, x_j)}$$

Kunegis et al. [100] introduce a dispersion parameter σ allowing to take into account the local dispersion of the data, and noted σ^2:

$$w_{ij} = \frac{1}{1 + \dfrac{d^2(x_i, x_j)}{\sigma^2}}$$

This similarity measure then makes it possible to obtain an overall maximum limited to 1 for a zero distance. It is frequently used in the field of document classification.

- The *cosine similarity* makes it possible to measure the similarity between two vectors (x_i, x_j), by calculating the angle between these two vectors :

$$w_{ij} = \left| cos(x_i, x_j) \right| = \frac{\left| x_i^T . x_j \right|}{\|x_i\| . \|x_j\|}$$

The smaller the angle between these vectors, the more similar the points are. This similarity function is also used in document content exploration and analysis. The major disadvantage of this type of similarity lies in the fact that the direction in which each point is projected takes more importance than the amplitude of the values of each of its attributes.

- *Gaussian similarity* is most commonly used in the field of classification. The relative importance of the values of the attributes, but also the neighborhood relations between data points are essential factors in the measurement of similarities between points. This function is defined by:

$$w_{ij} = exp\left(-\frac{d^2(x_i, x_j)}{2\sigma^2} \right)$$

With σ being a dispersion parameter (or scale parameter) allowing to take into account the local dispersion of the data, and $d(x_i, x_j)$ a function of distance (often, the Euclidean distance) between x_i and x_j. In contrast to the similarity based on the inverse of Euclidean squared distance, this function decreases exponentially when distances are large, giving a weight close to 1 for very similar points [100]. The dispersion parameter σ is generally set by the user. However, there are automatic calculation methods of σ such as that proposed in [101].

- The *locally adapted Gaussian similarity*, called *self-tuning* by [101], consists, instead of a single parameter σ^2 for all the data, to adapt this parameter to the local structure of each pair of data:

$$\sigma_{ij}^2 = \sigma_i \sigma_j$$

It is a question of approximating the dispersion σ_i in the neighborhood of a point x_i by the distance from this point to its $r^{\text{ème}}$ neighbor $x_{r(i)}$:

$$\sigma_i = d(x_i, x_{r(i)})$$

The selection of the rank r is independent of the scale factor and is often chosen between 7 and 10. Hence, for each pair of points (x_i, x_j), the weight of the connection w_{ij} is given by:

$$w_{ij} = exp\left(-\frac{d^2(x_i, x_j)}{2\sigma^2}\right)$$

In this sense, the similarity of the pairs of points is adjusted to the dispersion of the neighborhood of the data.

Once the similarity matrix is determined, the Laplacian matrix of the graph is calculated, an intermediate step to the representation in the spectral space of the data.

III.3.3.c. SPECTRAL REPRESENTATION

The Laplacian matrix plays a fundamental role in classification because it is its eigenvectors associated with its relevant eigenvalues (its spectrum) that define the spectral space. The spectral representation phase consists of the construction of the Laplacian matrix of the graph from the similarity matrix. There are several types of **Laplacian matrices** in literature:

Non-standardized Laplacian matrix

Non-standardized Laplacian matrix is a linear combination of the similarity matrix W and the matrix of degrees D. It is defined as follows:

$$L = D - W$$

It can be noticed that the non-normalized L matrix does not depend on the elements on the diagonal of the matrix of similarities W. Indeed, the values of self-similarity (that is to say the similarity of an object with it themselves) do not modify the Laplacian L matrix. Thus, any other matrix of similarities composed of off-diagonal values, equal to those of W, makes it possible to obtain the same solution as the matrix L.

Standardized Laplacian matrix asymmetric

Standardized Laplacian matrix asymmetric is defined by:

$$L_{as} = I - D^{-1}W$$

It is derived from Markov's random walk method [102].

Standardized Laplacian matrix symmetric

Standardized Laplacian matrix symmetric is defined by Shi et Malik [99]:

$$L_s = I - D^{-\frac{1}{2}} W D^{-\frac{1}{2}}$$

These Laplacian matrixes have common characteristics: matrices are semi-positive, "0" is an eigenvalue of these matrices associated with their respective unit eigenvectors.

III.3.3.d. CLASSIFICATION

Spectral classification methods use an unsupervised classification algorithm. The algorithm is of projections of given points in the spectral space which are defined by the eigenvectors of the Laplacian matrix. Generally, this step consists of the application of the K-means method. Initialization can be random or guided. Other alternative methods can be used: fuzzy K-means, K-median or density mixtures.

But, the main difficulty in spectral classification algorithms is the **estimation of the number of classes** that can be obtained by these different methods:

Analysis of eigenvalues

The analysis of eigenvalues is commonly used to estimate the number of classes. Ng et al. [103] have shown that, in the ideal case where the classes are very distant from each other, it is possible to generate the matrix of similarities in block matrix form. The smallest eigenvalue of the Laplacian diagonal-block matrix is a null eigenvalue, which repeats itself with a multiplicity equal to the number of classes desired. This implies that it is possible to easily estimate this number by counting the number of zero eigenvalues.

However, this estimation process is made possible only by the fact that it is an ideal case where the classes are compact and very distant from each other. In fact, if classes overlap, the first K eigenvalues are no longer all zero.

An alternative is then proposed by Shortreed and Meila [104] and taken up by von Luxburg in [98]. It consists in ordering the eigenvalues by order and looking for a significant difference between successive eigenvalues, this difference is called gap. The gap calculation is therefore defined as:

$$gap(i) = |\lambda_i - \lambda_{i+1}|$$

The number of classes is estimated by searching:

$$\hat{k} = arg \max_i gap(i)$$

However, if the maximum gap is relatively small, it becomes difficult to accurately estimate the number of classes. Indeed, if the distribution of eigenvalues does not present a clear "jump", the estimation of the number of classes proves difficult and irrelevant.

Modularity

In reference [105], there has been proposed an automated method to determine the number of classes based on the concept of modularity in the field of social networks introduced by Newman and Girvan [106]. This approach uses a graphic concept to identify classes. Their mod modularity function can be defined as [105]:

$$mod = \sum_{i=1}^{k} \frac{1}{|A_i|} \left[\frac{cut(A_i, A_i)}{cut(V, V)} - \left(\frac{cut(A_i, V)}{cut(V, V)} \right)^2 \right]$$

In this equation, $|A_i|$ is the cardinal of A_i, $cut(A_i, A_i)$ measures the sum of the weights (on the connecting arcs) intra-classes, while $cut(A_i, V)$ measures the sum of the weights of all the connecting arcs attached to the class A_i, and $cut(V, V)$ measures the sum of all the weights of the graph. The modularity function is calculated according to the number of classes, the maximum value gives an estimate of the number of classes.

Modularity measures the difference between the probability of connections of the graph whose nodes are in the same classes (probability of intra-class connections) and the probability that the connections are random between the nodes of the same graph.

More recently, Yu and Ding [107] proposed to solve modularity bundling via standard cut using the objective function:

$$nmod = \sum_{i=1}^{k} \frac{1}{cut(A_i, V)} \left[\frac{cut(A_i, A_i)}{cut(V, V)} - \left(\frac{cut(A_i, V)}{cut(V, V)} \right)^2 \right]$$

The relationship between the standardized modularity criterion and the standard cut criterion has been demonstrated in [107]:

$$nmod = \frac{1}{cut(V, V)} (k - 1 - ncut)$$

The technique of automatic determination of the number of classes most suitable for a real partitioning problem therefore seems to be that proposed by Yu and Ding that is to say that based on the calculation of the standardized modularity function. For experiments, it was therefore chosen to apply this method, but also based on the calculation of the gap [104] in order to compare the results obtained.

III.3.4.RESULT AND DISCUSSION

The input data of the unsupervised foot classification process were the vectors came from the feet shape descriptors. These vectors composed of the polar coordinates of the points P_1, P_2, P_3, P_4, P_5 and P_6 allowed us to conceive the similarity matrix W. This matrix defines the degree of resemblance of each foot. The Gaussian similarity was utilized, which has been most commonly used in the field of classification.

Afterwards, the eigenvectors and eigenvalues of the similarity matrix W lead to the spectral representation of data. This representation was carried out according to three main planes. This choice was defined during the eigenvectors projection, according to the eigenvectors which have the most important eigenvalues.

In this spectral representation, K-means method was applied. The criterion of intra-class grouping and inter-class separation of the K-means method takes into account the analysis of the five neighbors during the calculation.

During the calculation iterations, the K-means method has calculated the value of modularity by the criterion of White and Smith. **Figure 52** presents the representative curve of the computation results and shows a maximum of the number of clusters equals "3".
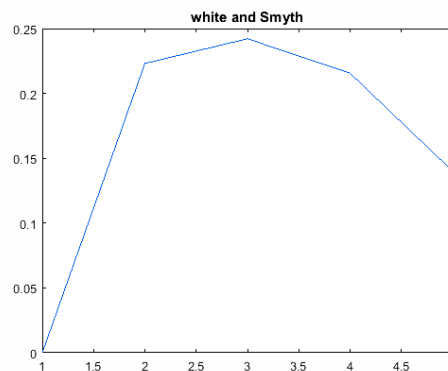
Figure 52 : Modularity value by White & Smith.

Figure 53 gives the spectral representation (two axis view) of this result according to the three projection planes. One might think that the reparability criterion is not sufficient following the superposition of clusters in certain zones which is not the case. Only the 3D space of our spectral representation (three axis view) shows a great separation of the "3" clusters with an appropriate choice of point of view (**Figure 54**).
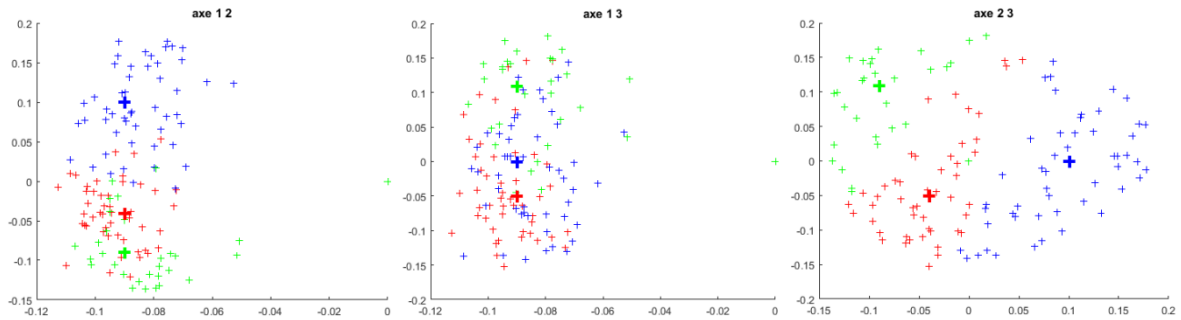
Figure 53 : Spectral representation of the 3 clusters (two axis view).
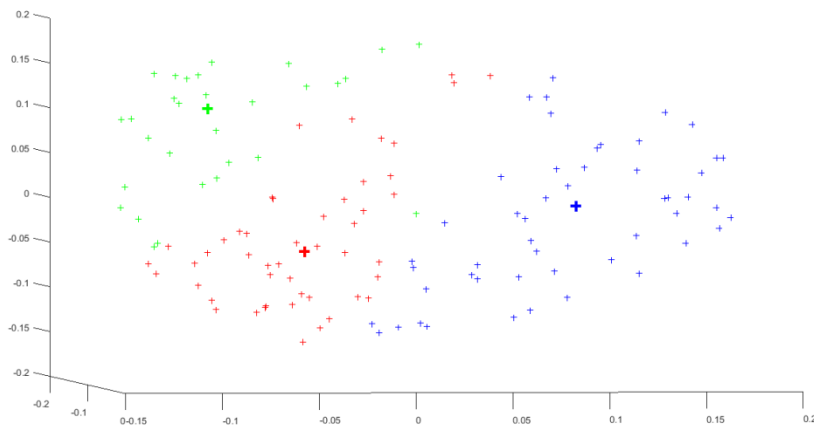
Figure 54 : Spectral representation of the 3 clusters (three axis view).

The 3 shape descriptors (top view) of the 3 centroids for each cluster are presented in **Figure 55**. These descriptors lead to three representative feet of the population. The above shapes have been aligned on the Brannock axis and give below shapes.
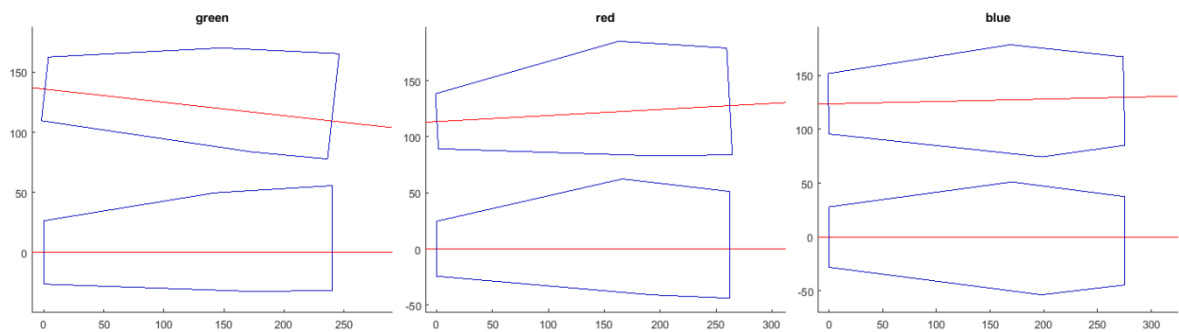
Figure 55: 3D shape descriptors of the centroids of the 3 clusters.

The 3 shape descriptors, 2D feet (bottom view) and 3D feet of the 3 centroids are presented in **Figure 56.**

The analysis of these last results shows a clear difference between the different foot centroids of each cluster. This difference is mainly perceived in 2D with this kind of descriptor which gives an image close to the footprint. By observing the 3D view, this difference is not as noticeable as the 2D view.

If the shapes of these three descriptors are compared, the difference comes from both the variance between the width of the heel and the width of the ball girth, and the difference between the angles of the 1st toes angle (A1: II.2.2) and the 5th toes angle (A2: II.2.2).
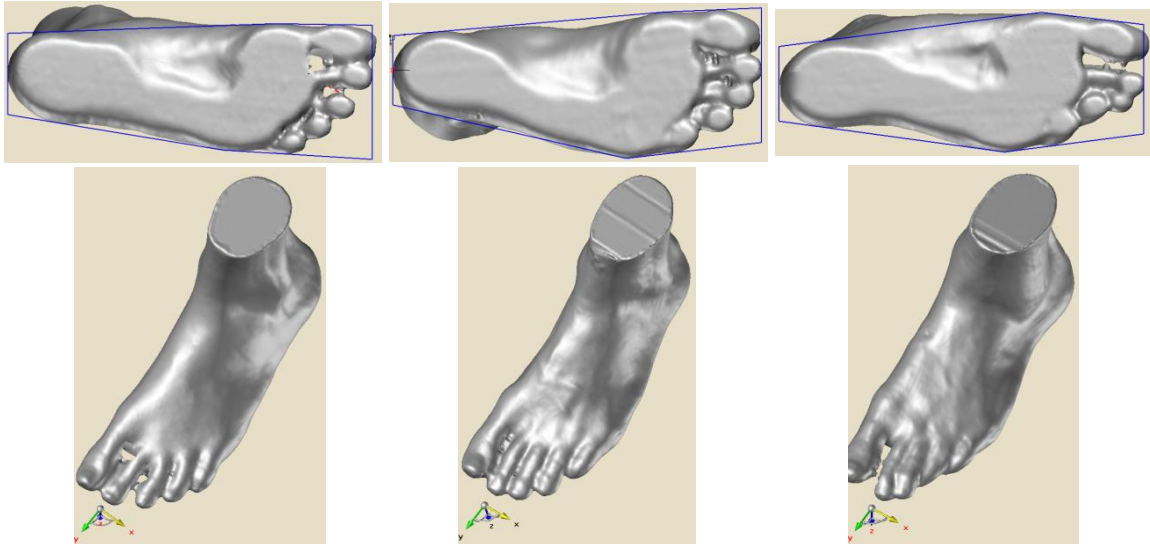
Figure 56 : 3 shape descriptors, 2D feet and 3D feet of the 3 centroids .

III.4.   CONCLUSION

In this chapter, two classification methods have been proposed. The first method was to analyze a male and female foot population to see if there are significant differences between the two sexes. The method has been able to verify the difference which can be taken into account in shoe manufacturing process. Since the method is based on a dimensional criterion, the results can be useful for updating existing size systems. The second method analyzes the shape of the feet irrespective of the gender. Using a 2D shape descriptor which represents the optimal outline encompassing the footprint, it has been classified the previous population into different morphological clusters. This result is very interesting because the different centroids of each cluster can be used to create morphotype shoe-last. These are very useful because they will significantly improve the comfort of the shoes, which is not the case with standard shoe-last that do not take into account this morphological disparity of the feet.

CHAPTER IV: INSOLE CUSTOMISATION

IV.1. INTRODUCTION

The insole creation is not as easy as one can imagine. Different parameters and technical criteria are involved in the creation process. A sole must cushion shocks when you put your foot on the ground, stabilize and align the body in its natural position, or even compensate for differences in leg length.

Bad insoles can cause fatigue in the feet, legs or create musculoskeletal disorders. A bad fit of the foot in the shoe does not optimize the unwinding of walking or running for people or athletes.

Depending on the needs of use (the city, running, hiking, the type of sport ..) or pathology that has been detected by the podiatrist, the role of the insole can be different and the designers of insoles act on the cushioning by gel, on the thickness, on the posture and hygiene, on its lightness and its dynamism, its protection, its insulating power. This product can then be designed in different natural or synthetic materials, multi-material with zoning. It is a very technical element very often using the distribution of the pressure during a medical analysis.

Matter is very important, but good fit foot into the shoe with specific insole is also very important. Also, this chapter is oriented on the implementation of a process of creation of sole adapted to the patient's morphology. This process is in 3D to follow the feet morphology and the inside shoe morphology represented by a shoe-last respecting the industrial size of the patient.

IV.2. MEASUREMENT TEST

Same feet of the patients as of chapter II.3 were taken for testing (**Figure 34**) and followed the same measurement protocol (**Figure 57**).
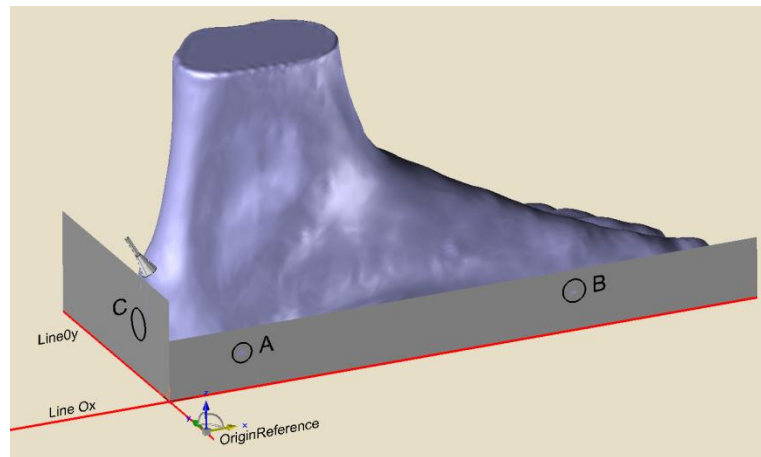
Figure 57 : Contact points detection by plane techniques.

IV.2.1. CUSHION SYSTEM OF THE FOOT

IV.3. PLANTAR SURFACE MODEL

The 3D method used to construct the plantar surface is close to the 2D graphical method proposed by Rigal [108]. The interest of the author's graphical method is to connect various technical data used to design the shoe-last representing the interface between the shoe style and the anatomical information of the foot. For various reasons, the shoe-last, the shoe, the foot and the insole have to be connected in the same design process. For example, the design, shape and volume of the shoe last are crucial for the fit of a shoe. The insole design whose upper form represents the lower part of the foot, have to be connected to the inside part of the shoe i.e. the lower shape of the shoe-last.

This 3D shape association has led us to a plantar surface design process in relation with the shoe-last which passes through four distinct steps which will be described hereinafter.

IV.3.1. GEOMETRY PLOT OF OPTIMAL OUTLINE ENCOMPASSING THE FOOTPRINT

In a first phase, the Rigal's method was carefully followed by adjusting only the dimensional characteristics obtained by the foot scan, i.e.:

- length of the foot (280.6 mm)
- perimeter of ball girth (278.7)
- perimeter of instep girth (282.1)

- length between heel to 5th toe (234)

For this foot size, others parameters have been chosen in the size chart of the database coming from the feet statistical analysis of the French population [108]. The author does not specify the date and the protocol of the measurement campaign, the unique information that has been given is that the statistical analysis has been realized with a men and women sample of 10000.

The data extracted of the size chart are essentially the angle measurements of the footprint, i.e.:

- metatarsophalangeal ball angle OCC' (71°06)
- 1st toe angle ACR' (13°94)
- 5th toe angle S'C'Q' (10°22)

The graphical method to trace outline encompassing the footprint follows the procedure described in the **Figure 58**.
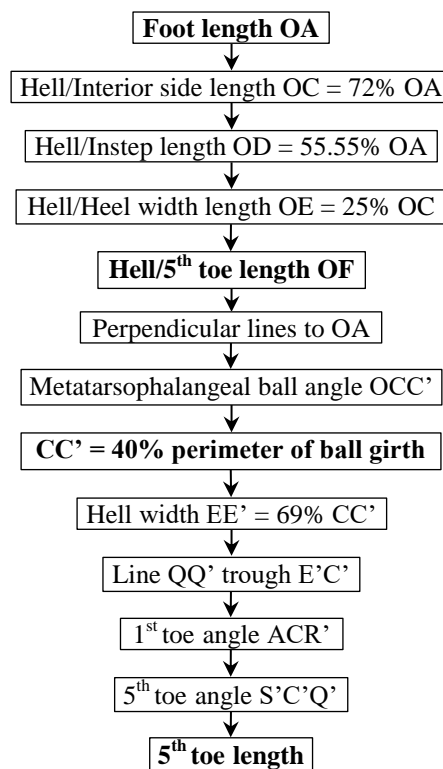
Figure 58 : Outline encompassing the footprint drawing procedure.

Figure 59 shows that the foot is not completely inscribed in the contour formed by the points OCR'S'C'Q. This gap was foreseeable as this procedure is applicable only to average data from the statistical analysis of the foot measurement campaign. By observing this result, it can be seen that a better detection of the contact zones and an adjustment of the different

angles could lead to better results. These two problems can be solved by our contact point's detection techniques by parametric plane (**Figure 60**).

Figure 59 : Rigal's method to draw outline encompassing the footprint.

Figure 60 : Contact points Method to define the optimal outline encompassing the footprint.

Thus, the line QQ' can be adjusted by a plane at two contacts (**Figure 59**). The two angles ACR ', S'C'Q' can then be adjusted by a plane at one contact pivoting respectively in C and C'.

The position of the pivot points C and C' are the two contact points resulting from the preceding search; the point C giving the position of the metatarsal tibiae, the point C' the position of the metatarsal fibular.

The results of the **Figure 61** show that the foot is perfectly inscribed in the new outline encompassing the footprint. The difference with the Rigal's method is that many parameters have been obtained automatically by a direct measurement and these parameters no longer control the shape of this new boundary.
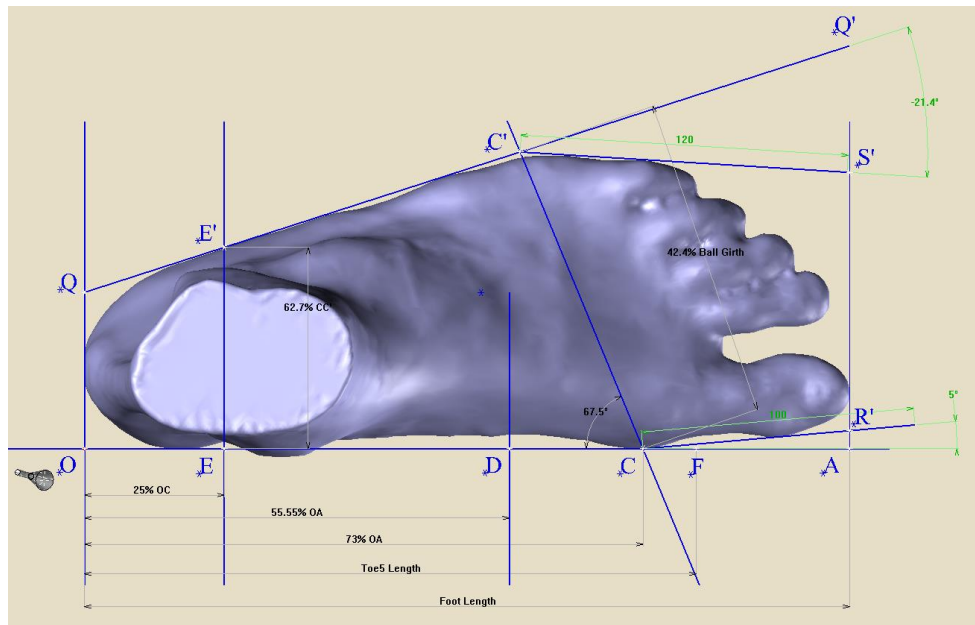
Figure 61 : Optimal outline encompassing the footprint**.**

The new values of these measurement data are:

OC = 73% OA, CC '= 42.4% Ball girth, EE' = 62.7% CC ', Angle ACR' = 5 °, Angle OCC '= 67.5 °, Angle S'C'Q' = 21.4 °.

The foot length can also be detected by a plane R 'S' perpendicular to the line OA and tangent on the extremity of the 1st toe. The new value OA defining the foot length is 280.2 mm which represents a French size close to 44. The conversion of the foot length to the French size (abacus from [108]) is given by the following equation:

$$Shoe\ size = \ 0.1602 * \text{FootLength} - 0.6607$$

IV.3.2. CONNECTION BETWEEN OUTLINE ENCOMPASSING THE FOOTPRINT AND THE SHOE-LAST

At this stage of the study, the good shoe last could be chosen according to the shoe size in order to know the inner shape of the shoe. **Table 8** gives us the evolution of the numbered shoe-last according to the shoe size. For example, if a shoe last of 6th was taken for a shoe size of 44, the finger perimeter of the shoe-last would take the value 250. This finger perimeter and the ball girth perimeter of the foot are connected by a value of ease allowance. For a better foot support in the shoe and increase comfort, the shoe last has to be longer and

narrower than the foot. Their length and volume depend on the type of shoe. For example, for a sandal, required increment in the length of 2%, of 3% for square toe, 4% for round toe and so on. In the case of this thesis, the number of the shoe last was 8th (ball girth perimeter = 277.4, finger perimeter = 260).

Table 8 : "Point de PARIS" of the shoe-last according to the shoe size (mm).

Shoe size	Width							
"Point de PARIS"	1st	2nd	3rd	4th	5th	**6th**	7th	8th
33	170	175	180	185	190	195	200	205
34	175	180	185	190	195	200	205	210
35	180	185	190	195	200	205	210	215
36	185	190	195	200	205	210	215	220
37	190	195	200	205	210	215	220	225
38	195	200	205	210	215	220	225	230
39	200	205	210	215	220	225	230	235
40	205	210	215	220	225	230	235	240
41	210	215	220	225	230	235	240	245
42	215	220	225	230	235	240	245	250
43	220	225	230	235	240	245	250	255
44	225	230	235	240	245	**250**	255	260
45	230	235	240	245	250	255	260	265
46	235	240	245	250	255	260	265	270
47	240	245	250	255	260	265	270	275
48	245	250	255	260	265	270	275	280

The graphical method to trace the lines connecting the outline encompassing the footprint and the shoe-last follows the procedure described in the **Figure 62**.

Foot last length OB = 1.04
↓
Perpendicular line BS'' to OB
↓
H & G Middle points of EE'& CC'
↓
Fitting axis HG
↓
II '= 42.4% finger perimeter centered on
↓
JJ '= 62.7% of II' centered on
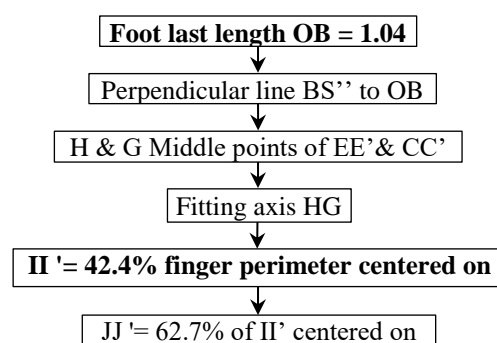
Figure 62 : Outline encompassing the footprint drawing procedure.

The procedure shows that the shoe last length is proportional to the foot length (increasing of 4% due to the round toe). The fitting axis is given by the direction of the line passing through the midpoints H of EE' and G of CC'. These red lines represent the projection of the outline encompassing the shoe-last (**Figure 63**).
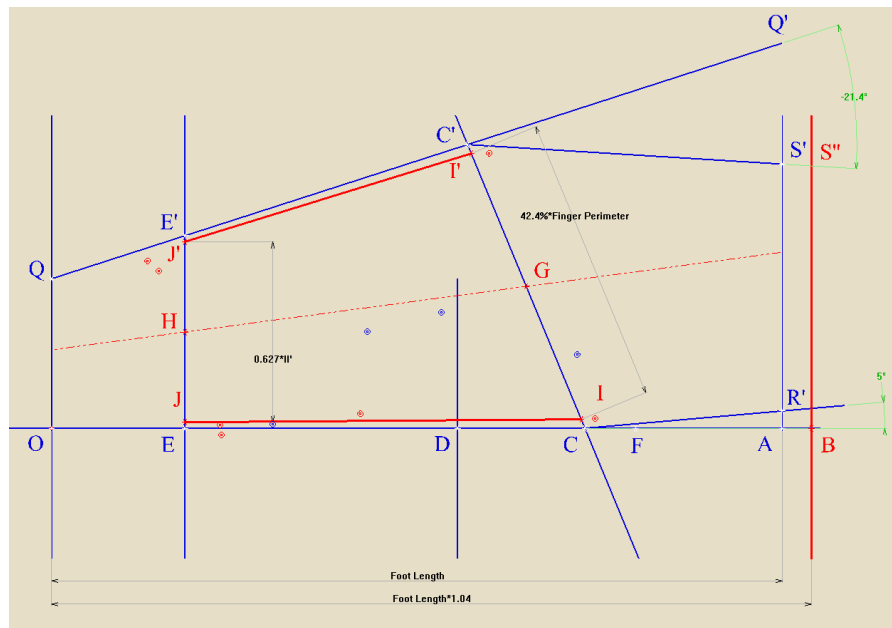
Figure 63 : Projection of the outline encompassing the shoe last.

IV.3.3. CHARACTERISTIC POINTS IDENTIFICATION OF PLANTAR SURFACE OF SHOE-LAST

The graphical method to locate the position of the characteristic points of the plantar surface follows the procedure described in the **Figure 64**.
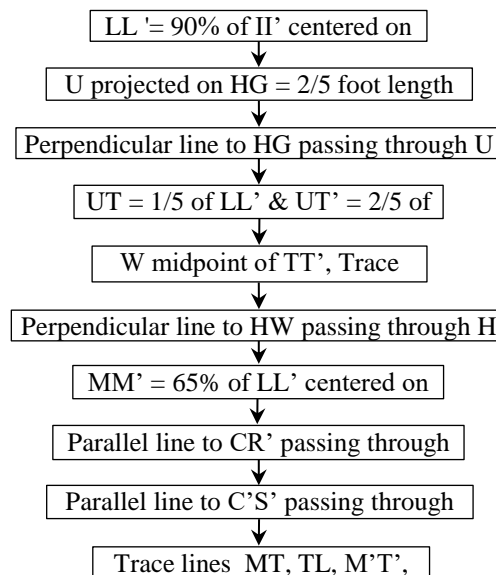
Figure 64 : Locating the position of the characteristic points of the plantar surface of the shoe last

The first step consists in positioning the points LL' distributed at an equal distance from the point G defining the plantar surface width (**Figure 65**). Then, the narrowest part of

the foot arch was to be located. Its position is defined with respect to a point situated on the axis OA, proportional to the length of the foot. U represents the projection perpendicular of this point on the fitting axis HG.

On a line perpendicular to the fitting axis passing through U, two points T and T' are located to define the width of the narrowest part of the foot arch. The midpoint W of the points T, T' and the point H make it possible to trace the symmetry axis of the heel. On a line perpendicular to the symmetry axis of the heel passing through H, two points J and J' are located to define the heel width. The heel extremity is generated by a circle of diameter MM' whose center can slide on the symmetry axis of the heel in order to control the distance between this circle and the axis OQ. This distance is conditioned by the shape of the rear curve of the shoe last. The extremity point of the plantar surface end is tangent to BS''.
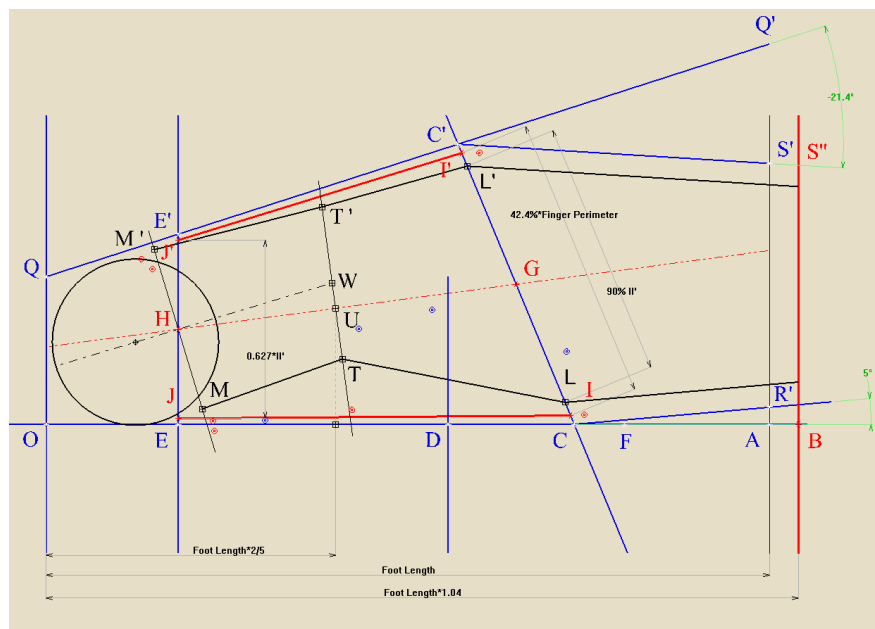
Figure 65 : Characteristic points of the plantar surface of the shoe last.

IV.3.4. OUTLINE OF PLANTAR SURFACE CONTOUR

The follow-up of this plot gives us a curve representing the plantar surface (**Figure 66**: red curve).
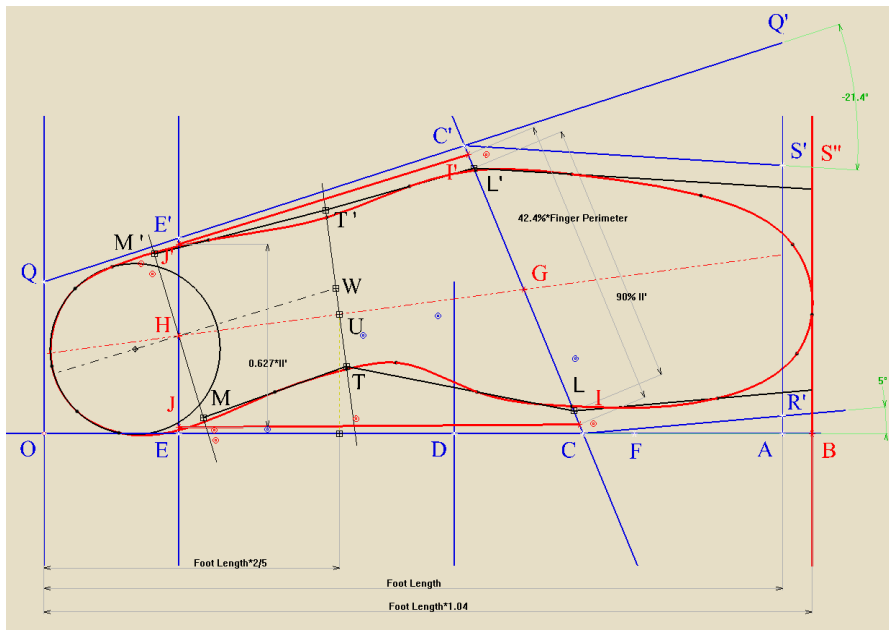
Figure 66 : Drawing the outline of plantar surface contour.

When the plantar surface compared with the foot, it was noticed that the curve perfectly follows the contour of the foot with a decreased ratio conforming to the design of a shoe-last (**Figure 67a**). The pressure of the foot on the scanner glass also gives a good match with the plantar surface (**Figure 67b**).
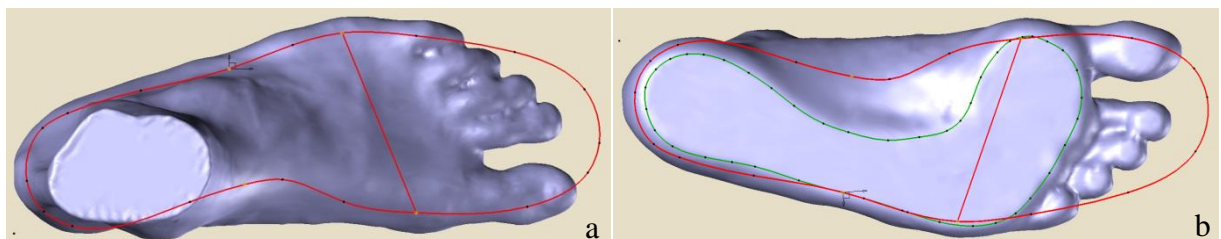
Figure 67 : Matching between the foot and the outline of plantar surface contour.

IV.3.5. ANALYSIS BETWEEN FOOT AND SHOE-LAST

In a first analysis, it can be interresting to compare the foot with the shoe-last choosen in the good range of size. **Figure 68a** shows that the two shape are quite close. It was noticed that the edge to the fingers corresponding to the 6th width of a shape was not verified because the shape was given for a width.

In this case, it is necessary to adjust the shoe-last to take into account the width of the foot larger. A homothetic ratio 1.076 on the shoe-last with ball girth value of 250mm was carried out in order to obtain the good ball girth value of 269mm (**Figure 68b**). It was considered considered that the number of the shoe-last was 9th, beyond the limit of **Table 8**.
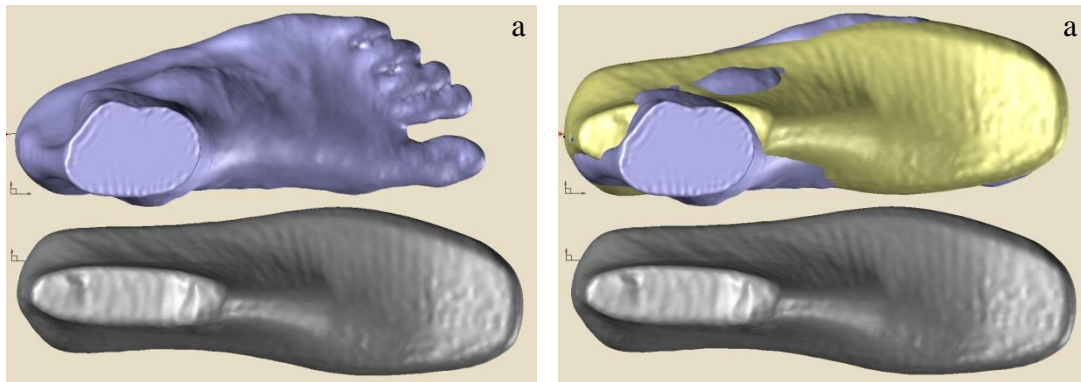
Figure 68 : Adjustment of the shoe-last.

This adjustment of the shoe-last makes it possible to check if the insole which has been adapted to the foot morphology correctly follows the shoe-last one which represents the inner part of the shoe. **Figure 69** shows that the front part of the plantar surface perfectly follows the shoe-last morphology. But the back part has an offset at the heel which will be necessary to take into account by slightly reorienting this area by the inclination of the axis TWT' (**Figure 66**). This adjustment will be made later on the lower part of the sole when it is created in 3D.
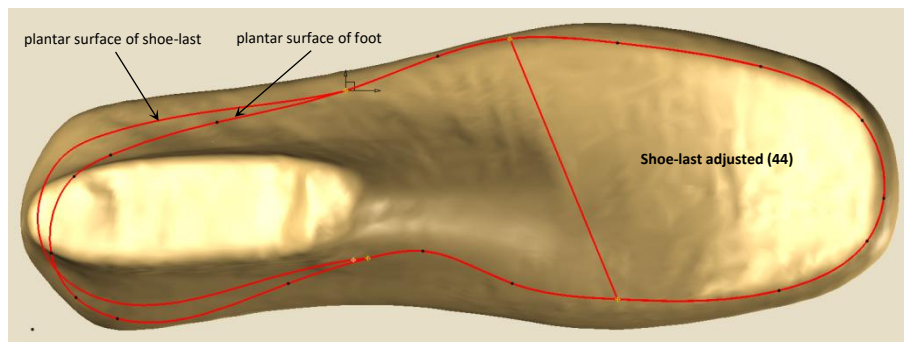
Figure 69 : Plantar surface difference between foot and shoe-last ajusted.

IV.4.   INSOLE 3D MODEL

The knowledge of the plantar surface is important because it represents the strategic outline to represent the 3D shape of the insole. At this stage of the design process, it was required to look for the contact areas between the foot and the shoe-last in order to create an insole morphologically fitted to the patient's foot. This creation required to take into account the previous constraints by using the two plantar surfaces: plantar surface of the foot and plantar surface of the shoe-last.

IV.4.1. 3D BELOW SURFACE OF INSOLE

The below of the insole should represent the contact area with the boot, i.e. the bottom surface of the shoe-last. The 2D contour is represented by the plantar surface of shoe-last in **Figure 69.** A printing of this 2D contour was first made on the shoe-last to obtain its 3D representation connected to the shoe-last (**Figure 70a**). Then, the mesh of the internal surface of this printed contour (**Figure 70a**) was made in order to create a 3D surface representing the bottom surface of the insole (**Figure 70b & c**).
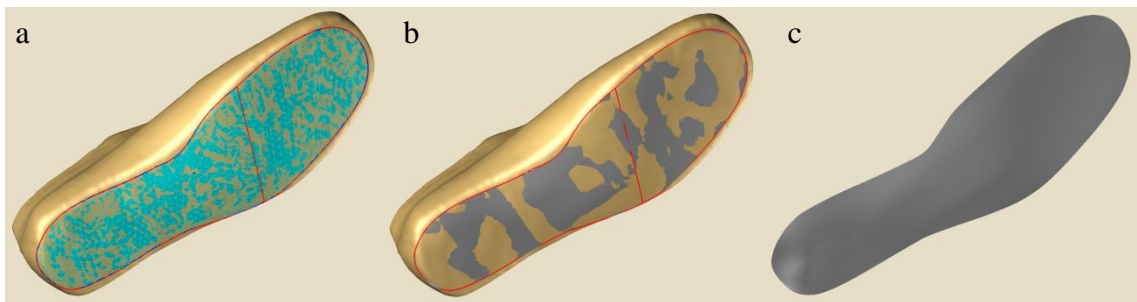
Figure 70 : Creation process of the insole below surface.

IV.4.2. 3D ABOVE SURFACE OF INSOLE

The above of the insole should represent the foot contact area, i.e. the bottom surface of the foot. The 2D contour is represented by the plantar surface of the foot in **Figure 69**. This outline was separated into two parts cut by the line of the ball girth (**Figure 71a**). This contour has been split into two sections cut by the ball girth line (**Figure 66a**). Two printings of this 2D line were made: one on the back part of the foot, the other on the front part of the shoe-last (forepart). It was printed on the front part to take into account the value of the toe spring measurement of the forepart, according to the 3D shoe-last shape. In addition, the forepart of the shoe-last does not present the misalignment of the backpart.
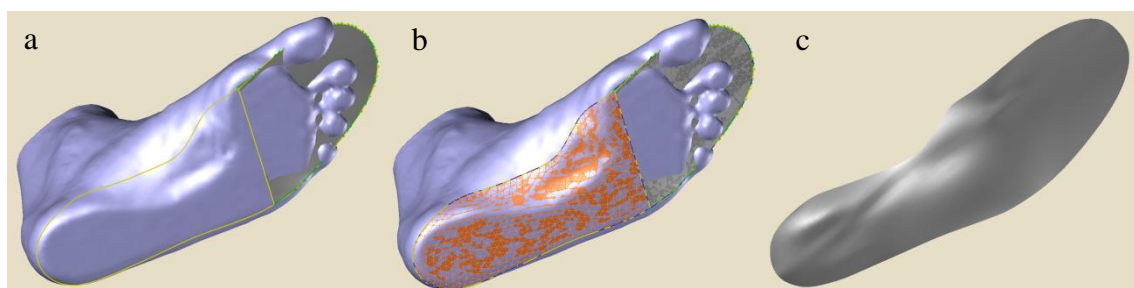
Figure 71 : Creation process of the insole above surface.

Then, the mesh of each inner surface of these printed contours (**Figure 71b**) was made to create two 3D surfaces. These surfaces were sewn to obtain the upper surface of the insole (**Figure 71c, Figure 72a**).

IV.4.3. 3D INSOLE

On the contours of the above and below surfaces of the insole (**Figure 72a**) is created a peripheral surface to create a closed continuous surface (**Figure 72b.c**). These three surfaces are then sewn to obtain the final surface of the 3D insole (**Figure 72d**).
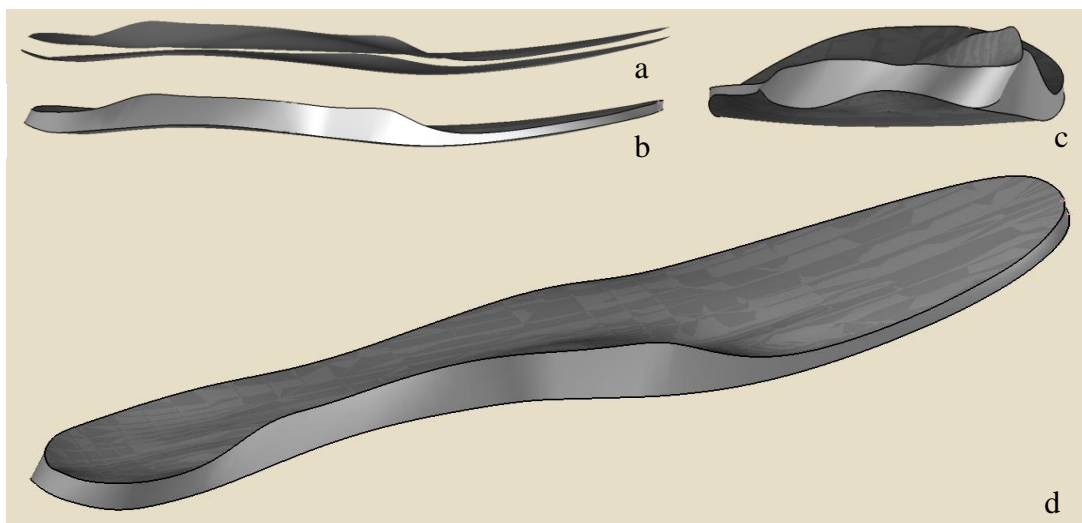
Figure 72 : Création process of 3D insole surface.

IV.5. CONCLUSION

This study was carried out with a shoe-last standard in order to respect the existing standards of the footwear industry. The analysis of the interface between the shoe-last and the adjusted insole showed a significant difference between the morphology of the shoe-last standard and the foot whose morphology was taken at random from our database. This gap forced us to adjust the underside of the footing showing an unbalanced 3D deformation (**Figure 72c**). This phenomenon can in some cases lead to a lack of comfort if this adjustment is too high. Also, future work has been focused on the implementation of shoe-last adapted to the feet morphology in order to perfectly adjust this inseparable block represented by the foot, the insole and the shoe-last.

CHAPTER V: SHOE-LAST CUSTOMIZATION

V.1.   INTRODUCTION

The shoe-last is the essential element to design a shoe as the style of the pattern is directly designed in 3D on the shoe-last. It is also a solid shape around which a shoe is molded with a specific paper. The fitting and comfortable of a shoe depend on the design, the shape and the volume of the shoe-last. A large number of forms exist because they are related to the style of the shoe. Thus, a given form corresponds to a shoe style. Many styles exist according to the rate of covering of the foot, the height of the heel ... But it was required not forget that the form must be associated with the measurements of the foot in order to bring the comfort and the good unfolding of the foot, criteria which were often degraded following a chosen style (example with heel). Therefore, a functional analysis of a shoe-last was required to be carried out in order to better understand the specificity of each zone. An analysis of the 2D/3D ease allowance between the foot and the shoe-last must then be performed. This will allow integrating the useful data of the comfort and the dynamics of the unfolding of the step on our 3D graphical model of the shoe-last customized. The respect of the shape of the foot and the comparison with works done in orthopedics will validate the overall concept of creation.

V.2.   SHOE-LAST ANALYSIS

To quantify the proportions and the volume of the shape, the anthropometry of the foot applied to the shoe-last makes it possible to extract its main measurements relating to the different lengths, heights, widths, and angles. Two main measures can be used to codify a given shape, i.e. the footwear length and the ball girth perimeter (In French; périmètre aux doigts). Depending on the type of items may be added other secondary measures such as the instep perimeter for items covering the upper foot area, heel/instep distance (55.5% total length LMF: Length Mean Form) for high stemmed items like boots or boots.

The characterization, the design of a shoe-last must follow basic rules. These rules define at first the vamp point, the front part and back part dividing the shoe-last in two lengthwise parts, and lead to measuring the total length of the shape (**Figure 73**).
The characteristic lines and contours defining the morphology and the measurements of the shoe-last are:

- Line AB is a line defined between the extremum points A and B of the shoe-last. This straight line is aligned with the Brannock axis of the shoe-last which makes it easy to detect these two extremum points. The distance between A and B represent the reference total length LMF.

    Chen [1] consider that A is a mid-toe point on the featherline, the point B is a mid-heel point at 1/3 way up from shoe-last featherline to the topline backseam tack point K. The back-hell height HS is about 66mm (22% of LMF). Now, line AB is a curve which passes around the lateral border of the shoe-last.

- Curve DE is drawn on the upper ball girth so that line DE intersects line AB at point C (1/3 of the total-length of the forefoot by Chen). The vamp-point G is located at the intersection between the metatarsal-line DE and the front center line of the forefoot.

- Curve GH is drawn on the upper ball girth. The point H is located at the intersection between the mid-last shoe curve (50% of LMF value) and the front center line of the forefoot.

    Chen considers that the mid-line AG is continued up and the topline marked at point H follows these proportions: AG: GH = 2/3:1/3.
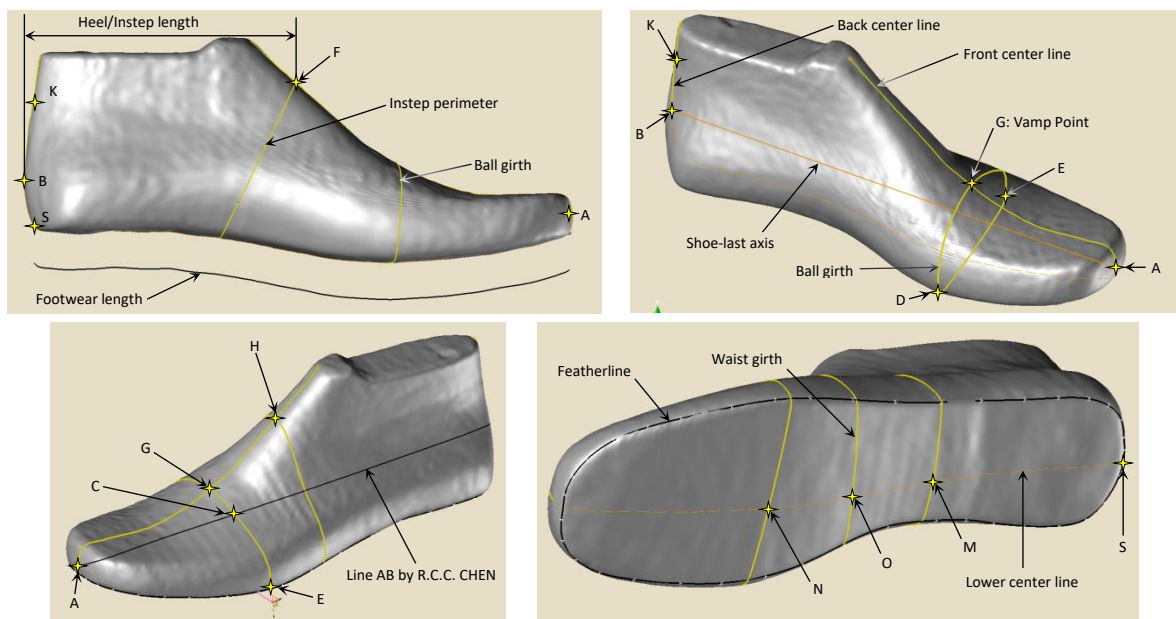
Figure 73 : Caracteristic lines of the shoe-last.

The waist girth is a curve defined between the ball girth and instep girth. This curve passes through two characteristic points. The first point L is located in the middle of the points GF on the front center line; the second point O is located in the middle of the points M, N representing the intersections between the lower center line and the ball and instep girths.

Other complementary lines can be represented on the shoe-last to help the designers to create the lines of styles delimiting the shoe's patterns (**Figure 74**), i.e.:

- Two points I and J are placed on either side of the point G on the ball girth DE, on the line GE for the point I, on the line GD for the point J. From these points are drawn two lines, one representing the lateral line IK and the other the medial line JK for join the top-line point of the heel.

- Two lines starting H are drawn on both side of the shoe-last to join the lines IK and JK. Their paths follow the mid-last shoe curve.

- To design the topline, a freehand line is drawn from the point K, using the lateral line IK and the medial line JK as a guide lines and dropping 5mm below these lines under the malleoli, then again blending upwards to the topline point H, following the two previous lines drawn from H.
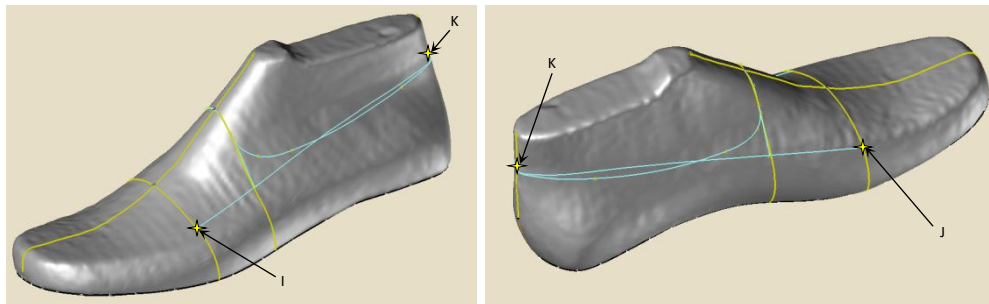
Figure 74 : Design curve on the shoe-last.

But the morphology of a shoe-last does not depend solely on the lines and contours previous, the shape and the camber of the bottom center line characterizes the reach of the shoe-last on the ground (**Figure 75**). This reach is conditioned by the height of the heel which, depending on its height (3.55 cm), rotates the shoe-last on the crucial point: tread point. From this point are defined two areas: the forepart and the backpart.

The forepart represents the raised part of the end of the shoe-last. It is characterized by the toe spring measurement. Raised the end of the shoe-last aims to facilitate the progress of the step when walking, so also depends on the activity (Dress, casual, sport hiking, work, sandal, mocassin, …). Raised the tip also acts on the upper part of the shoe because this curvature avoids the formation of folds on the top of the shoe at ball girth. The height or angle at the end is proportional to the height of the heel.
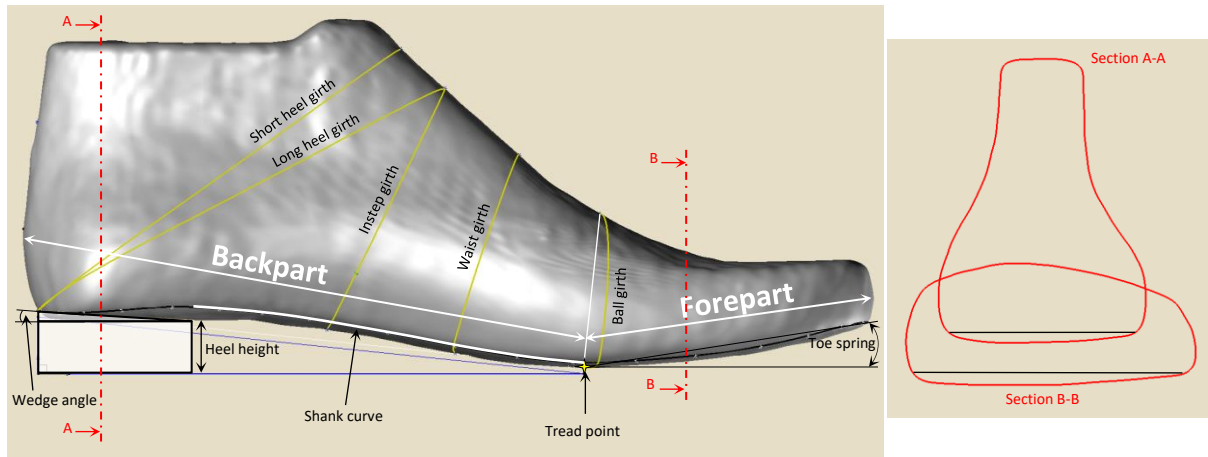
Figure 75 : Analysis of the shoe-last reach on the ground.

The backpart is separated into two areas: one depends on the wedge angle, elevation and length of heel, the other is represented by the shoe-last shank curve. The heel height is a parameter defined according to fashion trends and is very dependent on toe spring measurement. The curvature of the shoe-last shank curve, for a given length, also varies according to the height of the heel and follows the parametric shapes described by Luximon et al. [91] (**Figure 76**).

The alignment of the curves shows that the more the shape is arched, the more the posterior part approaches the anterior part while respecting that the length of the plantar arch of the shoe-last must be identical to that of the foot. This deformation imposed on the median curve of the plantar arch necessarily leads to a lack of comfort. Toe spring, heel height and tread point are the three key elements to ensure fitting well and comfortable.
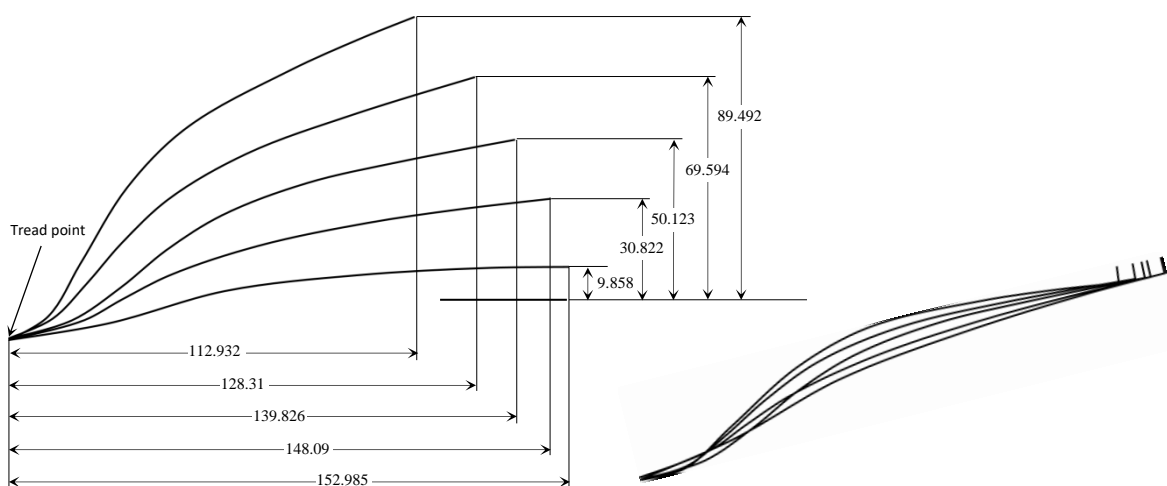
Figure 76 : Shoe-last shank curves (length curves = 155mm).

One of the particular morphologies of the shoe-last is the bulge of its lower part. The bulging of the underside of the forefoot acts on the shoe-last reach on the ground and limits the formation of folds on the top of the shoe. The bulge of the heel nesting favors the base of the foot in the shoe. The order of magnitude of this difference is 5 mm.

V.2.1. BOTTOM ANALYSIS

Data on the length, width and external shape of the bottom of the shoe-last are extracted from the plantar surface of the foot. It was from the outline encompassing the footprint of the foot placed on the ground that this plantar surface could be traced (**Figure 60, Figure 61**). The technique used was described in chapter IV.3.4 and gave the result of **Figure 66**. It is important to note that this technique already incorporates ease in the direction of the length of the shoe-last. This surface must be morphologically defined in its longitudinal section by the arching of the footwear line (bottom center line) described by the analysis of the shoe-last reach on the ground.

V.3.   ANALYSIS OF EASE ALLOWANCE BETWEEN THE FOOT AND SHOE-LAST

V.3.1. TOP ANALYSIS

The different morphological contours such as: instep girth, waist girth, ball girth, short and long heel girths, front and back center lines, contribute strongly to the definition of the shoe-last volume, i.e. the inner envelope of the shoe. The ease allowance between the foot and the shoe is therefore related to the different gaps between each respective contour between the foot and the shoe-last.

Few works have analyzed the ease allowance between the foot and the shoe-last. The research work that was chosen for this thesis was the most thorough in this field was done by Chen in 1993. Author's study is very complete because he analyzed the space between the foot of a person and two shoe-lasts, as well as the fit of a shoe according to the ease allowance for many carriers. A set of cross-sectional contours spread over the length of the foot at intervals of 5 mm and 15 mm according to these needs allowed him to analyze the gap between the foot and shoe-lasts. The interest of this study is that the first shoe-last was selected in the range of those used in orthopedics (model last (116028) for low-heeled shoes, the second shoe-last was chosen close to the shape of the shoe-last of the wearer (model last H6028S). The shape of the second shoe-last was adjusted to the wearer's measures by a senior orthopedic model last maker.

The adjustment procedure has been described in its document and follows the following steps:

- Draw the outline of the foot on a sheet and take the necessary measurements on the foot,

- Select le last shoe to match the required measures (stick length, heel to ball length, forepart width, ball girth and heel pitch height),

- Verify the shoe-last size with this formula:

    Last length = foot length + 1 1/2 shoe sizes (about 1.27 cm)

- Mark all reference positions on the last and the paper,

- Respect all ease allowances imposed by insole thickness (see **Figure 77**, **Table 9**),

- Modify the shape of the shoe-last by adding material or sanding off (the reference positions and measures have to be verified all time, especially for heel to ball length and ball girth).
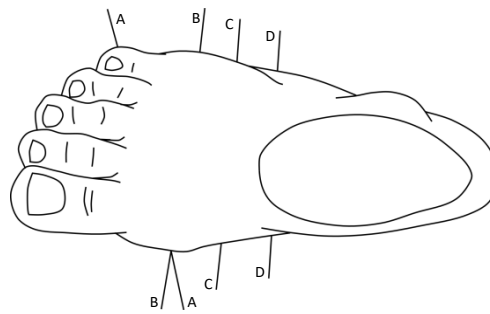
Figure 77 : Reference for shoe-last allowances.

Table 9 : Shoe-last allowances required vs. insole [1].

Insole	Allowances required			
	A	B	C	D
None	12 mm	6 mm	3 mm	3 mm
3 mm	25 mm	18 mm	12 mm	12 mm
4 mm	28 mm	25 mm	15 mm	15 mm
6 mm	31 mm	28 mm	18 mm	18 mm

This information is very interesting because it defines a strategy of ease allowance on the front of the shoe-last. It is noticeable that the ease allowance in the longitudinal direction of the shoe-last is defined from the shoe-last length, the foot length, and the shoe sizes. In the transverse direction of the shoe-last, it is necessary to take into account the thickness of the insole whose value depends on the place or contour to be taken into account.

But other factors intervene in the ease allowance of the top that led us to create and analyze cross-sectional contours with a similar approach to those of Chen. Cross-sectional contours were taken from toe-cap region (z = -230mm) to throat point (z = -95mm). The distribution of cross-sections taken at intervals of 15mm makes it possible to analyze toe-cap contours at z = -230 mm, toe-cap 2 at z = -215 mm, big-toe at z = -200 mm , little-toe at z = -185 mm, 1st metatarsal-head at z = -170mm, 5th metatarsal-head at z = -155 mm, instep at z = -140 mm, instep-throat 1 at z = -125 mm , instep-throat 2 at z = -110 mm, throat 2 at z = -95 mm. **Figure 78** shows the tracks taken from [1] such as: H6028S and a mixed (segmental) line for the original shoe-last stock H6028.
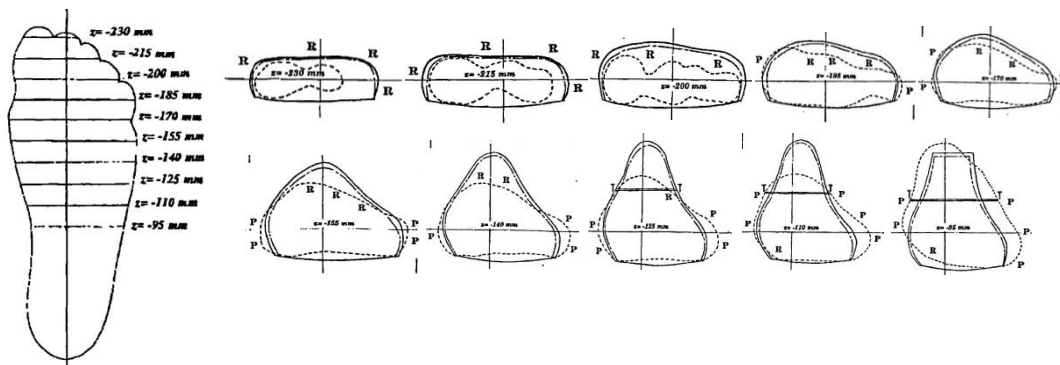
Figure 78 : Contours positions, cross-sectional contours [1] .

In order to make the most of these Cross-sectional contours and to understand how the 3D comfort is distributed between the shoe-lasts and the foot, it was necessary to set up a reverse process to visualize in 3D the 3 shapes. The process of 3D reconstruction of these 3D objects requires digitizing cross-sectional outlines, repositioning them spatially and creating a surface for each 3D object (foot, shoe-last H6028, shoe-last H6028S).

The 3D reconstitution process follows the following steps:

- Scan the different figures (foot surface, cross-sectional outlines) and import them into a 2D / 3D CAD (**Figure 79a.b**),

- Create a C-spline curve for each contour (**Figure 79b.c**),

- Scale the curve representing the outline of the foot with 230mm length measurement as a reference (**Figure 79a**),

- Position each contour on the end points A of the different lines representing the cutting plane (**Figure 79a.c**),

- Scale each curve representative of the cross-sectional contours by taking the scale ratio taken between the ends [A,B] et [A',B'] of the cut lines (**Figure 79c**),

> *Ratio = foot width of the plantar surface / foot width of the cut measured on the horizontal axis realigned with the plantar axis*

- Creation of new cross-sectional contours in a plane perpendicular to the plane of the plantar surface by rotation of 90° with respect to the axis of the plantar surface (**Figure 79f**),

- Rebuild of the 3 volumes by a surface nurbs (**Figure 79 g, h & i**).
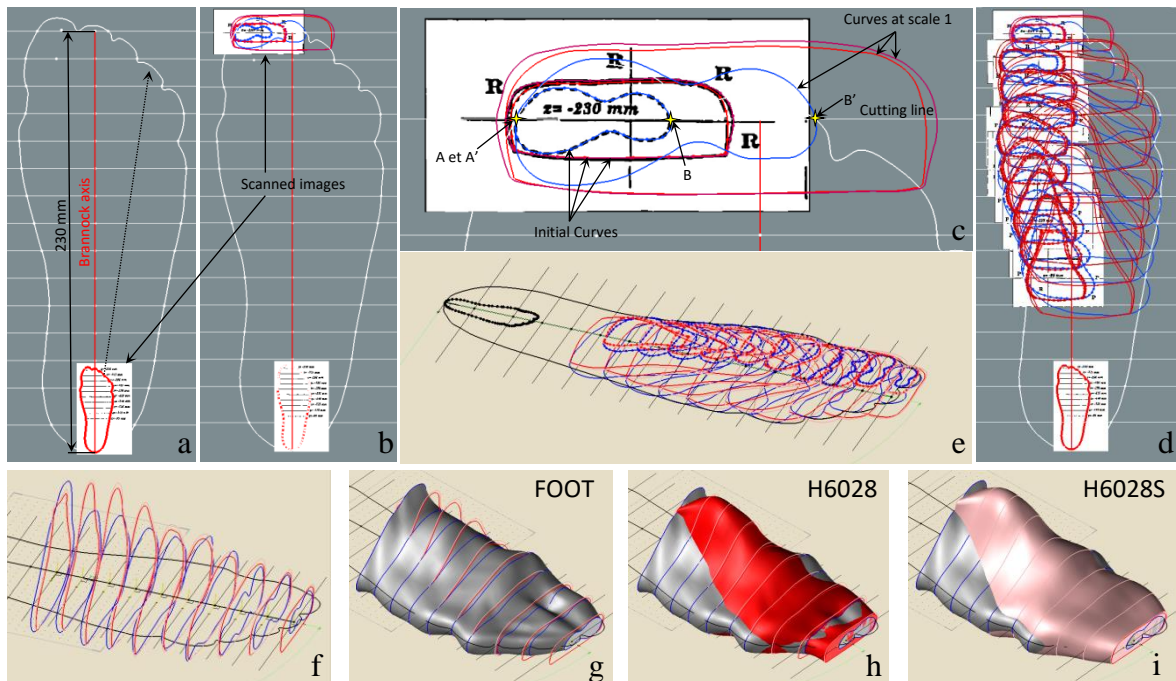
Figure 79 : Reverse engineering process to reshape the foot and the shoe-lasts.

The results show the interest of showing the wearer's foot, as well as the shoe-lasts in a 3D space that was not present in Chen's works. Imperfections appear in the area near the instep girth because it has been taken into account the last contour at z = -95 mm which cause these edge effects. The wearer's foot seems to have some imperfections at z = -95 mm which may be due to a deformation of wearer's foot induced by their diabetes (the heart of this work). On the other hand, the transparency allowed us to check a good coherence on the choice of shoe-lasts. The H6028S has a tendency to better follow the wearer's foot. The morphology of the shoe-lasts does not follow the foot morphology, it is only from the measurement of the ease allowance between the foot and shoe-lasts for each contour that the analysis can be more thorough.

The relationship between cross-sectional girth and width is illustrated as **Figure 80**. The results show that the original stock shoe-last H6028 is slightly smaller than made to measure shoe-last H6028S. The girth of the original stock shoe-last H6028 is about **1.7%** on average bigger than that of the foot and the girth of the made to measure shoe-last H6028S is about **6.1%** on average bigger than that of the foot. But between the value z= -170 mm and -155 mm, the averaged girth measurement of original stock shoe-last H6028 is about **0.3%** smaller than that of foot. This negative ease allowance can be explained because it is a region very close to the ball girth. The trend is to add more ease allowance value (**4-6%**) in the case of made to measure orthopedic shoe-last.
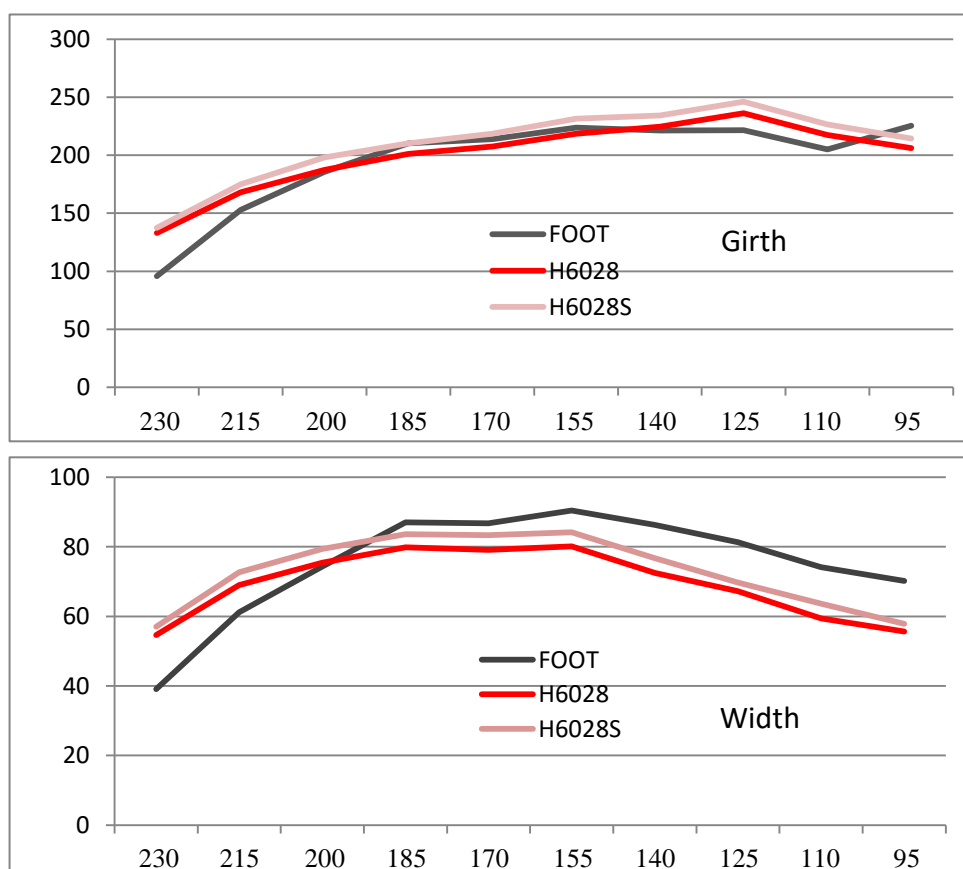
Figure 80 : Difference cross-section girth & width between foot and the two shoe-lasts.

The 1D ease allowances between cross-sectional width and stick length is illustrated as **Figure 81 .** The results show that the averaged width of the original stock shoe-last H6028 is about **8.6%** less than that of the foot. The averaged width of the made to measure shoe-last H6028S is about **6.3%** less than that of the foot. Further analysis shows that between z=-95 mm and z=-185, the cross-sectional measurements in both lasts are narrower than those of the foot, between z=-200 mm and z=-255 mm (ie. toe region) the cross-sectional measurements

are wider than those of the foot. Between z=-50 mm and z=0 mm (i.e. ankle-heel region), also that the cross-sectional measurements are wider than those of the foot.

The analysis of all the results on the forefoot shows that the 3D shape of the shoe-last is completely different from that of the foot. But, after analysis of the cross sectional contours, it was obvious that the difference between shoe and the last was not so different. In the ball girth area, ease allowance is close to 0 (tight). In the region of the toes, the ease allowance is very strong that can be explained later in the dynamics of the foot. In the region of the metatarsals, the ease allowance is slightly positive (loose) because this zone must allow the passage of the foot when one puts on their shoe while maintaining good support of the foot with the use. The area of the widest contour (ball girth) must be able to cross this zone.
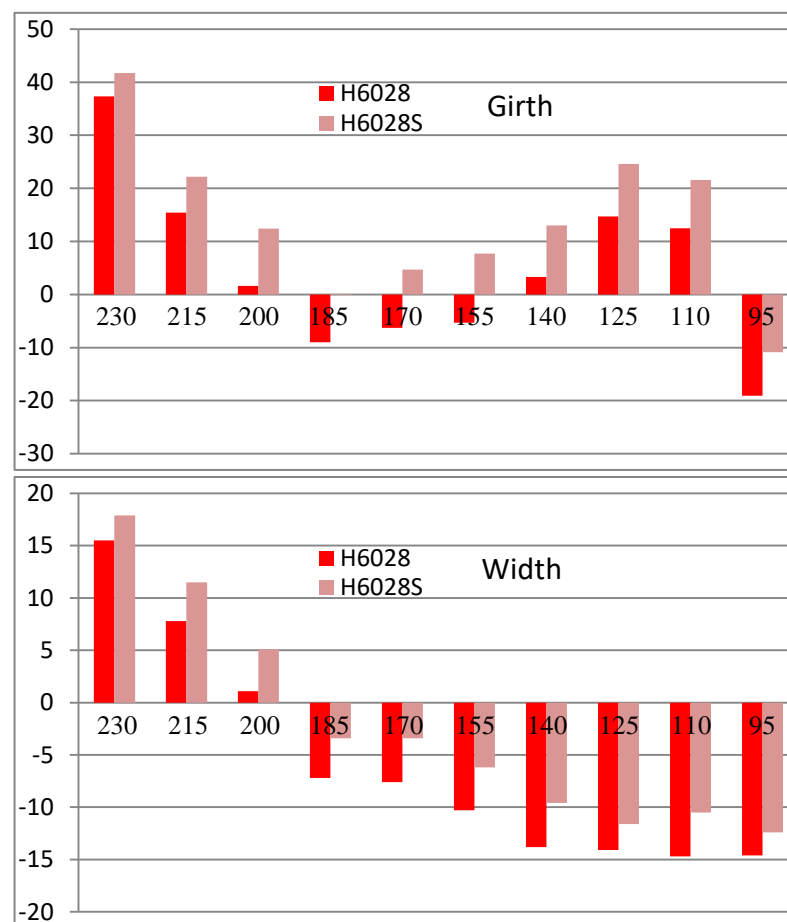
Figure 81 : 1D Ease allowance between foot and the two shoe-lasts.

Finally, worn under the well fitted, the shape and circumference of shoe and foot should be correctly matched at the ball joint region, i.e. the shape and girth of outer material (shoe) and the inner material (foot) should be conformed.

In order to achieve this fit, both the foot and shoe need to be molded together in order to find a new balanced shape. The shoe will be flattened to take the shape of the foot and will

be expanded to these sides. The foot will be deformed into a rounder shape. **Figure 82** illustrates the effects of this global deformation on the cross-sectional contours
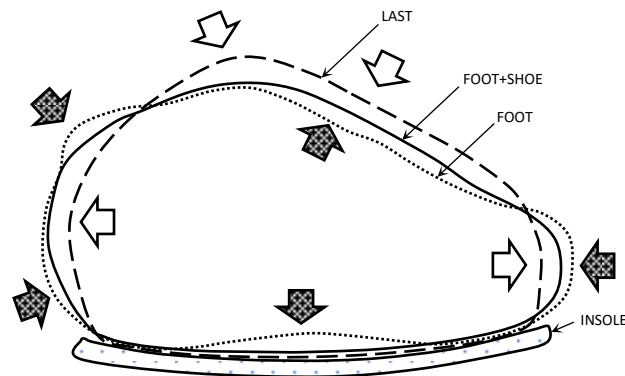
Figure 82 : Foot and shoe molded to be under the good-fit condition.

V.3.2. DYNAMIC ANALYSIS TOWARDS THE LENGTH

Previously, a first analysis of the bottom of the foot was carried out which was dependent on the plantar surface and the longitudinal section at the level of arching of the footwear line. But the morphology of the underside of the foot is also dependent on the dynamics of the foot. Two phenomena act at the level of the plantar vault and at the level of the toes, i.e.: the weight-bearing extension et the toe extension.

As shown in **Figure 83**, the weight-bearing extension is due to the weight of the wearer during standing who acts on the different arches. The principal functions of the longitudinal arches (medial and lateral arches) and the anterior arch of the foot are: keep the whole foot in balance, absorb major shocks. During the standing, the body weight acts on these arches and modify them in flattening of the longitudinal arches in length and the anterior arch in width which results in the weight-bearing extension. The overall value a+b, difference related the weight-off and weight-on positions, is in the range of **5.7 mm**
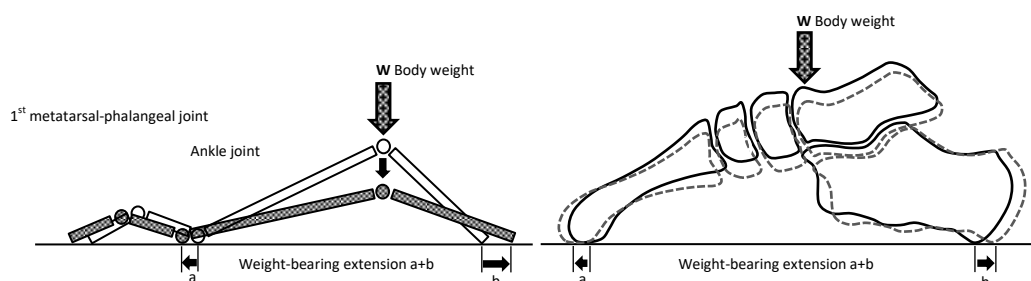
Figure 83 : Weight-bearing extension between weight-on and weight-off positions.

_

The toe extension is due to the unwinding of the foot during the walk. This extension is not the same depending on the type of toe and the morphology of the foot (the Egyptian foot, the Greek foot, The Polynesian foot). For example, **Figure 84.a** shows the extension c of the big toe during the evolution of the metatarsal-head from a position 1 (mid-stance position) to a position 2 (push-off position). During this evolution, the body weight thrust moves forward onto the region of the 1st metatarsal-phalangeal joint which causes the phalanges to move in a given direction. This displacement is due to the displacement of the notional axis of rotation during the pivot on the ground of the medial sesamoid bone.

For the other toes, the situation is different because they do not have sesamoid bones. It is the metatarsal-heads who play the role of pivot point in a rolling and gliding movement. **Figure 84.b** shows the extension d of the toes during the evolution of its metatarsal-heads from a position 1 (foot flat or mid-stance position), to a position 2 (early push-off position), to a position 3 (late push-off or early toe-off position). The overall value c or d, difference between the standing and walking measurements, can ranges from **2.5 mm** to **5.9 mm**. The average value can be taken at **4.1 mm**.

The global value of the weight-bearing extension and toe extension is **9.8 mm**. These values have been extracted from Chen's work. For the final ease allowance, the previous value has to be supplemented by a comfort value for good fit so that the toes do not touch the bottom of the shoe.
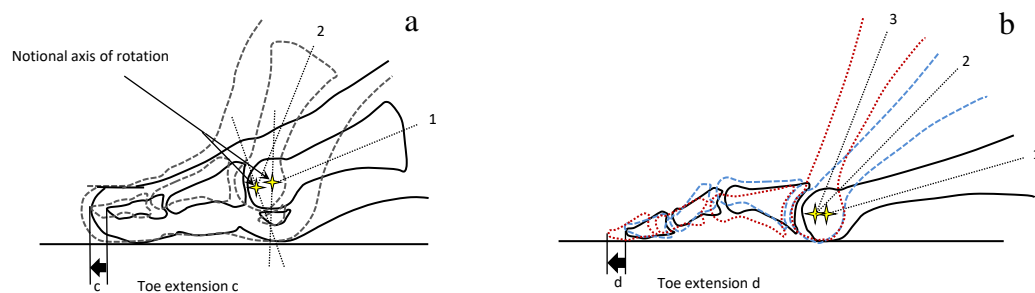
Figure 84 : Toe extension **c** at the big toe (a) & **d** at the other toes (b).

V.4.   3D GRAPHIC MODEL OF A CUSTOMIZED SHOE-LAST

In continuity with the work of the previous chapter, a first comparison between the standard shoe-last and foot to customize shows that the standard shoe-last has a volume smaller than that of the foot and does not follow perfectly the morphology of the foot (**Figure 85**). This led us to customize insole during the chapter IV. The volume between the ball girth

and the instep girth is much lower than that of the foot. From the instep girth to the back of the heel, the morphology difference is very pronounced which makes it very difficult to check who is the biggest. Among other things, the main axes (instep axis and heel axis) that was used to define the plantar surface can be very misaligned on the foot (**Figure 69**). These remarks confirm the need to put in place a new concept of shoe-last creation.
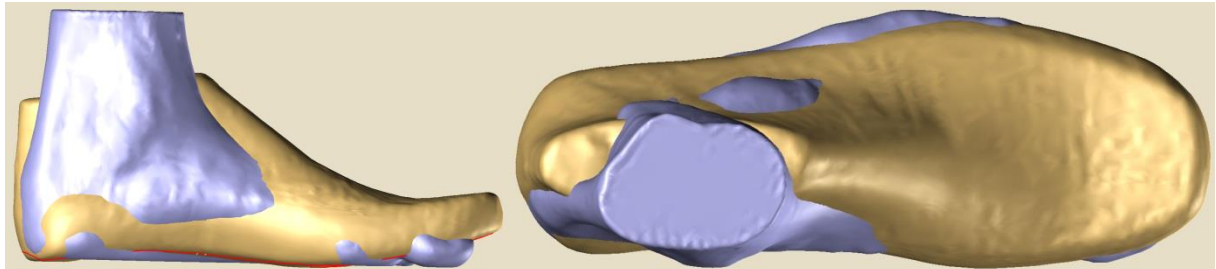
Figure 85 : Difference between shoe-last standard and foot to customize.

Hence, the morphology of the foot was used to create the graphical model of the shoe-last by following a specific process. It was from the morphological contours of the foot that the process of creation the shoe-last began. Also, the choice of these contours is very important because some must be linked imperatively to the anthropometry of the foot to take into account the measurements of it. These so-called primary contours are both morphological and dimensional references. Other so-called secondary contours are added in order to better follow the morphology of the foot during the creation of the shoe-last. They are associated or even connected to one or two primary contours so that their position and proportion evolve according to the neighboring primary contours. A 3D ease allowance is then applied and distributed on each contour. The values of ease allowance are different from one contour to another to ensure the comfort of the shoe induced by the shape of the shoe-last as shown by the analysis of the ease of a shoe-last described in the previous paragraph (**Figure 81**). This punctually managed 3D ease allowance control can be very useful in the event of a foot malformation that requires specific localized problems. This 3D well-distributed ease allowance on the surface of the foot allows creating a network of curves on which will be created a 3D surface representing the final 3D shape of the future customized shoe-last.

The previous analysis of the shoe-last led to the development of a 3D graphic model composed of three sub-models connected to each other:

- 3D model of the lower surface,
- 3D model of the upper front surface,
- 3D model of the upper back surface.

V.4.1. 3D MODEL OF THE LOWER SURFACE

The graphical model of the bottom shoe-last requires to create in a first step a 3D curve defining the path of the lower surface. In order to satisfy the conditions of dynamics and comfort, two constraints must be imposed. These constraints are noticeable in the views from below and from the side. In view from below, the preceding remarks show that the course of the shoe-last shank must follow two axes: insert axis, heel axis (**Figure 86**). In side view, the galb of the shoe-last shank curve must respect the constraints of product style and movement dynamics on the appropriate floor (**Figure 76**). Furthermore, it was chosen to extract the shape of this curve directly from the standard shoe-last corresponding to the size of the foot was to be treated. In practice, the projection of the HW and HG priority axes of the plantar surface (**Figure 65**) on the bottom of the standard shoe-last makes it possible to combine these two constraints (**Figure 86**).
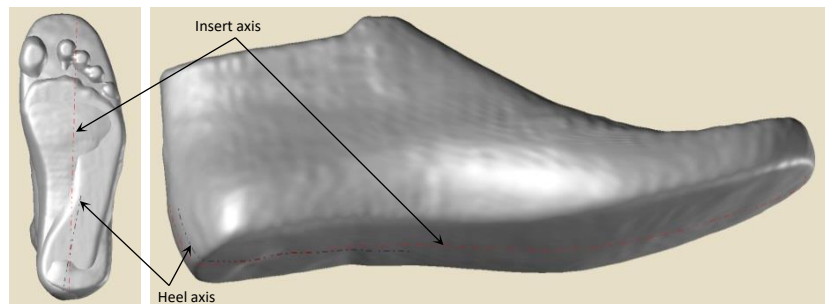
Figure 86: Insert axis and heel axis of the foot.

A 3D spline curve is then created from the projected axes to obtain the 3D shoe-last shank axis (**Figure 87**). Another constraint that was taken into account was the curved bottom of the shoe-last.
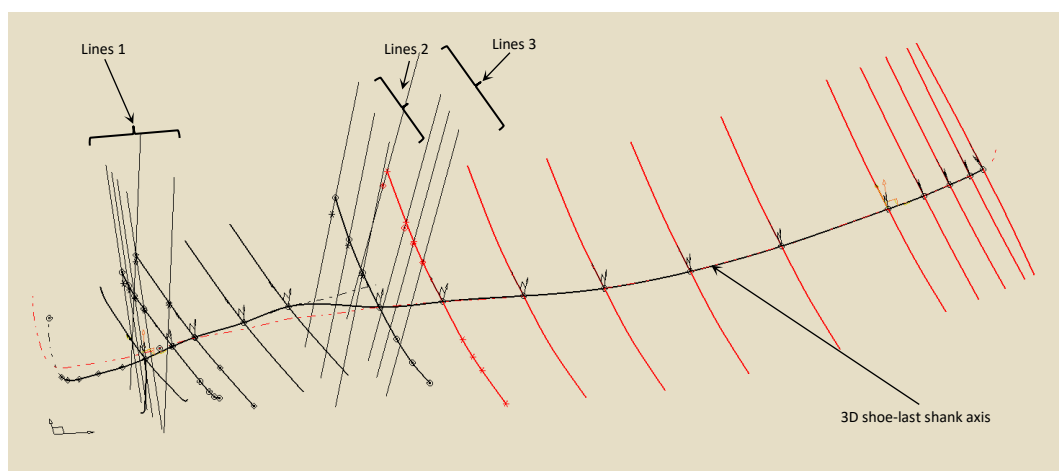
Figure 87 : Graphical model of the bottom last-shoe.

For this, three sets of curves perpendicular to the curve of the shoe-last shank axis must be created. The black curves give the curve of the heel which will be more or less pronounced depending on the relative position of the vertical lines 1 drawing in the definition plane of the initial curve. The red curves give the curvature of the front part which will be more or less pronounced depending on the relative position of the vertical lines 3 in the definition plane of the initial curve. The black curve associated with the vertical lines 2 controls the transition between the heel (black curves) and the front of the foot (red curves). The inspiration camefrom the standard shoe-last curve to define the shape of the black and red curves. But that did not prevent from generating a curvature clean to the patient to assure a better foot reach on the ground according to whether it was pronator or supinator.

Figure 88 shows the final surface of the bottom of the shoe-last. This surface is generated by the network of red and black curves and bounded by the outline of plantar surface contour (**Figure 66**).

Featherline (3D)

Outline of plantar surface contour (2D)
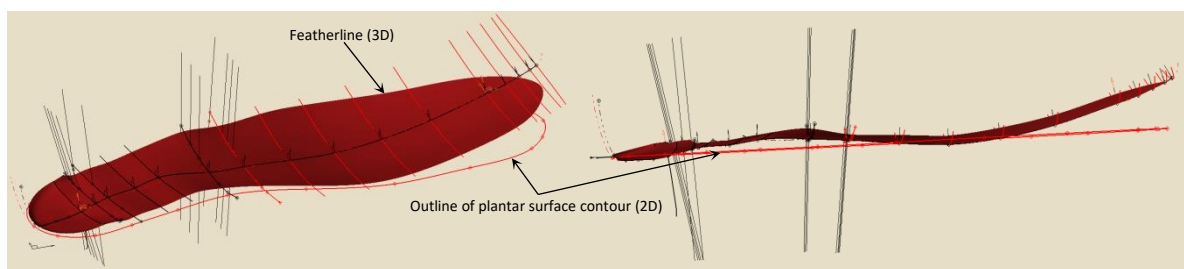
Figure 88 : 3D graphical surface of the bottom shoe-last.

V.4.2. 3D MODEL OF THE UPPER SURFACE

L'analysis of the shoe-last reach on the ground (**Figure 75**) shows that the upper part can be conceived in two distinct parts: Frontpart and Backpart. The ball girth is the junction outline that separates these two parts. The tread point is the intersection point between the ball girth and the 3D shoe-last shank axis. The general principle of our 3D model of the upper surface is to detect the morphological contours of the foot, to rely on these contours to generate other contours integrating the ease allowance necessary to the comfort and dynamics of the foot unroll on the floor. It was from these new contours that finally defined the 3D model of the upper surface of the shoe-last.

V.4.2.a. BACKPART

<u>Anthropometric model</u>

The backpart uses two categories of contours to represent the morphology of the foot (**Figure 89**).
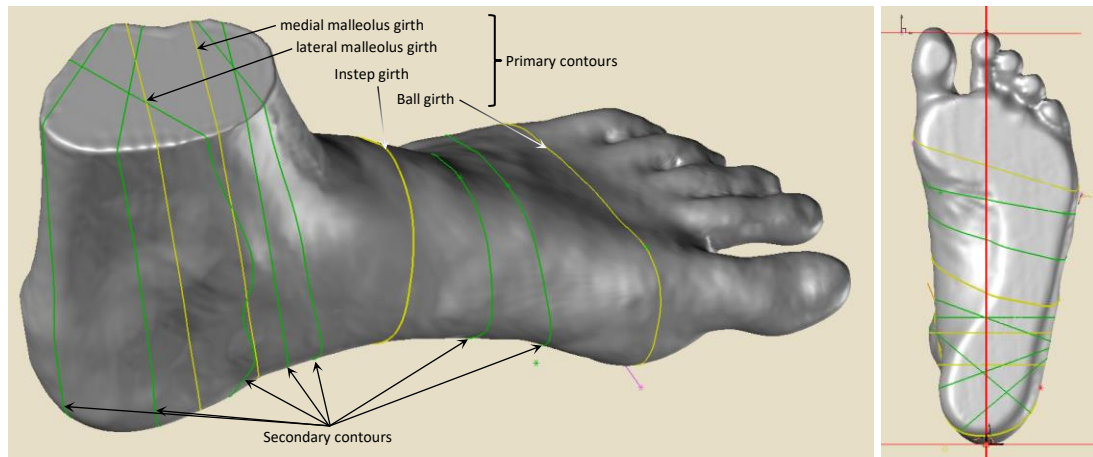
Figure 89: Primary and secondary contours of the backpart.

The first category of contours allows to design the front part of the shoe-last located between the ball girth and the instep girth (**Figure 89**). These two so-called primary morphological contours (**Figure 89:** in yellow) are detected by the method presented in chapter **II**. Between these two primary contours are added two other secondary contours (**Figure 89:** in green) distributed proportionally to the previous outlines. As it was explained previously, the secondary contours clearly improved the final shape of the shoe-last. The advantage of improving the shape of the shoe-last in this area is to provide a controllable comfort between instep girth and ball girth by the value of ease. This comfort value, which is different for each contour, varies greatly, progressively passing from a positive comfort value (instep girth) to a comfort value close to zero (ball girth). Of course, a positive comfort value at the level of instep girth improves the insteping of the foot in the shoe, while a value of negative ease in the ball girth ensures the locking of the foot in the shoe so that it does not slide to the end of it. Preliminary tests had been carried out with the waist girth (primary contour) to avoid creating these additional secondary contours but the shape obtained with the two other primary contours was not representative of a foot.

The second category of contour is located at the heel to take into account its morphology (**Figure 89**). Moreover, first two contours perpendicular to the Brannock axis were created whose objective was to detect the protruding parts of the two malleoli. These contours (**Figure 89:** in yellow) were considered primary because they passed through the

following two anthopometric points: medial malleolus 3 and lateral malleolus 4 (**Figure 31**). Other secondary contours (**Figure 89:** in green) were also added for the same reasons of morphological follow-up of the heel. These contours were obtained by cutting planes assigned to different coordinate systems (**Figure 89:** in black) positioned on the upper contour of the foot passing through the junction point 12 (**Figure 31, Figure 90**). This contour was connected later to the cone top surface outline of the shoe-last. The coordinate systems in which the cutting planes were defined were controllable both in position on the high contour and in angular value in order to manage the final shape of each secondary contour.

Two other contours were required to be detected in the direction of the Brannock axis. The first contour at the back of the foot alloed to control the shape of the shoe-last back center line/curve. The second contour allowed to position the shoe-last front center line/curve. It was from the impression of the Brannock axis on the front and the back of the foot that drew these two contours.
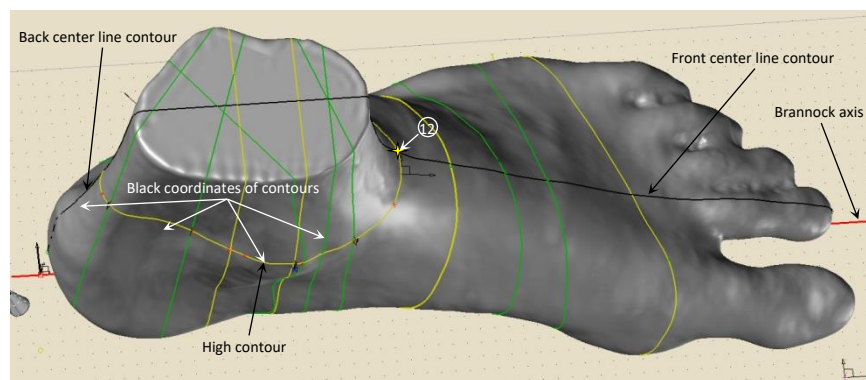
Figure 90 : High contour, back and front center line contours of foot.

3D ease allowance model

The 3D ease allowance model uses primary and secondary contours (**Figure 91**: green & yellow curves). The principle of this model is to judiciously distribute ease allowance points on these different contours. The number of ease allowance points on a contour depending on the position of the contour (the front part of the foot, the back of the foot i.e. the heel). The morphology of these two regions being very different, they impose a different surface model. There were nine ease allowance points on each contour of the front, while there were only have five ease allowance points on each contour of the back (**Figure 91**: white star points). On these ease allowance points were then created the lines of ease whose length depended on the value of ease allowance was to be affected at this point (**Figure 91**:

red straight thin lines). The lines of ease allowance are orientable in the plane of definition of the associated contour.

With this 3D ease allowance model, the distance between the foot and the shoe-last was managed in a punctual way. In this way, the pressure of the shoe on the fo ot could be managed more easily by this zoning principle. At the end of these ease allowance points passed a new contour (**Figure 91**: red curves), offset from the initial contour. The advantage of this new contour made by a spline curve made it possible to create a curve in accordance with the initial curve whose imperfections was eliminated by a smoothing effect induced by the spline function. The ends of these lines were attached to the featherline resulting from the 3D graphical surface of the bottom shoe-last (**Figure 88**).
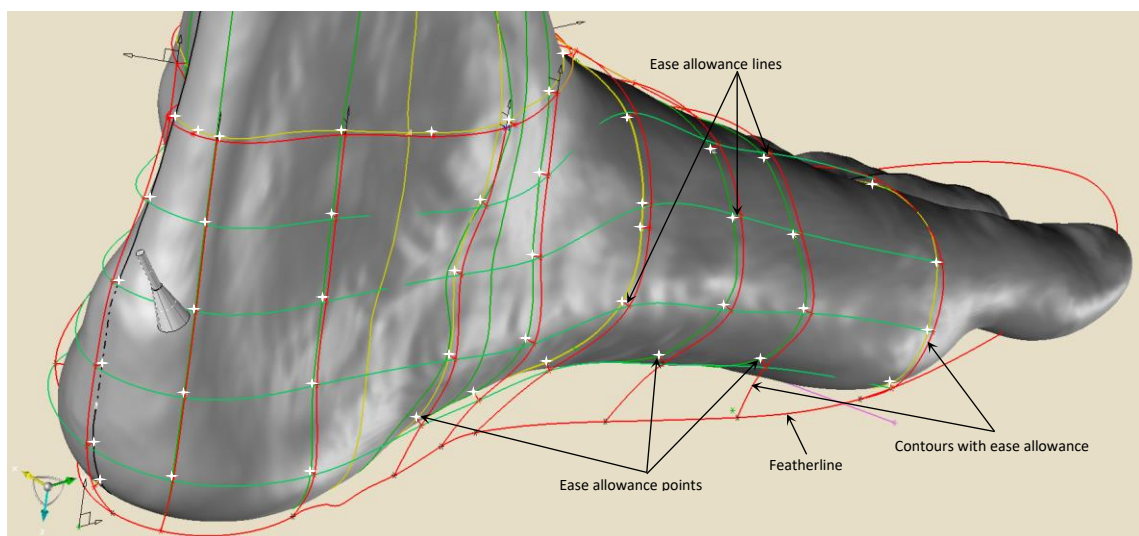
Figure 91 : 3D ease allowance model.

3D surface model

At this stage of the creation process, creation of the upper surface of the shoe-last backpart was possible (**Figure 92**). This surface leant on the network of curves of ease allowance contours (**Figure 91**: red contours ad curves).
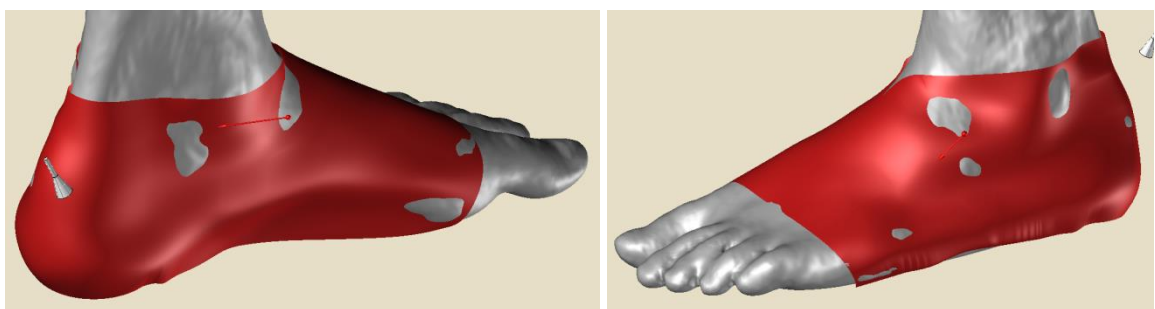
Figure 92 : Upper surface of the shoe-last backpart.

V.4.2.b. FRONTPART

Anthropometric model

The frontpart uses two types of contours to represent the morphology of the foot end (**Figure 93**). For the first type of contours, 5 sectional planes capture part of the morphology of the toes and create 5 secondary contours (**Figure 93** : green and pink curves). These planes perpendicular to the Brannock axis and the ground surface are positioned and shifted by an identical value with respect to the end points of each toe: anthropometric points 5_1, 5_2, 5_3, 5_4, 5_5 (**Figure 39**). The second type of contours is between the ball girth and the contour of the toe 5. Its role is to provide a surface continuity between the backpart and the frontpart. For this, it is necessary to tilt its cutting plane with an angle whose value represents the average value of the angle between the cutting planes of the ball girth and the toe 5.
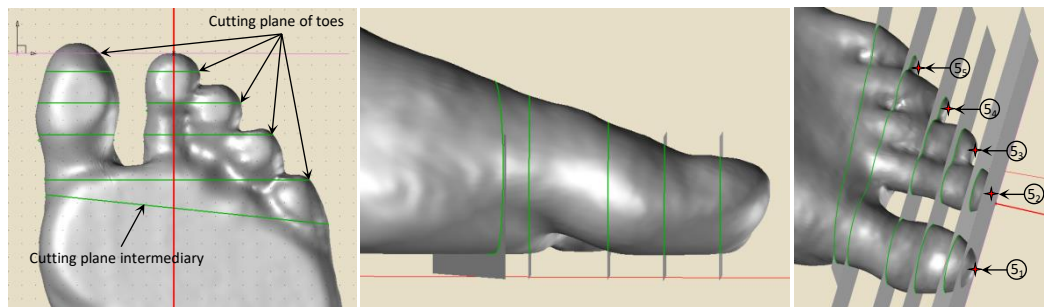
Figure 93 : Secondary contours and anthropometric points of the front part.

At this stage of the model, the position of the secondary contours must be adjusted to facilitate the smooth running of the step. This constraint imposes to raise the end of the frontpart taking into account toe spring measurement (**Figure 75**, **Figure 94a**). For this, each secondary contour must rotate around the tread point of a specific value in order to follow the curvature of 3D shoe-last shank axis.
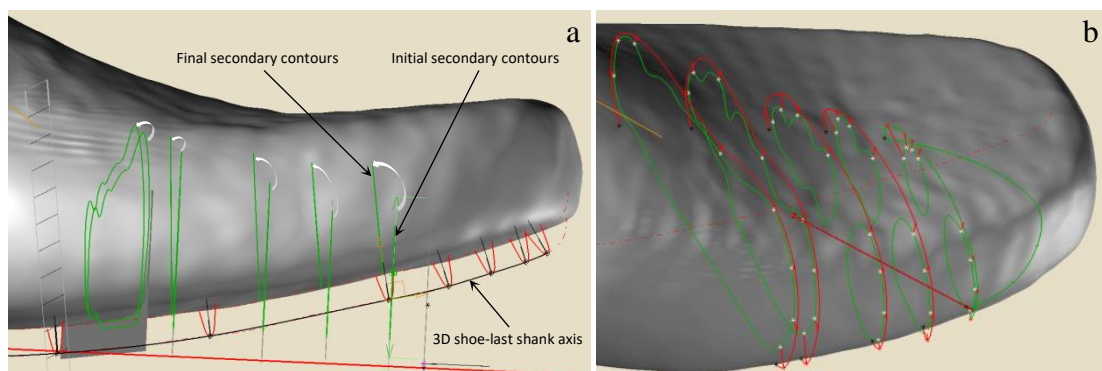
Figure 94 : Re-adjusted secondary contours (a), 3D Ease allowance model (b).

3D ease allowance model

Following the same principle as the 3D backpart ease allowance model, the secondary contours were used to distribute the ease allowance points on these contours (**Figure 94b**). In this case, eight ease allowance points were placed on each contour. On the top part, two points were sufficient since it was not required to follow exact morphology of the toes. The reason for this choice was that following the morphology generated ripples, that was to say, surplus material for the shoe, so harmful folds for comfort and bad roll of the foot on the ground. On the other hand, three ease allowance points on each side of a contour were necessary in order to follow the morphology of the sides of the foot. **Figure 77** and **Table 9 : Shoe-last allowances required vs. insole [1]**.shows the importance of controlling this area of comfort close to the sole as it contributed to the width of the shoe-last. On these ease allowance points ease lines (**Figure 94b**: red straight thin lines) were also created on which the new contours are hung (**Figure 94b**: red curves). Recall that the ends of these new outlines were also connected to the featherline to manage the width of the shoe-last and ease allowance of side together.

The ease allowance of the foot end was given by the green curve that is extracted from the end of the featherline. When drawing the outer contour of the plantar surface, the ease allowance of use for weight-bearing extension and toes extension was directly integrated into the proposed method.

3D surface model

The upper surface of the shoe-last frontpart is composed of two connected surfaces (**Figure 95**). The first is created from the 5 contours with ease allowance (**Figure 94b**: 4 red, 1 green) and the ball-girth contour. The second surface uses the last contour with ease allowance (**Figure 94b**: 1 green) and the green curve extracted from the end of the featherline (**Figure 94b**: 1 green).
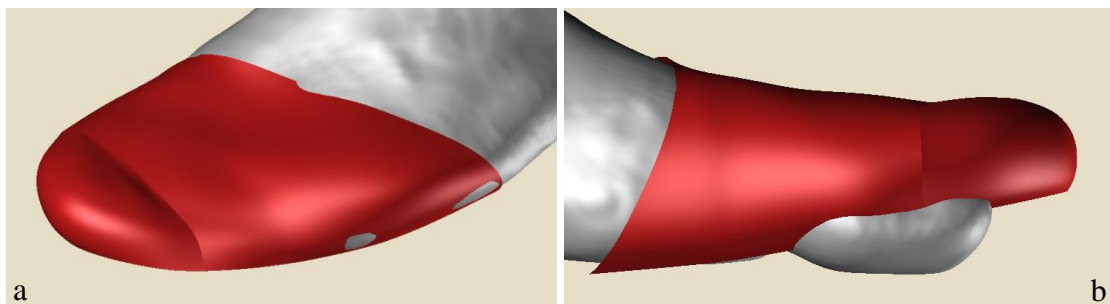
Figure 95 : Upper surface of the shoe-last frontpart.

113

V.4.3. 3D GLOBAL MODEL

The global 3D model of the customized shoe-last is an assembly of the three previous surface models: 3D model of the lower surface, 3D model of the upper backpart surface, 3D model of the upper frontpart surface. **Figure 96** shows a perfect morphological follow-up of the foot by the shape of the customized shoe-last. The 3D ease allowance values were chosen to show this type of result. These can be modified at any time and punctually depending on the area to be treated if a medical need requires it, or depending on the wearer's request for a specific comfort (in the case of non-orthopedic treatment). The gray areas would give the impression of a lack of ease allowance in these areas (eg zone of the lateral malleolus), which is not the case because when the overall ease allowance in a convex zone approaches zero, it gives this effect, but it is generally compensated by a neighboring concave zone (opposite effect).
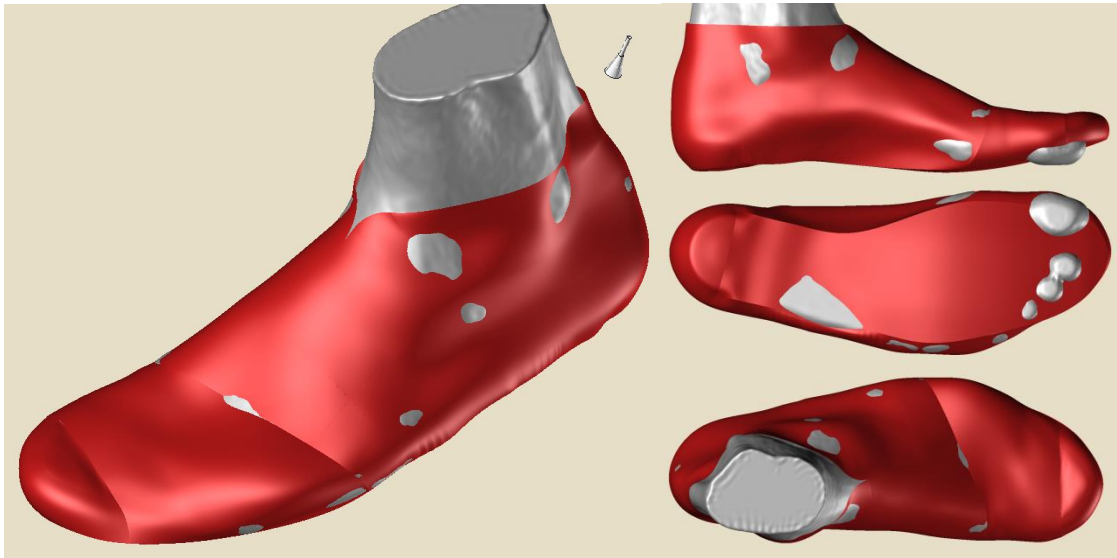
Figure 96 : 3D graphic model of a customized shoe-last.

So from the connection of the different surfaces (frontpart, backpart, bottom shoe-last), the tangents to the different surfaces to be connected do not always respect perfectly if one wishes to rigorously apply all the constraints imposed on the shoe-last. To solve this problem harmful to the harmonization of the shape and the final rendering of the object, the customized shoe-last is then smoothed in the junction areas of these different connected surfaces (**Figure 97**).
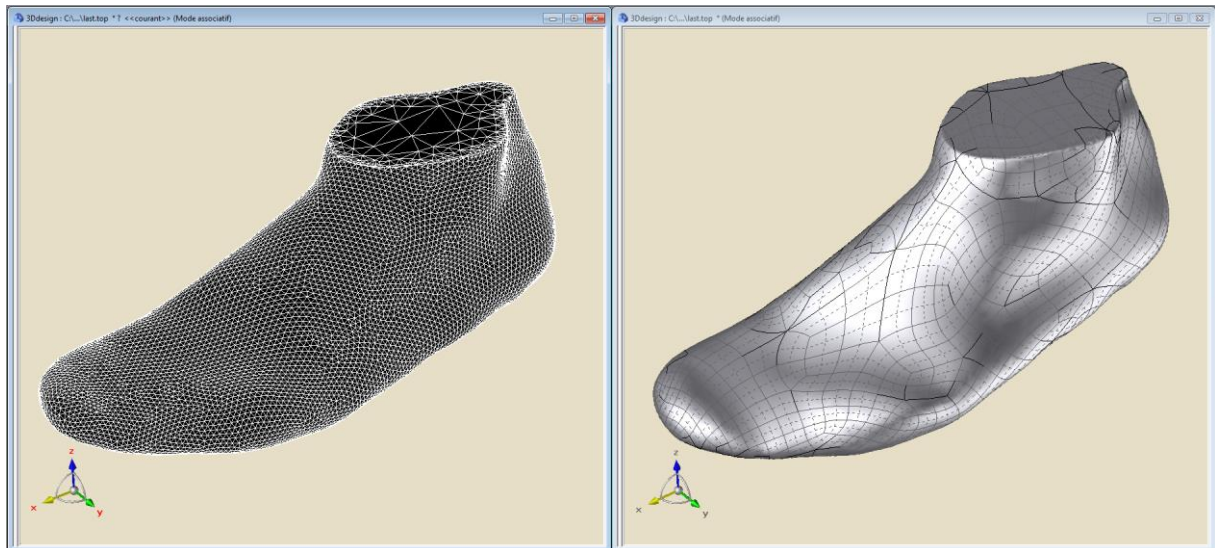
Figure 97 : Smooth customized shoe-last model.

V.5.   ANALYSIS OF **3D** EASE ALLOWANCE - RESULTS

Our global customized shoe-last model is not valid only by observing the good coverage of the foot surface. The validation must be completed by a 3D ease allowance analysis. It must be evenly distributed on the surface of the foot and contributed to the conditions of comfort and blockage of the foot in the shoe. **Figure 98a** gives a spatial representation of the gap between the foot and the shoe-last.
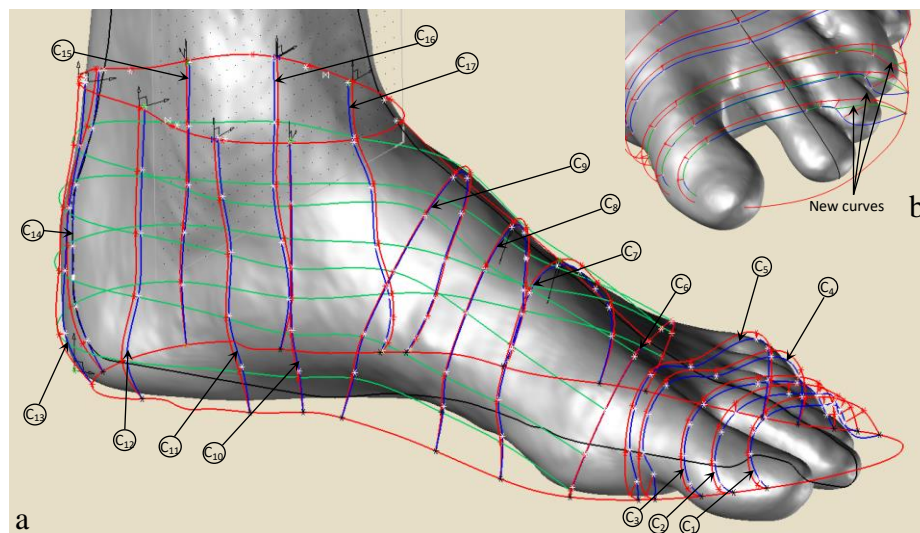
Figure 98 : 3D ease allowance between foot curves and shoe-last curves.

The blue curves represent contours in contact with the foot. As these move closer to the surface of the bottom shoe-last , these curves move away from the foot to take into account the tight areas of the material during the design of the shoe. The red curves represent

the set of contour curves with 3D ease allowance. These curves associated with the green curves represent the network of curves which made it possible to create the surfaces of the customized shoe-last. Each pair of blue and green curves for measuring ease in different areas has been identified and noted C_n.

Table 10 represents the length in mm of each curve marked by their position C_n (column 2). Column 3 represents the curves relating to the foot. Column 4 represents the curves relating to the shoe-last. Column 5 represents the gap between these two curves representing the 1D ease allowance. The curve C_6 is that of the ball girth, the curve C_9 is that of instep girth, the curve C_{14} is that of the back center line

Table 10 : Contour measurements and 1D ease allowance.

		Foot curves (blue)	Shoe-Last curves (red)	Ease allowance
	C_1	102.7	107.4	4.70
		100.6		6.8
	C_2	115.2	122.5	7.30
		113.5		9
	C_3	123.0	132.4	9.40
		123.8		8.6
	C_4	141.9	151.6	9.70
	C_5	156.6	165.5	8.90
	C_6	178.9	182.6	3.70
	C_7	185.0	192.7	7.70
	C_8	198.5	208.6	10.10
	C_9	218.4	228.2	9.80
	C_{10}	96.2	97.0	0.80
	C_{11}	96.2	96.9	0.70
	C_{12}	95.1	96.1	1.00
	C_{13}	99.5	100.5	1.00
	C_{14}	100.6	101.9	1.30
	C_{15}	98.3	99.6	1.3
	C_{16}	95.6	96.5	0.9
	C_{17}	98.1	100.5	2.4

Trends of the 1D ease allowance evolution in mm (**Figure 99:** blue) show a progressive increase in toes ease allowance (C_1 to C_5) that should not be as pronounced as the shape of the blue curve on the outer side of the foot deforms in opposition to that of the shoe-last (**Figure 98-b**). This greatly reduces the 1D ease allowance value, while the ease allowance lines show a very pronounced value. Also, an adjustment was made with curves C_1, C_2, C_3 (**Figure 98-b** : green curve) to correct the calculation. The value of these new curves are given in green

The new trends of the 1D easese allowance (**Figure 99:** green) are much closer to reality and needs. Curve C_6 shows a small ease allowance value because at the ball girth, the foot should not slide to the toes. Then, a gradual increase in ease allowance is required from C_7 to C_9 to facilitate sleeping the foot into the shoe. A low and constant ease allowance is imposed around the heel by the curves C_{10} to C_{17} in order to maintain it in the shoe and ensure its blockage in this area.
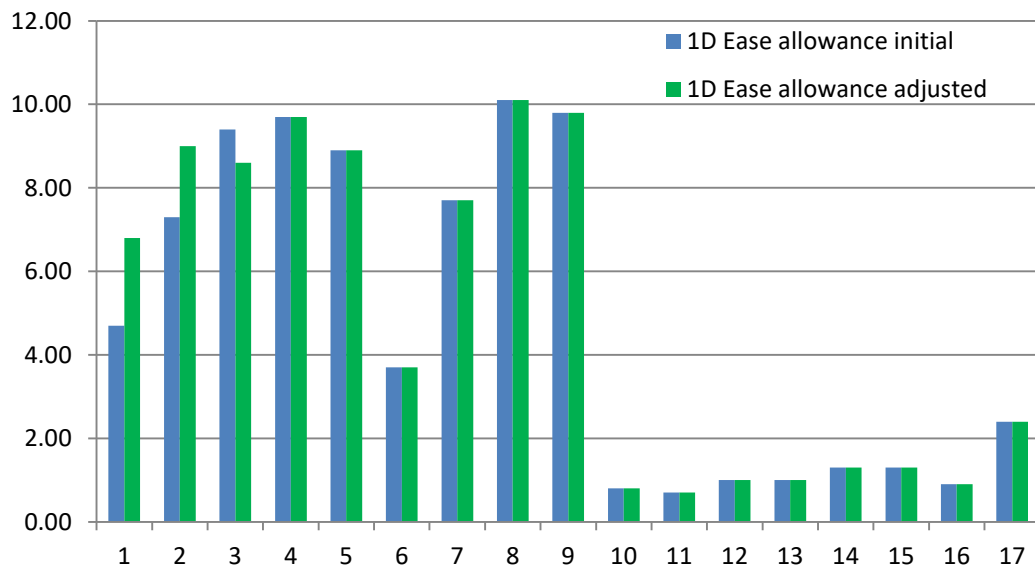
Figure 99 : Evolution of 1D ease allowance along the foot.

These evolutions are in line with the needs of the patients because they follow very closely the results of **Figure 81**. Here, only curves of C_1 to C_9 could be compared. The edge imperfections on the Chen results have been removed because the work in this thesis was directly done in 3D. These data were more realistic and exploitable because the morphology monitoring avoided the estimates that it was necessary to make on a standard shoe-last with a strong deformation between instep girth and ball girth.

V.6.   CONCLUSION

In this chapter, a new shoe-last creation process has been developed that directly takes into account the shape of the patient's foot and the 3D ease allowance necessary for comfort. Compared with the shoe industry sector, the existing CAD systems also offered 3D graphic processes for the creation of customized shoe-last, but the lack of precision could be challenged because their method of creation did not allow fine-tuning and zoning the 3D ease allowance. This imperfection was based on the fact that the customized shoe-last only takes

into account the deformation of a standard shoe-last in manual mode. Deformation techniques are very subjective.

The interest of our shoe-last creation process is that it takes into account the anthropometry of the foot because the curves defining the final shape of the shoe-last are attached to the anthropometric curves. Our process of creating shoe-last also takes into account the needs of the patient because the 3D ease allowance can very easily be adjusted according to these needs which can be therapeutic or comfort.

GENERAL CONCLUSION AND PROSPECT

Nowadays, the personalization of the products is more and more strong. The types of shoes are more and more varied. For example, one can choose to wear sandals, canvas, shoes, trainers, boots, safety footwear, wellies, and slippers. The difference is perceived in the style that carries names very fashion-oriented such as: slider, gladiator, wedge, mule, toe post flip flops, flat, heeled. This leads to an impressive shape diversity requiring design tools evolving to digital in order to create models quickly.

But the shoe, unlike the garment, is very technical and complex because it must support the weight of the body, suffer shock during walking by cushioning to relieve the foot, bring comfort in various ways. The shoe, designed to cover more or less feet depending on the type chosen, does not always meet the technical criteria mentioned above. Many people forget these aspects to privilege the beauty of the product. For example, high heels are not in the spirit of comfort and protection of a customer's foot. This type of product tends to adversely modify the posture of the wearer and lead to a biomechanical imbalance that can lead to pain in various areas of the body. Therefore, the proposed method is in disapproval to the world of medicine that uses plantar prostheses precisely to solve this kind of problems. Of course, the remedies for these medical foot problems must not follow this fashion that imposes tendencies shoe styles harmful to the patient. Obesity, diabetes, osteoarthritic pain of the knee, hip or legs, length defect between the right leg and the left leg, morphology of the cavus foot or the planus are all pathologies to be cautiously treated. These pathologies, usually detected by rheumatologists or podiatrists, finalize prescriptions by manufacturing custom-made orthopedic insoles or custom-made orthopedic shoes outside this fashionable spirit, unlike shoe manufacturers. But a problem remains because the manufacturers use digital tools of creation with means of foot's measurement with high technology like the 3D scanner. On the other hand, the profession of podiatrist remains a craft where the manual works persists, as much from a measurement point of view as from a manufacturing point of view.

All these considerations are intrinsically linked to the implementation of a new shoe and insole creation process from the 3D foot shape. This process will enable the design and validation of products in a virtual 3D environment close to patient data.

In this thesis works, it has been tried to integrate the concept of comfort and design of customized shoes and soles that has been implemented in a 3D digital solution perfectly adapted to the needs of podiatrists. This solution is also applicable in the ready-to-wear sector

which has been improved by the morphological knowledge of the feet of the brand's client population. In this context, three general approaches have been proposed.

First: Foot's morphology pattern recognition presented in Chapter 2 & 3:

The proposed method is to recognize the morphology of the patient's or consumer's feet using a supervised classification method associated with image processing procedures. The 3D measurement system provided the necessary quality of classification. The directions which were taken have made it possible to verify this clear dimensional difference between the man's and woman's feet, to also verify that the morphology could be very different morphologically. Thus, in ready-to-wear, creating shoe-lasts according to the morphology of each centroid of each cluster makes it possible to improve the wearing comfort of shoes.

Second: 3D insole customization presented in Chapter 4:

The 3D measurement system that has been put in place allowed to create by outline of plantar surface contour. This outline was the basic element to create the contour of the insole in 2D which adjusted to the 3D shape of the shoe-last taken to the right size, led to the 3D shape of the insole. But this result has shown that the shoe-last, although at the right size of the person, presented an inappropriate 3D shape. The position of the underside of the insole showed unbalanced 3D deformation detrimental to the foot's comfort when inserted into a shoe. This problem requires the creation of customized shoe-last in this case to obtain the right shoe.

Third: 3D ease allowance & 3D shoe-last customization presented in Chapter 5:

The next step in this research was to set up a new shoe-last creation process. The analysis of the 3D interface between the foot and the shoe, i.e. the 3D ease allowance, made it possible to connect the foot and the shoe in the same creation process. 3D ease allowance has the particularity of being parameterized to take into account the comfort and the dynamic aspect when walking. These notions are perfectly adapted to the needs of patients because the 3D ease allowance is zoned therefore adjustable to the location of the medical problem.

Future developments will be to create adaptive foot morphotypes from the results of the classification. The idea is to use the different morphological contours of a centroid to create other adjustable contours on which leans the new surface of the adaptative foot morphotype. This adjustment will be in the length direction to control the size and in the

cutting plane of the morphological contours to manage the volume. By applying the evolutions of size and volume of the selected cluster, this adaptive foot morphotype will represent a foot's model close to each individual of this cluster.

The 3D insole creation process, connected to this new foot surface, will provide 3D insoles adjusted to each individual. These insoles will be adjusted morphologically but it will always be possible to connect i.e. print on the lower part of this foot the plantar pressure of the patient to take into account the requirements of the podiatrist. By this method, the 3D distribution of the plantar pressure will precisely indicate the areas to be controlled by the use of different materials.

The shoe-last 3D creation process will use this set, adjustable foot and connected insole, to define the inside volume of the shoe. Finally, the connection of these three elements can be realized for the well being, the comfort of the consumers, or the therapeutic needs of the patient.

Of course, the creation of the shoe will pass by the design of the style curves on this new adjustable shoe-last according to all the aforementioned parameters (parameters foot, parameters of 3D ease allowance, parameters associated with the insole). The other interest of this digitization is that it will be possible to automatically detect the areas of each pattern and flat them in 2D for the manufacturing process.

BIBLIOGRAPHY

[1] R. C. C. Chen, "An investigation into shoe last design in relation to foot measurement and shoe fitting for orthopaedic footwear," London, 1993.

[2] B. Munro and J. Steele, "Foot-care awareness. A survey of persons aged 65 years and older," *http://dx.doi.org/10.7547/87507315-88-5-242*, Apr. 2014.

[3] H. B. Menz and S. R. Lord, "The Contribution of Foot Problems to Mobility Impairment and Falls in Community-Dwelling Older People," *J. Am. Geriatr. Soc.*, vol. 49, no. 12, pp. 1651–1656, Dec. 2001.

[4] D. M. Aaron, "Pied d'athlète (tinea pedis)," *Le Manuel MSD*, 2016. [Online]. Available: https://www.msdmanuals.com/fr/accueil/troubles-cutanés/infections-mycosiques-de-la-peau/pied-d'athlète-tinea-pedis.

[5] Centre Hospitalier, "Le pied," *Bois de l'abbaye*. [Online]. Available: https://www.chba.be/le_pied-1839.html.

[6] J. A. DeBello, K. I. DeCoteau, and E. Beatty, "Taking A Novel Approach To Hammertoe Surgery," *Podiatry Today*, 2006. .

[7] E. B. Neves, A. J. Almeida, C. Rosa, J. Vilaca-Alves, V. M. Reis, and R. Mendes, "Anthropometric profile and diabetic foot risk: a cross-sectional study using thermography," pp. 1–3, 2016.

[8] A. Ogundipe, "How to break in new pair of shoes without hurting your feet," *Memois by mide*. [Online]. Available: https://memoirsbymide.wordpress.com/2016/05/17/how-to-break-in-new-pair-of-shoes-without-hurting-your-feet/.

[9] "Foot friction blisters," *MASS4D*. [Online]. Available: https://www.mass-4d.com/blogs/clinicians-blog/foot-friction-blisters.

[10] S. K. van de Velde, M. Cashin, R. Johari, R. Blackshaw, A. Khot, and H. K. Graham, "Symptomatic hallux valgus and dorsal bunion in adolescents with cerebral palsy: clinical and biomechanical factors," *Dev. Med. Child Neurol.*, vol. 60, no. 6, pp. 624–628, 2018.

[11] "Hallux valgus: only the handicap leads to the operation of the onion - Why Doctor," *Pourquoidoctteur.fr*, 2016. .

[12] S. Taş and A. Çetin, "Mechanical properties and morphologic features of intrinsic foot muscles and plantar fascia in individuals with hallux valgus," *Acta Orthop. Traumatol. Turc.*, no. xxxx, pp. 3–7, 2019.

[13] J. Ragland, "How to get rid of bunions," *Getridofthings*. [Online]. Available: https://getridofthings.com/get-rid-of-bunions/.

[14] R. O. N. B. Killian, G. S. Nishimoto, and J. C. Page, "Fo and an," vol. 88, no. 8, pp. 365–374, 1998.

[15] A. Paiva de Castro, J. R. Rebelatto, and T. R. Aurichio, "The relationship between foot pain, anthropometric variables and footwear among older people," *Appl. Ergon.*, vol. 41, no. 1, pp. 93–97, 2010.

[16] K. J. Mickle and C. J. Nester, "Morphology of the Toe Flexor Muscles in Older Adults With Toe Deformities," *Arthritis Care Res.*, vol. 70, no. 6, pp. 902–907, 2018.

[17] "Corns and calluses," *NHS*. [Online]. Available: https://www.nhs.uk/conditions/corns-and-calluses/.

[18] D. Singh, G. Bentley, and S. G. Trevino, "Fortnightly Review: Callosities, corns, and

calluses," *Bmj*, vol. 312, no. 7043, pp. 1403–1406, 1996.

[19] A. Ladhani, "What are heel spurs?," *step-by-step foot care*, 2015. .

[20] U. Chundru, A. Liebeskind, F. Seidelmann, J. Fogel, P. Franklin, and J. Beltran, "Plantar fasciitis and calcaneal spur formation are associated with abductor digiti minimi atrophy on MRI of the foot," *Skeletal Radiol.*, vol. 37, no. 6, pp. 505–510, Jun. 2008.

[21] H. Lemont, K. M. Ammirati, and N. Usen, "Plantar fasciitis: a degenerative process (fasciosis) without inflammation.," *J. Am. Podiatr. Med. Assoc.*, vol. 93, no. 3, pp. 234–7, 2003.

[22] L. Özgönenel, "Plantar Fasciitis," *Tech. Foot Ankle Surg.*, vol. 12, no. 2, p. 109, 2013.

[23] M. J. Coughlin, "Mallet toes, hammer toes, claw toes, and corns," *Taylor Fr.*, vol. 75, 1984.

[24] N. M. DeLauro and T. M. DeLauro, "Onychocryptosis," *Clin. Podiatr. Med. Surg.*, vol. 21, no. 4, pp. 617–630, 2004.

[25] "Nagelerkrankungen." [Online]. Available: http://www.fusspflege-burgauner.at/leistungen/nagelerkrankungen/index.html.

[26] D. B. Jacoby, "PPT - Common Office Procedures Baby Health Service Lexington, KY Spalding University Louisville, KY PowerPoint Presentation - ID:4063511." [Online]. Available: https://www.slideserve.com/brick/common-office-procedures-baby-health-service-lexington-ky-spalding-university-louisville-ky.

[27] J. J. Heidelbaugh and H. Lee, "Management of the ingrown toenail.," *Am. Fam. Physician*, vol. 79, no. 4, pp. 303–308, 2009.

[28] B. Ezekian, B. R. Englum, B. F. Gilmore, J. Kim, H. J. Leraas, and H. E. Rice, "Onychocryptosis in the Pediatric Patient: Review and Management Techniques," *Clin. Pediatr. (Phila).*, vol. 56, no. 2, pp. 109–114, 2017.

[29] J. D.B., *Hollinshead's Functional Anatomy of the Limbs and Back*. Elsevier Health Sciences, 2008.

[30] Annette, "Shoes and Your Feet| Posturepro," 2016. [Online]. Available: https://posturepro.co/shoes-and-feet/.

[31] T. F. Novacheck, "Review Paper The biomechanics of running," *Gait Posture*, vol. 7, pp. 77–95, 1998.

[32] "Foot pain | Mast Cells & Collagen Behaving Badly." [Online]. Available: https://www.mendeley.com/reference-management/web-importer/#id_2. [Accessed: 19-Jun-2019].

[33] J. G. Atwater, "Cavus Foot (High-Arched Foot) Video | Orthopedic Doctor in Vero Beach, Florida." [Online]. Available: https://osamds.com/cavus-foot-high-arched-foot-video/. [Accessed: 01-Jul-2019].

[34] D. S. Williams, I. S. McClay, J. Hamill, and T. S. Buchanan, "Lower extremity kinematic and kinetic differences in runners with high and low arches," *J. Appl. Biomech.*, vol. 17, no. 2, pp. 153–163, 2001.

[35] G. Gijon-Nogueron, J. Montes-Alguacil, P. Alfageme-Garcia, J. A. Cervera-Marin, J. M. Morales-Asencio, and A. Martinez-Nova, "Establishing normative foot posture index values for the paediatric population: A cross-sectional study," *J. Foot Ankle Res.*, vol. 9, no. 1, p. 1, 2016.

[36] D. Carmody, P. Bubra, G. Keighley, and S. Rateesh, "Posterior tibial tendon dysfunction: An overlooked cause of foot deformity," *J. Fam. Med. Prim. Care*, vol. 4,

no. 1, p. 26, 2015.

[37]   "What Is Metatarsalgia? | Applied Biomechanics Orthotics & Bracing Guelph."
        [Online]. Available: https://appliedbiomechanics.com/orthotics-bracing-
        blog/metatarsalgia-symptoms-treatments/. [Accessed: 01-Jul-2019].

[38]   D. Bubnis, "The Beginner's Guide to Pronation." [Online]. Available:
        https://www.healthline.com/health/beginners-guide-to-pronation/.

[39]   M. Voracek, M. L. Fisher, B. Rupp, D. Lucas, and D. M. T. Fessler, "Sex Differences
        in Relative Foot Length and Perceived Attractiveness of Female Feet: Relationships
        among Anthropometry, Physique, and Preference Ratings. Perceptual and Motor
        Skills," 2007.

[40]   Printerest, "Ankle anatomy." [Online]. Available:
        https://www.pinterest.fr/hgbarrese/ankle-anatomy/. [Accessed: 18-Jul-2019].

[41]   A. Cichocka, P. Bruniaux, and I. Frydrych, "3D Garment Modelling - Creation of a
        Virtual Mannequin of the Human Body," *Fibres Text. East. Eur.*, vol. 22, no. 6(108),
        pp. 123–131, 2014.

[42]   C. P. Witana, S. Xiong, J. Zhao, and R. S. Goonetilleke, "Foot measurements from
        three-dimensional scans: A comparison and evaluation of different methods," *Int. J.
        Ind. Ergon.*, vol. 36, no. 9, pp. 789–807, 2006.

[43]   M. Hajaghazadeh, R. Emamgholizadeh Minaei, T. Allahyari, and H. Khalkhali,
        "Anthropometric Dimensions of Foot in Northwestern Iran and Comparison with Other
        Populations," *Heal. Scope*, vol. 7, no. 3, 2018.

[44]   M. Pantazi, A. M. Vasilescu, A. Mihai, and D. Gurau, "Statistical-mathematical
        processing of anthropometric foot parameters and establishing simple and multiple
        correlations. Part 1: statistical analysis of foot size parameters," *Leather Footwear J.*,
        vol. 17, no. 4, pp. 199–208, Dec. 2017.

[45]   Y. C. Lee, G. Lin, and M. J. J. Wang, "Comparing 3D foot scanning with conventional
        measurement methods," *J. Foot Ankle Res.*, vol. 7, no. 1, 2014.

[46]   D. Webb, D. V. Bernardo, and T. Hermenegildo, "Evaluating and Improving Footprint
        Measurement : Orientation and Lengths," *Anthropologie*, pp. 277–287, 2006.

[47]   R. B. Kennedy, I. S. Pressman, S. Chen, P. H. Petersen, and A. E. Pressman,
        "Statistical analysis of barefoot impressions.," *J. Forensic Sci.*, vol. 48, no. 1, pp. 55–
        63, Jan. 2003.

[48]   J. A. Akambase, T. V Kokoreva, and O. A. Gurova, "Racial and gender comparison of
        anthropometric parameters of the foot," *Arch. Euromedica N1*, vol. 8, pp. 55–56, 2018.

[49]   S. A. Özdinc and F. N. Turan, "Effects of ballet training of children in turkey on foot
        anthropometric measurements and medial longitudinal arc development," *J. Pak. Med.
        Assoc.*, vol. 66, no. 7, pp. 869–874, 2016.

[50]   T. G. McPoil, B. Vicenzino, M. W. Cornwall, and N. Collins, "Can foot
        anthropometric measurements predict dynamic plantar surface contact area?," *J. Foot
        Ankle Res.*, vol. 2, no. 1, 2009.

[51]   O. Vrdoljak, M. K. Tiljak, and M. Čimić, "Anthropometric measurements of foot
        length and shape in children 2 to 7 years of age," *Period. Biol.*, vol. 119, no. 2, pp.
        125–129, 2017.

[52]   K. Hasanzadeh and K. Salehzadeh, "The Relationship between Anthropometric Indices
        in Children and their Kinetic Performances of Agility , Balance and Foot Power The
        Relationship between Anthropometric Indices in Children and their Kinetic
        Performances of Agility , Balance and Foot Power," no. May 2015, 2016.

[53] "BFTS GmbH." [Online]. Available: https://www.bfts.de/. [Accessed: 19-Aug-2019].

[54] B. Nácher *et al.*, "A Footwear Fit Classification Model Based on Anthropometric Data," *SAE Tech. Pap. Ser.*, vol. 1, no. May 2014, 2010.

[55] "Boite à empreintes double - Salembier Pédicurie Podologie." [Online]. Available: http://salembier.fr/boites-a-empreintes-et-moulage/1146-boite-a-empreintes-double.html. [Accessed: 20-Aug-2019].

[56] S. Koley, J. Singh, and J. S. Sandhu, "Anthropometric and physiological characteristics on Indian inter-university volleyball players," *J. Hum. Sport Exerc.*, vol. 5, no. 3, pp. 389–399, Oct. 2010.

[57] So. Rademene, Oi. Anozeng, Oa. Mathias, and En. Michael, "Regression equations for estimating stature from anthropometric measurements of foot length and breadth in adults of efik ethnic group in cross river state," *J. Exp. Clin. Anat.*, vol. 16, no. 2, p. 127, 2017.

[58] E. Ogugua, J. Nto, E. Finbarr-Bello, and U. Ukoha, "Stature Estimation from Foot Dimensions of An Adult Nigerian Population," *Anat. Karnataka*, vol. 6, no. 2, pp. 8–12, 2012.

[59] O. Iheanyi, A. Godwin, and U. Godwin, "Stature prediction from foot length in a Nigerian population," *J. Exp. Clin. Anat.*, vol. 8, no. 1, Nov. 2009.

[60] D. Mansur, M. Haque, K. Sharma, R. Karki, K. Khanal, and R. Karna, "Estimation of stature from foot length in adult Nepalese population and its clinical relevance.," *Kathmandu Univ. Med. J. (KUMJ)*, vol. 10, no. 37, pp. 16–9.

[61] A. Ozaslan, B. Karadayi, M. O. Kolusayin, A. Kaya, and H. Afsin, "Predictive role of hand and foot dimensions in stature estimation," *Rom. J. Leg. Med.*, vol. 20, no. 1, pp. 41–46, 2012.

[62] B. Sarghie, M. Costea, and D. Liute, "Anthropometric Study of the Foot Using 3D Scanning Method and Statistical Analysis," *Int. Symp. Knitt. Appar.*, no. May, pp. 1–5, 2013.

[63] B. Sarghie, A. Mihai, M. Costea, and E. Rezuş, "Comparative Anthropometric Study Regarding the Foot of Elderly Female Population," *Procedia Eng.*, vol. 181, pp. 182–186, 2017.

[64] A. Mihai and M. Pastina, "Classification of foot types, based on plantar footprints," in *ICAMS 2012 – 4th International Conference on Advanced Materials and Systems*, 2012, pp. 347–352.

[65] Y. C. Lee and M. J. Wang, "Taiwanese adult foot shape classification using 3D scanning data," *Ergonomics*, vol. 58, no. 3, pp. 513–523, 2015.

[66] Y. C. Lee, W. Y. Chao, and M. J. Wang, "Foot shape classification using 3D scanning data," *2012 Southeast Asian Netw. Ergon. Soc. Conf. Ergon. Innov. Leveraging User Exp. Sustain. SEANES 2012*, 2012.

[67] Y. C. Lee, W. Y. Chao, and M. J. Wang, "Developing a new foot shape and size system for Taiwanese females," *19th Int. Conf. Ind. Eng. Eng. Manag. Manag. Syst. Innov.*, no. January, pp. 959–968, 2013.

[68] A. et al Bataller, "Morphological Grouping of Spanish Feet Using Clustering Techniques," no. February 2015, pp. 12–13, 2001.

[69] D. W. Grieve and T. Rashdi, "Pressures under normal feet in standing and walking as measured by foil pedobarography," *Ann. Rheum. Dis.*, vol. 43, no. 6, pp. 816–818, 1984.

[70] D. Rosenbaum and H.-P. Becker, "Plantar pressure distribution measurements.

Technical background and clinical applications," *Foot Ankle Surg.*, vol. 3, no. 1, pp. 1–14, Jan. 1997.

[71] T. Duckworth, R. P. Betts, C. I. Franks, and J. Burke, "The Measurement of Pressures under the Foot," *Foot Ankle Int.*, vol. 3, no. 3, pp. 130–141, 1982.

[72] N. Syed, H. Karvannan, A. G. Maiya, B. Binukumar, V. Prem, and R. D. Chakravarty, "Plantar Pressure Distribution Among Asymptomatic Individuals: A Cross-Sectional Study," *Foot Ankle Spec.*, vol. 5, no. 2, pp. 102–106, 2012.

[73] "iStep Luna." [Online]. Available: http://www.i-step.com/luna.php. [Accessed: 20-Aug-2019].

[74] A. Mihai, C. Dumitras, M. Pastina, and C. M. Harnagea, "Therapeutic footwear virtual prototyping based on gait analysis data.pdf," in *AUTEX 2010 World Textile Conference*, 2010, pp. 21–24.

[75] A. Almusallam, R. N. Torah, D. Zhu, M. J. Tudor, and S. P. Beeby, "Screen-printed piezoelectric shoe-insole energy harvester using an improved flexible PZT-polymer composites," *J. Phys. Conf. Ser.*, vol. 476, no. 1, p. 012108, Dec. 2013.

[76] L. Mateu and F. Moll, "Optimum piezoelectric bending beam structures for energy harvesting using shoe inserts," *J. Intell. Mater. Syst. Struct.*, vol. 16, no. 10, pp. 835–845, 2005.

[77] J. Zhao, Y. Guo, and L. Wang, "An Insole Plantar Pressure Measurement System Based on 3D Forces Piezoelectric Sensor," *Sensors & Transducers*, vol. 160, no. 12, pp. 49–54, 2013.

[78] M. Birtane and H. Tuna, "The evaluation of plantar pressure distribution in obese and non-obese adults," *Clin. Biomech.*, vol. 19, no. 10, pp. 1055–1059, 2004.

[79] S. A. Vela, L. A. Lavery, D. G. Armstrong, and A. A. Anaim, "The effect of increased weight on peak pressures: Implications for obesity and diabetic foot pathology," *J. Foot Ankle Surg.*, vol. 37, no. 5, pp. 416–420, 1998.

[80] K. G. Prabhu, D. Agrawal, K. M. Patil, and S. Srinivasan, "Parameters for analysis of walking foot pressures at different levels of diabetic neuropathy and detection of plantar ulcers at early stages," *Itbm-Rbm*, vol. 22, no. 3, pp. 159–169, 2001.

[81] M. A. Rahman *et al.*, "Analysis of plantar pressure in diabetic type 2 subjects with and without neuropathy," *Itbm-Rbm*, vol. 27, no. 2, pp. 46–55, 2006.

[82] E. Teh, L. F. Teng, R. Acharya U, T. P. Ha, E. Goh, and L. C. Min, "Static and frequency domain analysis of plantar pressure distribution in obese and non-obese subjects," *J. Bodyw. Mov. Ther.*, vol. 10, no. 2, pp. 127–133, 2006.

[83] A. Gefen, "Plantar soft tissue loading under the medial metatarsals in the standing diabetic foot," *Med. Eng. Phys.*, vol. 25, no. 6, pp. 491–499, 2003.

[84] P. R. Cavanagh, M. M. Rodgers, and A. Liboshi, "Pressure Distribution under Symptom-Free Feet during Barefoot Standing," *Foot Ankle Int.*, vol. 7, no. 5, pp. 262–278, 1987.

[85] M. Tenten-Diepenmaat *et al.*, "In-shoe plantar pressure measurements for the evaluation and adaptation of foot orthoses in patients with rheumatoid arthritis: A proof of concept study," *Gait Posture*, vol. 45, pp. 45–50, 2016.

[86] N. L. W. Keijsers, N. M. Stolwijk, B. Nienhuis, and J. Duysens, "A new method to normalize plantar pressure measurements for foot size and foot progression angle," *J. Biomech.*, vol. 42, no. 1, pp. 87–90, 2009.

[87] N. L. W. Keijsers, N. M. Stolwijk, J. W. K. Louwerens, and J. Duysens, "Classification of forefoot pain based on plantar pressure measurements," *Clin. Biomech.*, vol. 28, no.

3, pp. 350–356, 2013.

[88] A. Luximon and R. S. Goonetilleke, "Foot Shape Modeling," *Hum. Factors J. Hum. Factors Ergon. Soc.*, vol. 46, no. 2, pp. 304–315, 2004.

[89] H. P. Bao, P. Soundar, and T. Yang, "Integrated approach to design and manufacture of shoe lasts for orthopaedic use," *Comput. Ind. Eng.*, vol. 26, no. 2, pp. 411–421, 1994.

[90] T. J. Hwang, K. Lee, H. Y. Oh, and J. H. Jeong, "Derivation of template shoe-lasts for efficient fabrication of custom-ordered shoe-lasts," *CAD Comput. Aided Des.*, vol. 37, no. 12, pp. 1241–1250, 2005.

[91] Y. Zhang and A. Luximon, "Shoe-last design for mass-customized footwear," *Handb. Footwear Des. Manuf.*, pp. 236–253, 2013.

[92] N. Shi, S. Yi, S. Xiong, and Z. Jiang, "A CAD system for shoe last customization," *Proc. 2009 Int. Jt. Conf. Comput. Sci. Optim. CSO 2009*, vol. 1, no. June 2014, pp. 957–960, 2009.

[93] M. Hamad, S. Thomassey, and P. Bruniaux, "A new sizing system based on 3D shape descriptor for morphology clustering," *Comput. Ind. Eng.*, vol. 113, pp. 683–692, Nov. 2017.

[94] M. Hamad, "Classification non-supervisée de morphologies 3D de corps humain pour la mise en œuvre de mannequins morphotypes adaptatifs," Lille 1, 2015.

[95] M. Pantazi and A. M. Vasilescu, "3D Imaging Capture of the Foot and Data Processing for a Database of Anthropometric Parameters," pp. 387–392, 2017.

[96] PEARSON, Karl, "On Lines and Planes of Closest Fit to Systems of Points in Space," *Philosophical Magazine*, vol. 6, no. 2, pp. 559–572, 1901.

[97] H. Jia, S. Ding, X. Xu, and R. Nie, "The latest research progress on spectral clustering," *Neural Comput. Appl.*, vol. 24, no. 7–8, pp. 123–131, Jun. 2014.

[98] U. von Luxburg, "A tutorial on spectral clustering," *Stat. Comput.*, vol. 17, no. 4, pp. 395–416, Dec. 2007.

[99] Jianbo Shi and J. Malik, "Normalized cuts and image segmentation," *IEEE Trans. Pattern Anal. Mach. Intell.*, vol. 22, no. 8, pp. 888–905, 2000.

[100] J. Kunegis, A. Lommatzsch, and C. Bauckhage, "Alternative similarity functions for graph kernels," in *2008 19th International Conference on Pattern Recognition*, 2008, pp. 1–4.

[101] L. Zelnik-manor, L. Zelnik-manor, and P. Perona, "Self-tuning spectral clustering," *Adv. NEURAL Inf. Process. Syst. 17*, pp. 1601--1608, 2004.

[102] M. Meilă and J. Shi, "Learning segmentation by random walks," in *Advances in Neural Information Processing Systems*, 2001.

[103] A. Y. Ng, A. Y. Ng, M. I. Jordan, and Y. Weiss, "On Spectral Clustering: Analysis and an algorithm," *Adv. NEURAL Inf. Process. Syst.* , vol. 14, pp. 849--856, 2001.

[104] S. Shortreed and M. Meila, "Unsupervised spectral learning," in *the Twenty-First Conference Annual on Uncertainty in Artificial Intelligence*, 2005, pp. 534–541.

[105] S. White and P. Smyth, "A spectral clustering approach to finding communities in graphs," *Proc. 2005 SIAM Int. Conf. Data Mining, SDM 2005*, pp. 274–285, 2005.

[106] M. E. J. Newman and M. Girvan, "Finding and evaluating community structure in networks," *Phys. Rev. E*, vol. 69, no. 2, p. 026113, Feb. 2004.

[107] L. Yu and C. Ding, "Network community discovery: solving modularity clustering via normalized cut," in *Proceedings of the Eighth Workshop on Mining and Learning with Graphs - MLG '10*, 2010, pp. 34–36.

[108] R. RIGAL and D. MOTTIN, *La forme*, Lyon, CTC. 1991.

[109] Paul, "The Brannock Device | Ravelled Esoterica," 2016. [Online]. Available: https://ravelledesoterica.wordpress.com/2014/03/16/the-brannock-device/.

[110] D. Fauret, "Semelles Ortho 47."

APPENDIX

Published and submitted papers/conferences:

Articles in international peer-reviewed journals listed in international databases:

M.K.MISHRA, P.BRUNIAUX, G.TARTARE & C.CAMPAGNE,
Insole customized Part 1: Non-contact Method of Anthropometric Measures Detection of Feet
The Journal Leather & Footwear (In writing).
M.K.MISHRA, P.BRUNIAUX, G.TARTARE & C.CAMPAGNE,
Insole customized Part 2: 2D/3D graphical process
The Journal Leather & Footwear (In writing).

Communications with proceedings in an international conferences:

M.K.MISHRA, P.BRUNIAUX, D.CREPIN & B.HAMAD,
Studying foot anthropometric measures using 3d scanning method
CLOTECH 2017, 12th International Conference on Innovative Materials & Technologies in Made-up Textiles Articles, Protective Clothing and Footwear, Lodz, Poland, 11-14 October 2017.

M.K.MISHRA, P.BRUNIAUX, C.CAMPAGNE, D.CREPIN & A.CAYLA,
New method of detection of anthropometric measures of 3D foot models obtained by foot scanner
FTC 2018, Functional textiles & Clothing Conference, New Delhi, India, 9-11 February 2018.

Communications by poster in international or national conferences:

M.K. MISHRA, P. BRUNIAUX, C. CAMPAGNE, D. CREPIN, A. CAYLA,
Customization of insole using antibacterial nonwoven
NIA 2017 (Nonwovens innovation academy), EDANA poster competition, Innovation day on nonwovens, Chemnitz, Allemagne, 25-26 October 2017.

M.K. MISHRA, P. BRUNIAUX, C. CAMPAGNE, D. CREPIN, A. CAYLA,
Customization of Orthopedic Insoles for Different Foot-Morphologies
GEMTEX Day, ENSAIT, Roubaix, France, 01 December 2017.